The Chemistry of the Noble Gas Elements Helium, Neon, and Argon – Experimental Facts and Theoretical Predictions

Gernot Frenking[1] and Dieter Cremer[2]

[1] Fachbereich Chemie, Universität Marburg, Hans-Meerwein-Straße, D-3550 Marburg, FRG
[2] Theoretical Chemistry, University of Göteborg, Kemigården 3, S-41296 Göteborg, Sweden

The results of 65 years of experimental and theoretical research in light noble gas chemistry is reviewed, with particular emphasis on recent quantum chemical studies on the structures, stabilities and bonding of molecules containing He, Ne, or Ar. The scattered experimental results reported mainly for cations are interpreted using a chemical bonding model which is based on donor-acceptor interactions. A systematic view of bonding in Ng compounds (Ng = He, Ne, Ar) is presented that allows the prediction of new compounds which are theoretically predicted to be stable or metastable. The nature of the Ng,X interactions is studied with the help of the analysis of the electron density distribution and its associated Laplace field. Covalent noble gas bonds are found for many cations and dications, while closed-shell interactions are responsible for the unusually stable van der Waals compounds NgBeO.

Structure and Bonding 73

1 Introduction

For many chemists the title of this article may sound strange and even obscure. After all, are there any compounds containing either helium, neon or argon? A quick look into a recent textbook of inorganic chemistry confirms the suspicious reader. There are no revolutionary research reports on chemical reactions involving He, Ne or Ar that the reader may have missed. Of course, most standard textbooks devote a chapter to "noble gas chemistry". However, these chapters are exclusively restricted to the chemistry of the heavier noble gas elements krypton, xenon (this in particular), and radon. In this sense, noble gas chemistry started with Neil Bartlett's landmark experiment in 1962 [1, 2]. The lighter homologues helium, neon and argon are only mentioned as chemical elements for which all attempts to isolate a chemical compound failed. So what is the topic of this article?

The answer to this question depends on the chemists judgement whether or not a particular atom or molecule is the subject of chemical research. In orthodox chemistry, one would say: "As long as a compound cannot be filled in a bottle, it is not a subject of chemical research. A molecule has to have stable chemical bonds and a well-defined molecular structure in order to become the topic of a research report."

Of course, the position of orthodox chemistry has been abandoned as chemistry has moved more into the border areas to investigate molecules with low stability, fluxional, or nonclassical geometries. But even in modern chemistry, it is common chemical thinking that there are two classes of noble gas elements, namely those that chemically react (Kr, Xe, Rn) and those that do not react at all, the "truly" noble gas elements He, Ne, Ar. The former possess quite an interesting chemistry, the study of which has deepened chemists' understanding of chemical bonding, while the latter should be left to physicists and engineers to do work on super conductors and to prepare light bulbs.

This somewhat provocative view is not correct. The gas phase chemistry of the light noble gas elements has been known ever since HeH^+ was observed by Hogness and Lunn in 1925 [3]. Nevertheless, it has failed to qualify as a truly chemical research field because it did not meet the criteria of orthodox chemistry for a long time. Until today, all experimentally observed species containing He, Ne, or Ar, are only stable in the gas phase under unusual conditions, or they are weakly bound neutral complexes that do not qualify as molecules in the chemical sense. As a result, research of species containing light noble gas elements is exclusively a domain of physics or chemical physics, a view which is confirmed by the list of references in this review.

Physicist consider different aspects and properties of molecular species to those chemists do. This explains why the chemical aspects of light noble gas elements, in particular their reactive behavior, have not been the subject so far of a review article. Chemists ask whether He, Ne or Ar can form stable covalent bonds with other elements; they are interested in the resulting electronic structure, the stability, and the shape of the molecules containing light noble gas elements. They lose interest, however, if there are just van der Waals or dispersion forces that lead to a weakly stable associate, or if the molecule in question can only be observed under extreme conditions.

This report is aimed to (re)activate chemical interest in light noble gas elements by demonstrating that these elements should undergo interesting chemical reactions, provided the right reaction partners are found. We give an overview on the results of roughly 65 years of experimental and theoretical research on molecular species containing the light noble gas elements. We discuss in more detail recent quantum chemical investigations that predict stable molecules containing either He, Ne or Ar [4–15]. These predictions are extraordinary in so far as they are based on nothing but electronic structure calculations and *they are predictions before the (experimental) fact and not after the fact.*

The modern techniques of quantum chemistry, in particular the ab initio methods, and the availability of supercomputers which perform several million operations in a second have given a variety of tools that help to predict experimental events with chemical accuracy [16]. The power of these methods has long been overlooked by orthodox chemists, since the methods of quantum chemistry have often only been used to predict a molecular property or the existence of a certain species *after* the fact. This is valuable for theoretical chemistry itself, but not for experimental chemistry in search of new compounds and new reactions. The value of theoretical predictions beyond the realm of theory is obvious only in new areas. In such a situation, theory can guide experimentalists by predicting the existence of yet unknown compounds, describing their electronic structure and properties, in particular their chemical behavior, and suggesting experiments that eventually may lead to the observation of these compounds. All this has been done in the theoretical investigations that represent the kernel of this review [4–15].

This review has four aims:

(a) To summarize the experimental and theoretical research on the chemistry of He, Ne, Ar, during the past roughly 65 years.
(b) To give an overview of the results and their interpretation laid down in five major theoretical studies and several communications, where the chemistry of the light noble gas elements is presented with an attempt to unify the various results, utilizing techniques of modern quantum chemistry.
(c) To (re)awaken the interest of experimentalists in a research area that can be explored using the theoretical predictions as a guide line.
(d) To demonstrate the predictive power of quantum chemical calculations, in particular those based on ab initio methods.

Special consideration will be given to a description of the electronic structure and the nature of bonding in noble gas (Ng) containing compounds. Because it is the peculiar electronic structure of the Ng atoms which cause their resistance to forming a chemical bond, we review briefly some of the atomic properties of Ng

in Sect. 2. Then, in Sect. 3, various ways of analyzing chemical bonding are discussed, where special emphasis is given to a description of bonding based on the electron density distribution calculated for Ng containing molecules. In Sect. 4, we will systematically discuss diatomic ions NgX^{n+} with Ng = He, Ne, Ar, and X being any chemical element. In Sect. 5 we will extend our discussion to polyatomic ions of He, Ne, and Ar. On the basis of these results, we will discuss in Sect. 6 the attempts to synthesize neutral Ng compounds and the prospect for future experiments.

2 Atomic Properties of Light Noble Gas Elements

The light noble gases helium, neon, and argon are known to resist chemical bonding with other atoms or molecules. What is the origin of the peculiar resistance? The formation of a chemical bond is characterized by sharing of electrons by the atoms that are bonded. The strengths of such interactions depends on some key properties of the corresponding atoms. The energy necessary to share an electron with another atom or to accept an additional electron can be estimated from the ionization potential I_n and the electron affinity A_n, where n denotes the number of electrons removed from or accepted by a neutral atom. Another useful property, that can be used to describe the bonding ability of an atom, is the static electric dipole polarizability α which reflects the degree to which the electronic structure of an atom can be deformed by a potential binding partner.

In Table 1, first and second ionization potentials, I_1 and I_2, and dipole polarizabilities α of the noble gas elements and some first row elements are listed. The electron affinities of the noble gas elements are not shown, because they are essentially zero. This indicates that none of the noble gas elements accepts an electron from any other neutral atom or molecule.

The atomic data given in Table 1 show that in going from He to Xe there is a regular decrease in I_1 and I_2, and an increase in α. The first ionization potentials of He and Ne are higher than that of any other element. The highest I_1 for a non-noble gas element is found for fluorine (Table 1), but I_1(F) is still approx. 3 eV and 6 eV below the I_1 value of Ne and He, respectively. Accordingly, no other element should be capable of withdrawing electrons from either He or Ne, thereby forcing them into chemical bonding. This is in line with all experimental observations reported so far.

Argon, however, is different from He and Ne in so far, as its first ionization potential I_1 is *smaller* than that of fluorine (Table 1). Also, there is a very large change in the dipole polarizability when going from Ne to Ar. This suggests that Ar should be closer to Kr in its chemical behavior than to Ne. As a matter of fact, there are many theoretical and experimental observations that support this assumption. Whether this implies that Ar can form chemical bonds in the same

Table 1. First and second ionization potentials[a] I_1 and I_2 (in eV) and static electric dipole polarizabilities[b] α (in Å^3) for noble gas elements and first-row atoms

	I_1	I_2	α
He	24.587	54.416	0.205
Li	5.392	75.638	24.3
Be	9.322	18.211	5.60
B	8.298	25.154	3.03
C	11.260	24.383	1.76
N	14.534	29.601	1.10
O	13.618	35.116	0.802
F	17.422	34.970	0.557
Ne	21.564	40.962	0.395
Ar	15.759	27.629	1.64
Kr	13.999	24.359	2.48
Xe	12.130	21.21	4.04

[a] Ref. 85; [b] Ref. 171

way as Kr does will be discussed in detail later on. Here, it is sufficient to stress that when discussing light noble gas elements one should distinguish between He and Ne on the one side and Ar on the other side.

3 Ways of Describing the Electronic Structure and the Nature of Bonding in Ng Compounds

While the atomic properties shown in Table 1 reflect the reluctance of the light noble gas elements to undergo chemical reactions with other elements, they do not exclude the possibility of chemical bonding totally. For example, the data in Table 1 reveal that the second ionization potential of carbon is of the same magnitude as the first ionization potential of He. *Hence, carbon dications should be sufficiently strong electron acceptors to withdraw electrons from He (or Ne and Ar) and to establish a chemical bond with these noble gas elements. This assumption was the basis of the quantum chemical investigations reviewed in this article. They lead to the prediction of strongly bound helium (neon, argon) containing organic cations* [7, 11–13].

It is essential for the quantum chemical investigation of potential compounds containing light noble gas elements that a clear distinction is made between bonding and nonbonding situations. For example, if there are interactions between He and C^{2+} the question has to be answered whether these interactions lead to chemical bonding.

3.1 The Problem of Defining and Describing a Bond Ng–X

Chemists tend to describe chemical bonds either by comparing appropriate energies such as bond energies and dissociation energies, by analyzing interatomic distances and by describing the forces exerted on the nuclei of a molecule. However, none of these methods leads to a clear distinction between bonding and nonbonding situations or helps to differentiate between covalent and noncovalent bonds. Dissociation energies depend on both the stability of the target molecule and that of the dissociation products. Therefore, they cannot provide an accurate measure for the bond strength and the character of a bond. Bond energies, on the other hand, are arbitrarily defined. Even if this were not the case, it would be problematic, if not impossible, to define an energy value that indicates the change from nonbonding to bonding situations. For example, an interaction energy of 30 kcal/mol and more does not necessarily indicate covalent bonding [4]. It can be due to electrostatic forces, e.g. charge-dipole, dipole-dipole or other multipole interactions between two atoms that do not undergo covalent bonding. We will give several examples for such cases in Sects. 4.5 and 5.5.

It is similarly problematic to define bonding on the basis of measured or calculated atomic distances. In order to identify a certain interatomic distance as typical of covalent bonding, suitable reference distances have to be found. Normally, this is not very difficult in cases where there is no doubt about the nature of bonding. However, for nonclassical structures or in the case of exceptional long bonds or bonds between "unusual" atoms the problem of the reference bond cannot be solved in an unique way. The same difficulties arise when other molecular properties are used to define and to describe chemical bonding [17].

Theoreticians often resort to an analysis of the molecular orbitals. However, orbitals are not observable entities, they have only a mathematical meaning. Furthermore, they can be transformed by any unitary transformation into a new set of orbitals without changing energy or other properties of the molecule. For example, they can be presented as delocalized or localized MOs. A unique definition of chemical bonding, however, should be independent of the form of the MOs. The chemical bond should preferentially be described with the help of a molecular quantity that is observable.

In many textbooks of chemistry, the electrostatic picture of chemical bonding is presented. Electron density accumulates in the region between bonded atoms. Since electron-nuclear attraction dominates the forces stabilizing the molecule, the negative charge in the bonding region is thought to act like a glue that keeps the atomic nuclei together thereby establishing a chemical bond.

However, the electrostatic force description is flawed in several ways. Electrons should prefer those locations in the molecule where the potential energy is most negative and electron-nuclear attraction is a maximum. Hence, they should be found in the vicinity of the nuclei rather than the internuclear region. Nevertheless, those electrons that are responsible for chemical bonding prefer

the internuclear region. The reason why they behave different can only be described by quantum mechanics and not by a classical electrostatic argument. Accordingly, any description of chemical bonding based on electrostatic force arguments must be flawed as has been pointed out by several authors [18].

Because of the reasons outlined above we have refrained from using any of the traditional ways of describing chemical bonding in molecules containing light noble gas elements. Instead we have used a three-step procedure to elucidate the nature of the electronic interactions that He, Ne, and Ar can undergo with other elements. First, we have qualitatively assessed the degree of interactions between a light noble gas element and a potential binding partner with the aid of a simple donor-acceptor model. Then, we have calculated the potential NgX system and have analyzed the computed electron density distribution $\rho(\mathbf{r})$ in order to describe chemical bonding in a more quantitative way with the aid of the properties of $\rho(\mathbf{r})$. For this purpose we have utilized a model of the chemical bond suggested by Cremer and Kraka [19].

In the last step, we have complemented the information gained in the first steps by an analysis of the Laplace field $\nabla^2 \rho(\mathbf{r})$ associated with $\rho(\mathbf{r})$. It has been shown that the Laplaceian of $\rho(\mathbf{r})$ indicates where electrons concentrate in the molecule which is useful for a description of electronic structure and chemical bonding [20].

This procedure has been very successful when used to describe compounds containing noble gas elements [4, 5, 7, 13, 15]. Therefore, we will briefly outline some of the details of the three steps of describing chemical bonding.

3.2 The Donor-Acceptor Model

Since the electron affinity of noble gas atoms is zero (see above), chemical bonding can only be established if the very weak electron donor Ng is combined with a strong electron acceptor X. While the donor ability of Ng is reflected by the ionization potential I_1, the acceptor ability of X can be assessed from its electron affinity. This, in turn, depends on the energy of the lowest unoccupied MO (LUMO) of X. Furthermore, the nature of the LUMO, σ or π, symmetric or asymmetric, influences the acceptor ability of X with regard to Ng electrons.

Ab initio calculations provide a means of describing both the energy and nature of the LUMO of X and thereby its acceptor ability. All necessary data can be calculated to establish a donor-acceptor model for any combination of Ng and X and to predict the nature of Ng,X interactions in a potential molecule or complex. While these predictions are only qualitative, they are particularly useful when viewed together for a series of NgX molecules. For example, it is easy to see from the data in Table 1 that the donor ability of Ng increases from He to Ar and that for a given X the largest chance of finding a compound NgX should exist for Ng = Ar. Also, the strength of the binding interactions in NgX for a given Ng will be stronger when the acceptor ability of X increases.

On the basis of the donor-acceptor model the first calculational search for bonded systems between He and doubly charged cations was performed [7, 11, 12]. Also, the analysis of NgX systems for varying X has been facilitated by the use of the donor-acceptor model. For example, the trend in interatomic distances and bond strength for first-row diatomic ions NgX^+ and HeX^{2+} (X = Li–Ne) in their electronic ground and excited states could be rationalized [4, 5] by a qualitative discussion of the HOMO of Ng and LUMO of X^{n+}. The donor-acceptor model turned out to be very helpful not only for an understanding of the binding features of light noble gas compounds, but also for the search for new and strongly bound molecules [4–15, 21].

While a qualitative understanding of the structures and stabilities of Ng molecules was achieved by the donor-acceptor model, the quantitative analysis of the binding properties was provided by the analysis of the electron density distribution.

3.3 *Analysis of the Electron Density Distribution*

The electron denstiy distribution $\rho(\mathbf{r})$ of an atom or molecule is an observable property that can be measured by a combination of X-ray and neutron diffraction experiments [22]. Also, it is easy to calculate $\rho(\mathbf{r})$ once the MOs and the wave function of a molecule have been determined. The distribution $\rho(\mathbf{r})$ is invariant with regard to any unitary transformation of the MOs. It has been shown by Hohenberg and Kohn that the energy of a molecule in its (nondegenerate) ground state is a unique functional of $\rho(\mathbf{r})$ [23]. In other words, the physical and chemical properties of a molecule can be related to $\rho(\mathbf{r})$. Thus, $\rho(\mathbf{r})$ represents the best starting point for an analysis of chemical bonding.

Bader and coworkers have shown that properties of the electron density distribution $\rho(\mathbf{r})$ can be used to partition the molecular space into subspaces in a unique way [24]. This has been used by Cremer and Kraka (CK) to establish a model of the chemical bond that it easy to use, that allows a simple distinction between bonding and nonbonding situations, and that helps to characterize covalent bonds [19]. Therefore, the CK model has been applied when quantitatively describing chemical bonding in molecules containing light noble gas elements. In the following, we will briefly review the essentials of the Bader analysis and the CK bond model [25].

In Fig. 1, a perspective drawing of the calculated electron density distribution $\rho(\mathbf{r})$ of the N_2 molecule is shown with regard to a plane containing the N nuclei. At the positions of the nuclei, $\rho(\mathbf{r})$ adopts a maximal value, while in the off-nucleus direction $\rho(\mathbf{r})$ decreases exponentially. In the region between the two N atoms, however, the behavior of $\rho(\mathbf{r})$ is different. Along the internuclear connection line $\rho(\mathbf{r})$ first decreases, then reaches a minimum at a point $\mathbf{r}_B$ in the bonding region (which is identical with the bond midpoint in the case of homonuclear diatomics) and, finally, increases again to the value it possesses at the second nucleus. At the minimum $\mathbf{r}_B$, the value of $\rho(\mathbf{r})$ is still substantial

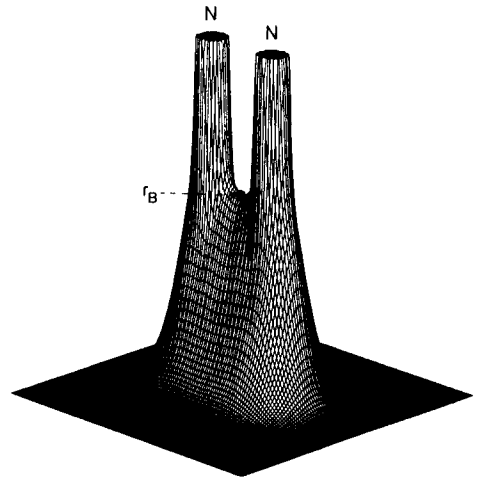

Fig. 1. Perspective drawing of the electron density distribution $\rho(\mathbf{r})$ of N_2 shown with regard to a plane containing the two nuclei (HF/6-31G(*d*) calculations). In this and the following figures the function value has been cut off above (below) a predetermined value in order to improve the representation

because $\rho(\mathbf{r})$ is at this point (as well as all other points along the internuclear connection line) a maximum in any direction perpendicular to the molecular axis. In other words, *the nuclei are connected by a path of maximum electron density (MED) path.* Any lateral displacement from the MED path leads to a decrease in $\rho(\mathbf{r})$. The position $\mathbf{r}_B$ corresponds to a saddle point of $\rho(\mathbf{r})$ in three dimensions.

The saddle point $\mathbf{r}_B$ is fully characterized by the first and second derivatives of $\rho(\mathbf{r})$ with regard to $\mathbf{r}$. The gradient of $\rho(\mathbf{r})$, $\nabla\rho(\mathbf{r})$, vanishes at $\mathbf{r}_B$. The Hessian matrix of $\rho(\mathbf{r}_B)$ is of rank 3, i.e. there are three eigenvalues $\lambda_i = 0$ (i = 1, 2, 3). The eigenvalues of the Hessian matrix of $\rho(\mathbf{r})$ give the curvatures of $\rho_B = \rho(\mathbf{r}_B)$ along the principal axes. The curvatures λ_1 and λ_2 perpendicular to the MED path are negative while the curvature λ_3 along the MED path is positive due to the minimum of $\rho(\mathbf{r})$ in this direction. This is expressed by the signature $s = \Sigma_i \lambda_i/|\lambda_i|$ which is $+1$ for the saddle point of $\rho(\mathbf{r})$ in the bond region. According to rank and signature, ρ_B classifies as a (3, +1) critical point [26].

Analysis of the electron density distribution $\rho(\mathbf{r})$ of numerous molecules [27–30] has revealed that there exists a one to one relation between MED paths and saddle points $\mathbf{r}_B$ on the one side and chemical bonds on the other side.

This relation is the basis for a definition of a chemical bond [19, 27]: *Two atoms will be bonded if and only if there exists a MED path linking them (necessary condition).*

This definition is not sufficient since there are MED paths that link the atoms of a van der Waals complex such as He_2. Even at larger distances than the van der Waals distance, the two He atoms are connected by a MED path indicating that there are still small dispersion forces active between the atoms. In order to distinguish closed-shell interactions such as van der Waals interactions,

hydrogen bonding or ionic (electrostatic) bonding from covalent bonding, a second criterion is needed. This has been formulated with the aid of the local energy density distribution H(**r**) [19, 27]:

$$H(\mathbf{r}) = G(\mathbf{r}) + V(\mathbf{r}) \tag{1}$$

Where G(**r**) is a local kinetic energy density distribution and V(**r**) is the local potential energy density distribution [31]. If H(**r**) is negative at $\mathbf{r}_B$, then the local potential energy density distribution V(**r**) will dominate, and accumulation of electronic charge in the internuclear region will be stabilizing. In this case, one can speak of a covalent bond.

*A covalent bond implies that the local energy distribution H(**r**) is negative at the* (3, +1) *critical point* $\mathbf{r}_B$, (*sufficient condition*).

The MED path is an image of the covalent bond and, therefore, it is called the *bond path*. For the same reason, the (3, +1) critical point $\mathbf{r}_B$ is termed *bond critical point* [32].

If H(**r**) is zero or positive in the internuclear region, then there will be closed shell interactions between the atoms in question, typical of ionic bonding, hydrogen bonding or van der Waals interactions [19].

On the basis of these definitions one can describe chemical bonding in molecules containing noble gas elements with the aid of the properties of ρ(**r**). One starts by searching for the bond paths and their associated bond critical points $\mathbf{r}_B$ in the molecular electron density distribution. If all bond paths are found, then the properties of ρ(**r**) along the bond paths will be used to characterize the chemical bonds. For example, the value of ρ_B can be used to determine a bond order, the anisotropy of ρ_B can be related to the π character of a bond, the position of the bond critical point $\mathbf{r}_B$ is a measure of the bond polarity and the curvature of the bond path reveals the bent-bond character of a bond [17, 19].

All these features are used to describe bonding in potential Ng compounds. The two conditions for covalent bonding can be applied for each combination of Ng and X. If NgX is calculated to be a potential energy minimum, then the sufficient condition for covalent bonding is utilized to distinguish between van der Waals or electrostatic complexes and chemically bonded molecules NgX.

3.4 The Laplacian of the Electron Density Distribution

The analysis of ρ(**r**) leads to useful information about chemical bonding. Additional information on the electronic structure of Ng molecules can be gained by analyzing not only ρ(**r**) but also $\nabla^2\rho(\mathbf{r})$, the Laplacian of the electron density distribution. The Laplacian of a scalar function f indicates where this function concentrates ($\nabla^2 f < 0$) and where it is depleted ($\nabla^2 f > 0$) [33]. For f = ρ(**r**), the *Laplace concentration* $-\nabla^2\rho(\mathbf{r})$ reveals where the electrons lump together in the molecule [34].

In Fig. 2a, this is illustrated for the N atom in its ^4S ground state. Contrary to ρ(**r**), which is characterized by a maximal value at the position of the nucleus and an exponential decay in the off-nucleus direction, the Laplace concentration of N(^4S) reveals an interesting fine structure. Close to the nucleus there is a peak of high electron concentration, which is surrounded by a sphere of charge depletion. Further away from the nucleus, in the valence region, a second sphere with concentration of negative charge is found (Fig. 2a). Again, this sphere is surrounded by a sphere with (small) depletion of negative charge although this becomes only obvious in a quantitative analysis of $-\nabla^2\rho(\mathbf{r})$. It is appealing to assign the inner sphere of charge concentration to the *1s* electrons and the outer sphere to the valence electrons. Accordingly, one can speak of an inner shell and a valence shell of the Laplacian of ρ(**r**): *The distribution* $-\nabla^2\rho(\mathbf{r})$ *reflects the shell structure of the electron distribution in an atom.*

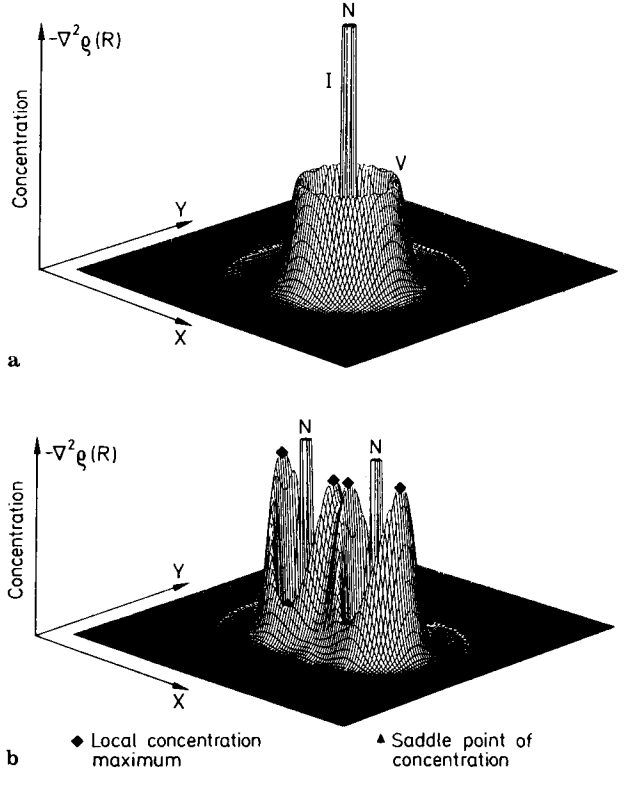

Fig. 2a and b. Perspective drawings of the Laplace concentration, $-\nabla^2\rho(\mathbf{r})$, of (**a**) the N atom in its ^4S ground state and (**b**) the N_2 molecule (HF/6-31G(*d*) calculations). Inner shell and valence shell concentrations are indicated

If two atoms bind, the shell structure of the Laplacian of $\rho(\mathbf{r})$ is deformed in a characteristic way as is shown in Fig. 2b for the N_2 molecule. Electrons lump together in the bonding and in the nonbonding regions. Again, it is very appealing to assign regions with large concentrations of $\rho(\mathbf{r})$ to electron bond and electron lone pairs. The holes in the valence concentrations, which develop when two N atoms form the N_2 molecule, may be considered as positions prone to a nucleophilic attack.

In the case of the N_2 molecule, the valence shell holes are in the direction of the π-orbitals and may be called π-holes to distinguish them from σ-holes in the σ-region. The concentration holes are located in those regions where the LUMO possesses its highest amplitudes. *The size of the hole is a measure of the acceptor ability of the corresponding molecule as is the energy of the LUMO.* Accordingly, both quantities can be used to assess the extent of donor-acceptor interactions between the noble gas element Ng and an acceptor X.

It is important to note that the Laplace concentration reflects the effects of all occupied MOs and, therefore, provides a more reliable description than the frontier MOs that often must be supplemented by the next lower (higher) orbital to the HOMO (LUMO) to reproduce experimental findings. However, it must be born in mind that the analysis of the Laplace concentration as well as the frontier orbital model are both not sufficient to distinguish between bonding and nonbonding situations and to draw a border line between electrostatic and covalent Ng,X bonding.

In Fig. 3, perspective drawings of the Laplace concentration of He, Ne, and Ar are shown. The He atom possesses a single concentration peak surrounded by a sphere of depletion of negative charge (Fig. 3a). For Ne (Fig. 3b), two concentration and two depletion spheres can be distinguished. The inner concentration sphere is at the nucleus while the outer concentration sphere is about in the valence region. Again, one can associate the inner shell with the *1s* electrons and the outer concentration shell with the valence electrons of Ne. Similarly one can speak of an inner shell depletion sphere and a valence shell depletion sphere.

For Ar (Fig. 3c), three pairs of spheres with concentration or depletion of negative charge exist in the Laplace concentration $-\nabla^2\rho(\mathbf{r})$: The most inner can be associated with the *1s* electrons of Ar; the next with the *2s2p* electrons, and the most outer with the valence electrons of Ar.

There is a direct relation between the degree of charge concentration and charge depletion in the valence shell. For example, the more electronegative an atom is, the smaller are the radii of the valence spheres and the higher is the concentration of negative charge in the valence region. With the contraction of the valence sphere the outer depletion sphere becomes more pronounced and much deeper. It seems as if negative charge residing further away from the nucleus is pulled into the valence concentration sphere to increase electron-nucleus attraction and to leave a hole surrounding the valence sphere. The extent of charge concentration and the extent of charge depletion are indeed

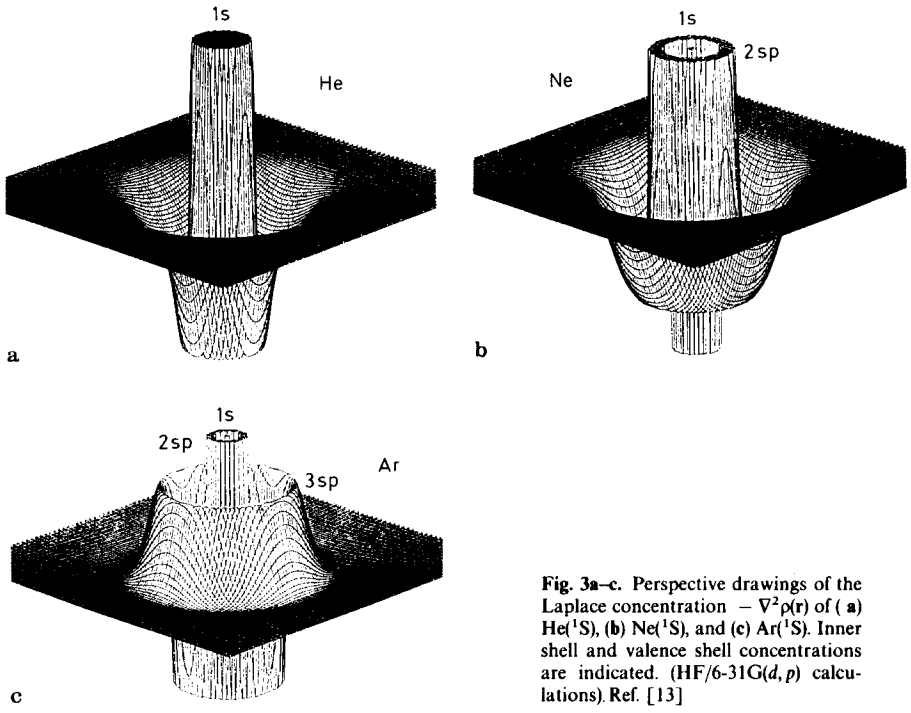

Fig. 3a–c. Perspective drawings of the Laplace concentration $-\nabla^2\rho(\mathbf{r})$ of (**a**) He(^{1}S), (**b**) Ne(^{1}S), and (**c**) Ar(^{1}S). Inner shell and valence shell concentrations are indicated. (HF/6-31G(*d*, *p*) calculations). Ref. [13]

related as becomes obvious from the local virial theorem [35]:

$$1/4\ \nabla^2\rho(\mathbf{r}) = 2G(\mathbf{r}) + V(\mathbf{r}) \tag{2}$$

which states that the kinetic energy density distribution G(r) and the potential energy density distribution V(r) add up at each point r in space to the Laplace distribution. Integration over the total space must yield the virial theorem, which says that twice the total kinetic energy T of a molecule is equal to the negative total potential energy V:

$$1/4 \int \nabla^2\rho(\mathbf{r})d\mathbf{r} = 2\int G(\mathbf{r})d\mathbf{r} + \int V(\mathbf{r})d\mathbf{r} = 2T + V = 0 \tag{3}$$

Equation (3) reveals that fluctuations in the Laplace distribution summed over all space vanish. The more negative charge is concentrated in the valence shell, the deeper is the surrounding depletion shell. This can be seen for He and Ne, where in the latter case the extension of the valence shell from two *2s* electrons to additional six *2p* electrons has a distinct effect on both the value of charge concentration and charge depletion in the valence shell.

For Ar, the *2sp* shell shields to some extent the nucleus. As a consequence, the *3sp* valence shell is less contracted as can be seen from the Laplace

concentration shown in Fig. 3c. Also, the outer depletion sphere is rather shallow and less pronounced as that of Ne in accordance with the lower electronegativity of Ar (Table 1). *He and Ne are more related than Ne and Ar since the former atoms both possess deep valence shell depletion spheres while Ar does not.*

Formation of a bond leads to a distortion of both the valence shell concentration and the valence shell depletion sphere. In the direction of the bond, depletion of negative charge is reduced while in other directions depletion may become larger. For He and Ar, these effects are so pronounced that there can be even charge concentration in the interatomic region between Ng and its next neighbor. For Ne, however, charge concentration along a bond does not overcompensate atomic depletion in the outer valence sphere. Charge concentration in the bond region can be even impeded by electron repulsion. Ne possesses $4p\pi$ electrons in linear structures, which cause destabilizing electron interactions if a potential binding partner also possesses $p\pi$ electrons. This has to be born in mind when analyzing the electronic structure of Ng compounds.

4 Diatomic Ions of Helium, Neon and Argon

The chemistry of all noble gas elements Ng is characterized by the fact that, in a molecule, Ng can only donate electrons [192], and a binding partner must be capable of withdrawing electrons from Ng forming partially or completely charged Ng^+. Thus, a suitable binding fragment X in NgX should either be strongly oxidizing, i.e. having a high electron affinity, or it should be a strong Lewis acid, i.e. it should have an energetically low-lying unoccupied orbital (LUMO). Until 1962, no neutral species X was known which had a sufficiently high attracting power to bind the noble gases chemically. However, molecular ions containing noble gas elements have been observed as early as 1925 when Hogness and Lunn [3] attributed a peak found in a mass spectrometer at m/e = 5 to the helium hydride ion HeH^+. Thus, we will begin our discussion of light noble gas compounds with cations.

4.1 Noble Gas Ions $NgNg^{n+}$

The first observation of He_2^+, Ne_2^+ and Ar_2^+ was made in 1936 by Tüxen [36], using a mass spectrometer. The formation of Ng_2^+ (Ng = He, Ne, Ar, Kr, Xe) produced by electron impact at 10^{-4} to 10^{-2} mm Hg in a mass spectrometer was later studied by Hornbeck and Molnar in 1951 [37]. It was suggested by Inghram in 1953 [38] that all possible diatomic cross-ions of the noble gas atoms and their isotopes are formed from appropriate mixtures in a mass spectrometer, and most of them have been observed spectroscopically.

Table 2 exhibits the dissociation energies of $NgNg^+$ ions in their ground states. The trends in the bond strengths of heteroatomic ions $NgNg^+$ can be explained by frontier-orbital interaction [39] between the highest occupied orbital (HOMO) of neutral Ng and the lowest unoccupied orbital (LUMO) of Ng^+. For example, in the series $HeNg^+$, which dissociates into $He + Ng^+$, the energy level of the LUMO of Ng^+ increases with atomic size and therefore, orbital interaction decreases because the HOMO–LUMO energy difference becomes larger [39]. Consequently, the dissociation energies for $HeNg^+$ show the order He > Ne > Ar > Kr.

For the $XeNg^+$ ions in their electronic ground states, which dissociate into $Xe^+ + Ng$, the order for the binding energy is Ne < Ar < Kr < Xe because the energy level of the HOMO of Ng increases, which causes smaller HOMO–LUMO differences and thus larger orbital interaction. $HeXe^+$ is the only cation in this series for which no experimental D_0 value for dissociation of the ground state is available. In a mass spectrometric study of homonuclear and heteronuclear noble gas molecular ions, Munson et al. [40] were able to obtain appearance potentials for all species except $HeXe^+$, although a signal for the ion was observed. The intensity of $HeXe^+$ was too low to estimate its dissociation energy. From the data in Table 2 it can be concluded that $HeXe^+$ is the weakest bound $NgNg^+$ ion with $D_0 < 0.6$ kcal/mol. The donor-acceptor model also explains the results of scattering experiments by Weise and Mittmann [41] for elastic scatttering of He^+ on Ne, Ar, Kr and Xe. The potential depths correspond to excited states of $NeNg^+$ and show the order $HeNe^+$ (1.2 kcal/mol) < $HeAr^+$ (4.4 kcal/mol) < $HeKr^+$ (5.1 kcal/mol) < $HeXe^+$ (6.5 kcal/mol). This is because the donor ability of Ng increases with atomic size.

The decrease in binding energies for the homoatomic dimers Ng_2^+ with He > Ne > Ar > Kr > Xe is not so simple to explain. At first approximation, the donor strength of Ng increases with atomic size as the acceptor strength of Ng^+ becomes weaker, thus cancelling each other. The difference in the dissociation energy between He_2^+ and Ne_2^+ is clearly larger than for the following diatomics. The relation in the number of electrons in bonding valence orbitals (2) at antibonding electrons (1) is the highest for He_2^+ but is lower (8 to 7) for the

Table 2. Dissociation energies[a] D_0 of diatomic noble gas cations $NgNg^+$ (in kcal/mol)

	He	Ne	Ar	Kr	Xe
He	54.5[a]				
Ne	15.9[b]	31.3[d]			
Ar	1.1[c]	1.8[e]	29.2[f]		
Kr	0.6[j]	1.3[e]	12.2[g]	26.5[h]	
Xe		0.9[e]	4.1[g]	8.9[g]	23.7[i]

[a] Ref. 45; [b] Ref. 172; [c] Ref. 173, slightly lower values have been reported in Refs. 174 and 56; [d] Ref. 175; [e] Ref. 176; [f] Ref. 177; [g] Ref. 178; [h] Ref. 179; [i] Ref. 180; [j] Ref. 181

heavier Ng_2^+ ions. Wadt [42] calculated that the decrease in well depth from Ar_2^+ to Kr_2^+ and Xe_2^+ is mainly because of spin-orbit effects. He_2^+ is clearly the strongest bound diatomic noble gas ion $NgNg^+$.

The dihelium cation He_2^+ is of particular interest not only because of its high binding energy, but possibly also for interstellar chemistry. It has been speculated that He_2^+ may exist in the atmospheres of helium-rich stars and in ionized nebulae in sufficient quantities to affect the chemistry of those objects [43]. An important step toward the identification of this ion in outer space has recently been made by the first report of the vibration-rotation spectrum of the isotope $^3He^4He^+$ by Yu and Wing [44].

It is illuminating to compare the bond strength of $NgNg^+$ with isoelectronic non-noble gas ions. Very similar D_o values are found when the homonuclear cations Ng_2^+ are compared with isoelectronic X_2^-, especially for halogen anions. There are nearly identical D_o values for F_2^- (29.5 kcal/mol) and Ne_2^+ (31.3 kcal/mol), Cl_2^- (29.0 kcal/mol) and Ar_2^+ (29.2 kcal/mol), Br_2^- (26.5 kcal/mol) and Kr_2^+ (26.5 kcal/mol), and J_2^- (24.0 kcal/mol) and Xe_2^+ (23.7 kcal/mol) [45]. H_2 does not form a stable molecular anion in the gas phase, but taken the D_o value for H_2 (103.2 kcal/mol [45]) and the electron affinity of H atom (17.4 kcal/mol [46]), a dissociation energy of 85.8 kcal/mol can be deduced for hypothetical H_2^-. This is much larger than D_o of F_2^- which agrees with $D_o(He_2^+) \gg D_o(Ne_2^+)$. Isoelectronic reasoning is not valid for the comparison of heteronuclear ions $HeNg^+$ with HX^- because HX^- dissociates into halogen anions $X^- + H$, whereas the fragmentation products of $HeNg^+$ are $He + Ng^+$. For example, HF^- has a purely repulsive ground state curve which dissociates into $H + F^-$ [47].

The difference between unbound Ng_2 and bound Ng_2^+ in the ground state is readily explained by the removal of one electron from the highest lying, strongly antibonding (σ) orbital of the neutral molecule. What happens when two (or more) electrons are taken off? Orbital interactions in Ng_2^{2+} should be even more attractive than in Ng_2^+. However, doubly charged cations encounter Coulomb repulsion which favors dissociation into two singly charged cations. Both forces act in opposite direction which makes the bonding situation for multiply charged cations more complicate than for singly charged species. For the most simple case involving noble gas atoms, i.e. He_2^{2+}, Pauling predicted as early as 1933 [48] on the basis of quantum chemical arguments that He_2^{2+} should be an observable molecule. Only recently has this been proven experimentally by charge-stripping mass spectrometry [49].

Bonding in doubly charged cations XY^{2+} may qualitatively be discussed [4, 50, 51] in the following way which is based on Pauling's investigation of He_2^{2+} [48]. The interactions between cations X^+ and Y^+ are mainly determined by repulsive Coulomb forces which exhibit a $1/r$ curve as shown in Figs. 4a–d. In contrast, the potential energy curve between X^{2+} and Y (and $X + Y^{2+}$) will show a minimum caused by attractive interactions. If mixing of the two states is symmetry allowed, there will be an avoided crossing. Depending on the nature of X and Y, four different cases can qualitatively be distinguished. Figure 4a

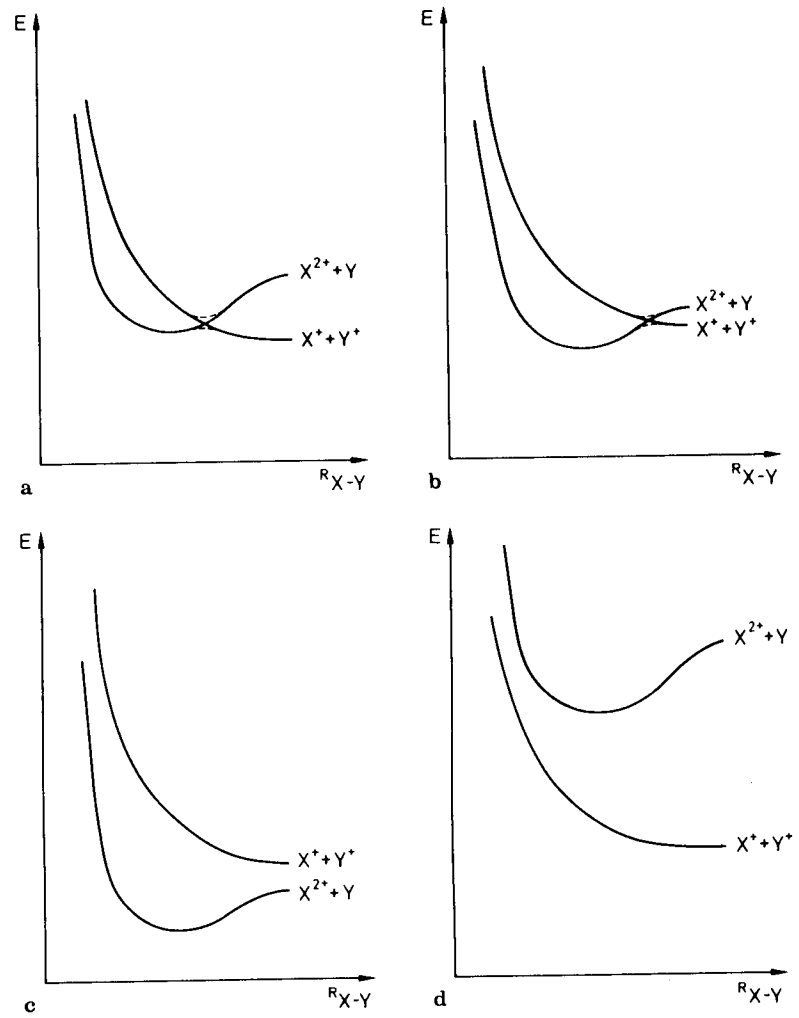

Fig. 4a–d. Schematic representation of the potential energy curves for molecules XY^{2+} dissociating into $X^+ + Y^+$ and $X^{2+} + Y$. (**a**) The dissociation products $X^+ + Y^+$ are lower in energy than $X^{2+} + Y$ and the XY^{2+} minimum energy is higher than $X^+ + Y^+$. XY^{2+} is thermodynamically unstable. (**b**) The same as (a), but the energy difference of the dissociation products is smaller, and the XY^{2+} minimum energy is lower than $X^+ + Y^+$. XY^{2+} is thermodynamically stable. (**c**) The energy of $X^+ + Y^+$ is higher than $X^{2+} + Y$, XY^{2+} is thermodynamically stable. (**d**) The energy of $X^+ + Y^+$ is much lower than $X^{2+} + Y$, XY^{2+} does not form a minimum energy structure. Ref. [4]

shows the situation when $X^+ + Y^+$ are lower in energy than $X^{2+} + Y$ (and $X + Y^{2+}$, only one possibility is shown for simplicity). The energy difference between the two dissociation limits is small enough to allow sufficiently high interactions of the two states which yields a minimum in the ground-state curve,

but higher in energy than the dissociation limit. The resulting XY^{2+} species is metastable, i.e. the dissociation is exothermic, but XY^{2+} may be observed if the barrier is high enough. Figure 4b depicts the situation when the energy difference between the dissociation limits is smaller, thus allowing stronger interactions so that the potential energy minimum is lower than the dissociation products. Now XY^{2+} is thermodynamically stable although Coulomb repulsion is released in the charge separation reaction. In Fig. 4c the relative stabilities of the dissociation products are reversed, $X^{2+}+Y$ is lower in energy than $X^{+}+Y^{+}$, and the ground state potential energy curve is completely determined by the interactions of the former product. Finally, Fig. 4d shows the situation where the two curves are too far apart in energy to interact significantly. In this case, XY^{2+} is not observable as a ground state species.

It follows from the above that the well depth of the ground state potential energy curve for XY^{2+} is mainly determined by (i) the strength of the interactions between $X^{2+}+Y$ and (ii) the mixing of the two curves, which depends on the energy difference between the dissociation limits. The curves shown in Figs. 4a–d are, of course, idealized cases. However, it will be seen that they are well-suited to understand experimental and theoretical results of doubly charged cations not only for diatomics. He_2^{2+} is an example for the case shown in Fig. 4a. The energy difference between the two curves at the dissociation limits ($He^{+}(^2S)+He^{+}(^2S)$ and $He(^1S)+He^{2+}$) is 29.829 eV ($I_2(He)-I_1(He)$, see Table 1). Bonding in ($X^1\Sigma_g^+$) He_2^{2+} is quite strong: high-level ab initio calculations [52] predict an interatomic He,He distance of only 0.704 Å, which is even shorter than in He_2^+ (1.018 Å [45]). The barrier for dissociation is calculated as 37.3 kcal/mol, although the dissociation reaction is strongly exoenergetic by 199.6 kcal/mol [52a]. In the case of ($^1\Sigma^+$) $HeNe^{2+}$, the energy difference between the two dissociation limits ($He^{+}(^2S)+Ne^{+}(^2P)$ and $He(^1S)+Ne^{2+}(^1D)$) is 19.579 eV [55]. Theoretical studies predict only a shoulder [53] or an extremely low (< 0.1 kcal/mol) minimum [54] for the $^1\Sigma^+$ ground state curve of $HeNe^{2+}$. Although the two curves are closer in energy than for He_2^{2+}, the mixing does not yield a genuine minimum in the ground state curve because Ne^{2+} is a weaker Lewis acid than He^{2+}. In the case of ($^1\Sigma^+$) $HeAr^{2+}$, the two curves are very close in energy, the dissociation limits ($He^{+}(^2S)+Ar^{+}(^2P)$ and $He(^1S)+Ar^{2+}(^1D)$) are only 4.779 eV apart [55]. Although the interactions between Ar^{2+} and He are even weaker than between Ne^{2+} and He, the much smaller energy difference of the two curves yields strong mixing [56]. Consequently, a rather deep well depth of 45.7 kcal/mol at $r_e = 1.43$ Å is theoretically predicted [57]. Clearly, the $(1)^1\Sigma^+$ state of $HeAr^{2+}$ should be experimentally observable, but not $(1)^1\Sigma^+$ $HeNe^{2+}$.

The ionization energies shown in Table 1 indicate that I_2 of Kr and Xe are lower than I_1 of He. This means that $HeKr^{2+}$ and $HeXe^{2+}$ are examples for the situation shown in Fig. 4c, and they are predicted to be thermodynamically stable. There are no theoretical studies reported for the two dications. Experimental attempts to observe $HeKr^{2+}$ and $HeXe^{2+}$ by double ionization of the respective neutral van der Waals dimers in a mass spectrometer were hampered

by the overlap of their mass spectra with those of the much more abundant Xe^{2+} and Kr^{2+} atomic ions [58]. However, in the same experiments done by Helm and coworkers, doubly charged $NeXe^{2+}$ and $ArXe^{2+}$ [58] and also $NeKr^{2+}$ [59] were identified. In the context of the binding model, $NeXe^{2+}$ is an example of the case shown in Fig. 4c, and $ArXe^{2+}$ and $ArKr^{2+}$ are examples for Fig. 4a.

It is tempting to use isoelectronic arguments to discuss the stability of the noble gas dications. The rather strong bond in He_2^{2+} is often compared with H_2. However, the analogy fails for the heteroatomic species, similar as in case of the singly charged species. He_2^{2+}, $HeNe^{2+}$ and $HeAr^{2+}$ are isoelectronic with H_2, HF and HCl, respectively. The bond strengths of the three neutral molecules (H_2: 104.1 kcal/mol; HF: 136.2 kcal/mol; HCl: 103.1 kcal/mol [45]) do not correlate with the stabilities of the isoelectronic noble gas dications, especially not in case of $HeNe^{2+}$/HF. A systematic comparison of isoelectronic hydrogen and helium (+) compounds has shown the limits of this approach [50].

4.2 *Noble Gas Hydride Ions NgH^{n+}*

The noble gas hydride ions NgH^+ are rather stable species which have been observed and extensively studied by means of mass spectroscopic techniques [60]. The proton affinities shown in Table 3 increase regularly with the sequence He < Ne < Ar < Kr < Xe indicating stronger binding for the heavier noble gases. This can be explained by the increase in donor ability (Lewis basicity) of Ng in the same order. The two-electron system HeH^+ was subject to a quantum mechanical treatment as early as 1936 by Beach [61] when he calculated the potential well depth as 46.6 kcal/mol, which is in excellent agreement with the experimentally derived value for $D_e = 46.1$ kcal/mol [62]. A more sophisticated calculation of the James-Coolidge type by Kołos and Peek using an 83-term function [63] predicts a dissociation energy $D_e = 47.0$ kcal/mol. Very high quality calculations for NeH^+, ArH^+, KrH^+ and XeH^+ have also been made, most notably by Rosmus [64]. The high-resolution vibration-rotation spectra of HeH^+ [65], NeH^+ [66–68], ArH^+ [67, 69] and KrH^+ [70] have been reported. Generally, the NgH^+ cations are well-understood diatomic systems.

In the same theoretical paper by Beach [61], the one-electron system HeH^{2+} was also calculated and it was predicted to have a purely repulsive potential energy curve for the $^2\Sigma^+$ ground state. The same result was found in more recent

Table 3. Proton affinities[a] $(PA)_e$ of noble gas atoms (in kcal/mol)

	He	Ne	Ar	Kr	Xe
$(PA)_e$	46.1	52.1	96.1	106.0	133.4

[a] From Ref. 45

calculations of HeH^{2+} [71]. Also for NeH^{2+} [72], the ($^2\Pi$) electronic ground state is theoretically predicted to be repulsive. The two energetically lowest lying $^2\Pi$ states, which dissociate into $Ne^+(^2P)+H^+$ and $Ne^{2+}(^3P)+H(^2S)$, respectively, apparently do not mix strongly enough to yield a minimum in the ground state curve [72]. The energy difference of the two curves become smaller for the heavier noble gases. For ArH^{2+}, the lowest lying $^2\Pi$ state has a shoulder or a very shallow minimum [73] which, however, is not sufficiently deep to make experimental detection feasible. It seems possible that KrH^{2+} and XeH^{2+} exhibit a minimum in the ground state potential energy curve, which makes them potentially observable as metastable species. There are no theoretical or experimental studies reported on KrH^{2+} and XeH^{2+}.

4.3 Noble Gas Ions NgX^{n+} with First-Row Elements X = Li–Ne

The comparative study of the strength of the interactions of helium, neon, and argon atoms with first row atomic ions Li^+ to Ne^+ is an excellent probe to elucidate the principle of bonding between the light noble gases in other elements. For only a few NgX^+ cations have experimentally determined dissociation energies been reported, mainly for Ng = argon, but theoretical results are available for all 24 different species. Also for dications NgX^{2+}, some experimental and theoretical data are reported. Most experimental data for NgX^+ result from atomic scattering experiments which will not be discussed in detail. Very often, the experimental studies were carried out together with theoretical calculations of the potential energy curves, and there is generally good agreement between theory and experiment concerning the dissociation energies of NgX^+ cations.

Atomic scattering results show weak attractive interactions between Li^+ and the light noble gas elements. The reported data for the potential wells are 1.1–1.6 kcal/mol for $HeLi^+$ [74], 2.6 kcal/mol for $NeLi^+$ [74c] and 7.0–7.2 kcal/mol for $ArLi^+$ [103c, 75]. For other NgX^+ systems, experimental data are available only for argon ions (except for $HeNe^+$ and $NeNe^+$ which have already been discussed). $ArBe^+$ has a dissociation energy $D_e = 12.9 \pm 0.15$ kcal/mol [76]. For the $X^1\Sigma^+$ ground state of ArB^+, the D_e value is given as 6.9 kcal/mol and for the $^3\Pi$ excited state, it is 34.6 kcal/mol [77]. The ground states of $ArC^+(X^2\Pi)$, $ArN^+(X^3\Sigma^-)$ and $ArO^+(^4\Sigma^-)$ are bound with D_e values of 21.6 kcal/mol [78], 53.0 kcal/mol [79], and 15.7 kcal/mol [80], respectively. The reported data indicate that there is no systematic increase in binding energies for ArX^+ cations along the first-row elements. For ArF^+, the bond energy has been established experimentally as $D_o > 38.1$ kcal/mol [81].

There are numerous theoretical studies reported for diatomic cations NgX^+ for He, Ne or Ar and first-row atoms X, but only few of them address the comparison of bond strengths and trends in dissociation energies for various X. Perhaps the first attempt was made by Liebman and Allen [82], who reported

ab initio calculations at the Hartree-Fock level for several helium, neon and argon diatomic cations in ground and excited states with boron, nitrogen, oxygen and fluorine. Later Cooper and Wilson [83] performed Hartree-Fock calculations for HeC^+, HeN^+ and HeO^+ as well as higher charged cations. They found that the doubly-charged ions HeX^{2+} are more strongly bound than their singly-charged counterparts. From their data, they concluded that the various trends in stability can be understood in terms of the effective nuclear charges of the two centers which show the order $HeO^{n+} > HeN^{n+} > HeC^{n+}$ [83]. Very recently, Frenking et al. made a complete "first-row sweep" of HeX^{n+} (n = 1, 2) [4], NeX^+ and ArX^+ [5] reporting ab initio calculations including correlation energy for the ground and selected excited states. Their theoretical data agree very well with experimentally observed binding energies and other high-level calculations and will be used to discuss the trends in binding energies.

Table 4 shows the calculated dissociation energies D_e for the ground states of HeX^+, NeX^+ and ArX^+ as reported by Frenking et al. [4, 5]. With two exceptions, the NgX^+ cations dissociate into $Ng+X^+$, the exceptions being ArF^+ and $ArNe^+$ (the latter is not really an exception, because it should be considered as an NeX^+ species). In the two cases, the energetically lowest lying dissociation products are Ar and X^+ (X = F, Ne). The data in Table 4 show that for a given X there is an increase in binding energy $HeX^+ < NeX^+ < ArX^+$. $ArNe^+$ is only seemingly an exception because the dissociation limit is different than for the respective He and Ne analog. The trend is observed if the dissociation energy D_e for $ArNe^+$ into $Ar+Ne^+$ is considered (134.6 kcal/mol [5]). The increase in bond strength for He < Ne < Ar can be expected because the polarizability increases in the same order, which means stronger charge-induced dipole interactions, and also the ionization energy decreases for He < Ne < Ar, which means an increase in Lewis basis strength (donor-acceptor interactions).

More information can be gained from the trends in Ng, X^+ binding energies along the first-row atoms X = Li–Ne, which are not so trivial. The trends are

Table 4. Theoretically predicted[a] dissociation energies D_e (in kcal/mol) and equilibrium distances r_e (in Å) for the ground states of HeX^+, NeX^+ and ArX^+

	D_e			r_e		
X	He	Ne	Ar	He	Ne	Ar
Li	1.5	3.0	5.7	2.062	1.986	2.441
Be	0.3	0.9	10.9	3.132	1.856	2.045
B	0.5	1.2	5.6	2.912	2.474	2.738
C	1.1	3.0	20.6	2.406	2.077	2.059
N	4.1	9.2	48.7	1.749	1.767	1.836
O	0.8	1.2	10.0	2.473	2.273	2.292
F	1.4	3.6	49.6	2.123	1.960	1.637
Ne	10.4	29.8	1.8	1.406	1.717	2.410

[a] Refs. 4 and 5

nearly the same for the three noble gases He, Ne and Ar. For HeX^+ and NeX^+, there is a decrease in D_e from X = Li to Be, but an increase for ArX^+. The three systems show a regular increase in binding energy from X = boron to carbon and nitrogen. The calculated binding energies for HeN^+ and NeN^+ are the highest in the two series, and the dissociation energy for ArN^+ is only slightly smaller than the highest value in the ArX^+ series, i.e. ArF^+. For the three cases, the D_e value is significantly smaller for NgO^+ than for NgN^+. There is a regular increase in binding energy from NgO^+ to NgF^+ and $NgNe^+$ for the helium, neon and argon contains (if for $ArNe^+$ the dissociation into $Ar+Ne^+$ is considered).

Clearly, these results do not exhibit the trends for the dissociation energies of NgX^+ cations which are expected when the effective charges at X are considered. An explanation for the irregular behavior of the dissociation energies has been given by Frenking et al. [4, 5, 50] based on the donor-acceptor model described in Sect. 3.2. Figure 5 shows schematically the valence orbitals of the first row ions X^{n+} (n = 1, 2) in the ground and selected excited state for the situation of an approaching Ng atom. In this situation, the triply degenerate *2p* AOs split into doubly degenerate $p(\pi)$ AOs and a $p(\sigma)$ orbital. Then, the dominant orbital interactions between $Ng(^1S)$ and X^+ in its ground state involve the following orbitals of X^+. For $Li^+(^1S)$ and $Be^+(^2S)$, it is the *2s* AO, which is empty in Li^+ and singly occupied in Be^+. This orbital is lower in energy in Be^+ than in Li^+ invoking stronger interactions. However, HOMO–LUMO interactions with singly occupied orbitals are weaker than with empty orbitals, and they may even be repulsive when the HOMO–LUMO overlap is very small [84].

In the case of He and Ne, the binding energy is weaker with Be^+ than with Li^+. For Ar, the interactions with Be^+ are stronger than with Li^+ because argon is a better donor and the HOMO–LUMO overlap becomes larger. In case of $B^+(^1S)$, $C^+(^2P)$ and $N^+(^3P)$, the dominant orbital interaction with Ng involves the empty $p(\sigma)$ AO. Because the energy of the orbital decreases with increasing nuclear charge, there is a regular increase in dissociation energy D_e for the three series of NgX^+ cations with B < C < N. As noted above, there is a substantial decrease in ground state binding energy in all three cases from NgN^+ to NgO^+ (Table 4). Figure 5 shows that the $p(\sigma)$ AO, which is empty in $N^+(^3P)$, is singly occupied in the ground state of $O^+(^4S)$, causing a significant decrease in stabilizing interaction with the HOMO of Ng. The ground states of O^+, F^+ and Ne^+ all have a singly occupied $p(\sigma)$ AO as lowest lying orbital, which can interact favorably with the HOMO of Ng. Consequently, there is a regular trend for the three NgX^+ series in dissociation energies O < F < Ne (see above for the apparent anomaly of $ArNe^+$). However, the result for ArF^+ differs from that of NeF^+ and HeF^+ in that the ground state of ArF^+ has $^1\Sigma^+$ symmetry. ($X^1\Sigma^+$) ArF^+ is not the product of $Ar(^1S)+F^+(^3P)$, but rather dissociates into $Ar^+(^2P)+F(^2P)$.

Argon is the lightest noble gas for which there is still an element besides the noble gases, i.e. fluorine, that has a higher ionization energy (17.422 ev [85]).

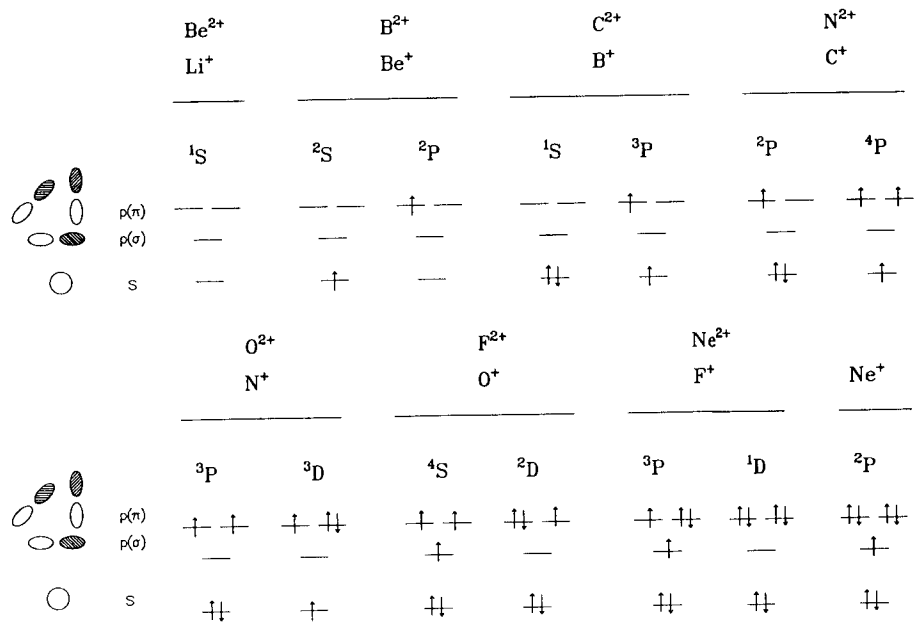

Fig. 5. Schematic representation of the valence atomic orbitals of first-row atomic ions in the ground and selected excited states shown for the situation of an approaching Ng atom. Ref. [4]

This peculiarity is the reason that ArF^+ salts were suggested early [86, 87] as the best candidates for isolating neutral argon compounds. This has been supported by more recent, accurate calculations of the Ar, F^+ bond energy and by estimating the stabilization energies of suitable salt compounds, for which SbF_6^- is suggested as the best candidate counter anion [6]. However, the systematic comparison of NgX^+ cations shows that ArN^+ as the strongest bound cation of the "normal" dissociating species is nearly as strongly bound in its ground state as ArF^+.

Associated HeN^+ was experimentally observed by Jonkman and Michl [88] in cluster ions $(HeN)^+(N_2)_n$ (which may have been $(HeN_3)^+(N_2)$) via secondary ion mass spectrometry. In the same paper, the observation of ArN^+, ArN_2^+ and ArN_4^+ was reported [88].

The orbital model discussed above not only provides a rationale for the trends in dissociation energies found for the NgX^+ ground states, it also explains the often dramatic increase in bond strengths and shortening in the bond lengths for some excited states. Figure 5 exhibits several excited states of X^+ where one electron is excited from the HOMO of the X^+ ground state. For example, the *2s* AO is doubly occupied in the ^1S ground state of B^+, but it is half empty in the ^3P excited state which allows stronger HOMO–LUMO interactions. In agreement with this, the corresponding $^3\Pi$ state of NgB^+ is stronger

bound for Ng = He [4], Ne and Ar [5]. For all excited states of X^+ shown in Fig. 5, the corresponding state of NgX^+ has a shorter interatomic distance and higher dissociation energy than the ground state [4, 5].

The same reasoning has also successfully been applied to HeX^{2+} dications [4]. Here, the binding interactions are between He and X^{2+}. Depending on the second ionization energy of X, dissociation of HeX^{2+} will yield either X^{2+} or X^+, besides He and He^+, respectively. The calculated dissociation energies D_e and the interaction energies IA between He and X^{2+} are shown in Table 5. There are two first-row elements, beryllium and carbon, which have a second ionization energy lower than I_1 of He (18.211 eV for Be, 24.383 eV for C; [85]). Consequently, $HeBe^{2+}$ and HeC^{2+} are energetically stable in their ground states with dissociation energies D_e of 21.1 and 17.7 kcal/mol, respectively [4]. $HeBe^{2+}(X^1\Sigma^+)$ and $HeC^{2+}(X^1\Sigma^+)$ are examples of the case shown in Fig. 4c. Boron has a slightly higher I_2 (25.154 eV, [85]) than I_1 of helium. The interaction energy of B^{2+} with He is sufficiently strong to yield a minimum in the $^2\Sigma^+$ ground state potential energy curve that is lower than the dissociation limit $He^+(^2S) + B^+(^1S)$. $HeB^{2+}(X^2\Sigma^+)$ is energetically stable by 16.6 kcal/mol [4] and represents a case as shown in Fig. 4b. HeN^{2+} $(X^1\Pi)$ and HeO^{2+} $(X^3\Sigma^-)$ are predicted to be unstable, but have a minimum in the ground state curve as schematically shown in Fig. 4a. $HeLi^{2+}(X^2\Sigma^+)$, $HeF^{2+}(X^4\Sigma^-)$, and $HeNe^{2+}$ $(X^3\Pi)$ are calculated with purely repulsive ground state curves; these systems are examples for Fig. 4d. Like the singly charged HeX^+ cations, bound HeX^{2+} dications exhibit significantly shorter interatomic distances and higher interaction energies IA (which are in case of HeX^+ identical with dissociation energies D_e) in the calculated excited states than in the ground states (Table 5). The calculated trends in HeX^{2+} from X = Li to Ne and the differences between

Table 5. Calculated dissociation energies D_e (in kcal/mol), interaction energies IA between He and X^{2+} (in kcal/mol) and equilibrium distances r_e (in Å) of HeX^{2+} dications[a]

Struct.	Symm.	D_e	IA	r_e
$HeLi^{2+}$	$X^2\Sigma^+$			Diss.
$HeBe^{2+}$	$X^1\Sigma^+$	+ 20.1	+ 20.1	1.453
HeB^{2+}	$X^2\Sigma^+$	+ 16.6	+ 26.8	1.339
	$^2\Pi$	+ 18.6	+ 64.5	1.191
HeC^{2+}	$X^1\Sigma^+$	+ 17.7	+ 17.7	1.575
	$^3\Pi$	− 74.2	+ 63.0	1.167
HeN^{2+}	$X^2\Pi$	− 71.1	+ 45.4	1.321
	$^4\Sigma^-$	− 151.4	+ 122.7	1.060
HeO^{2+}	$X^3\Sigma^-$	− 151.4	+ 93.6	1.164
	$^3\Pi$	− 288.2	+ 223.3	1.003
HeF^{2+}	$X^4\Sigma^-$	—	—	Diss.
	$^2\Pi$	− 197.3	+ 135.4	1.044
$HeNe^{2+}$	$X^3\Pi$	—	—	Diss.
	$^1\Sigma^+$	− 214.1	+ 235.3	1.025

[a] Taken from Ref. 4

ground and excited states have been explained using frontier orbital interactions between He and X^{2+} in the same manner as the HeX^+ species [4].

Experimental information concerning the stability of noble gas first row dications NgX^{2+} is very scarce. No data are available for HeX^{2+} species. Very recently, Jonathan et al. [89] reported results of charge-stripping mass spectrometry for several diatomic dications containing one inert gas atom. Using the singly charged cations NgX^+ with Ng = Ne, Ar, Kr, Xe, and X = C, N, O, the doubly charged species NeN^{2+}, ArN^{2+}, ArO^{2+}, KrO^{2+}, XeC^{2+}, XeN^{2+} and XeO^{2+} were observed in the charge-stripping experiments. The NgN^{2+} cations seemed to be the most stable and NgC^{2+} the least stable species [89]. A possible explanation for the failure to detect NeC^{2+} and NeO^{2+}, while NeN^{2+} had been observed, was later given by Frenking and Koch [21]. The explanation is based on the stabilities of the precursor ions NeX^+ which show the trend N > C > O, as shown above. However, the observed species were not always in their electronic ground states. From the translational energy release measured in the unimolecular dissociation reactions it was concluded that in some cases, for example ArO^{2+} and KrO^{2+}, the observed cations correspond to excited states and not to the electronic ground states [89].

Detailed information on the stabilities of some NgX^{2+} dications with first-row elements X are available from theoretical studies, but many systems have not been studied yet. Besides the comparative study of Frenking et al. [4] which covers a complete first-row sweep for HeX^{2+} dications, ab initio calculations are reported for only a few NgX^{2+} systems. Results for $HeBe^{2+}$ are available from several studies [90] which give similar values for the dissociation energy as noted above (18.9 kcal/mol). $NeBe^{2+}$ has been calculated together with $HeBe^{2+}$ by Hayes and Gole [90a] and it was predicted that the ground state of $NeBe^{2+}$ is 5.4 kcal/mol less bound than $HeBe^{2+}$. Like for helium, I_1 of Ne is higher than I_2 of beryllium. Thus, $NeBe^{2+}(X^1\Sigma^+)$ dissociates into $Ne(^1S) + Be^{2+}(^1S)$. The greater stability of $HeBe^{2+}$ over $NeBe^{2+}$ was explained by the assumption that the binding energy in the dications be mainly due to charge induced dipole interactions between Ng and Be^{2+} which follows r_e^{-4}. This result does not agree with the donor-acceptor model used by Frenking et al. for noble gas compounds [4, 5, 7, 21, 50]. Neon is a better donor than helium and HOMO–LUMO interactions with Be^{2+} should therefore be stronger in $NeBe^{2+}$. A recent high-level ab initio calculation shows that the dissociation energy D_0 for $NeBe^{2+}$ is 35.3 kcal/mol, considerably higher than $HeBe^{2+}$ which is calculated at the same level of theory with a D_0 value of 17.2 kcal/mol [90d].

For HeC^{2+}, Hartree-Fock SCF calculations were reported for the $X^1\Sigma^+$ ground state by Harrison et al. [91] and by Cooper and Wilson [83] who also calculated HeN^{2+} and HeO^{2+}. The potential energy curves of the low-lying electronic states of HeC^{2+} [8] and NeC^{2+} [9] were calculated by Koch et al. using a complete active space SCF (CASSCF) approach. From these calculations it is predicted that the $(X^1\Sigma^+)$ ground state of HeC^{2+} is thermodynamically stable with D_0 = 16.6 kcal/mol [8] while $NeC^{2+}(X^1\Sigma^+)$ has a barrier for the exothermic dissociation into $Ne^+(^2P) + C^+(^3P)$ of 37.3 kcal/mol.

NeC^{2+} dissociates as shown in Fig. 4a, while HeC^{2+} is an example for Fig. 4c. The low-lying electronic states of NeN^{2+} have been studied at the CASSCF+CI level by Koch et al. [10]. The $X^2\Pi$ ground state is predicted to be metastable with a barrier for dissociation into $Ne^+(^2P)+N^+(^3P)$ of 21.7 kcal/mol.

4.4 *Noble Gas Ions NgX^{n+} with Metal Atoms X Having Z Above 10*

Two of the eight first-row atoms, beryllium and carbon, have a second ionization energy I_2 lower than I_1 of helium. As discussed above, $HeBe^{2+}$ and HeC^{2+} are quite strongly bound. Also HeB^{2+} is thermodynamically stable, because I_2 of B is only slightly higher than I_1 of He. Looking at the ionization energies of the elements it can be recognized that there are several elements, especially metals, which have I_n values, even for n = 3, lower than I_1 of He and also I_1 of Ne. That means that triply charged ions NgX^{3+} are thermodynamically stable for many metals X if Ng is helium or neon. Table 6 shows a list of atoms which have low-lying third and fourth ionization energies. It seems conceivable that even quadruply charged ions HeX^{4+} ions might be detected.

Several HeX^{2+} and HeX^{3+} ions with X being metal atoms such as V, MO, Rh, Pt, Ir, Ta, W, Re were observed experimentally by Müller, Tsong and co-workers [92] by means of time-of-flight mass spectrometry. While no direct information about the bond strength of the highly charged molecules could be extracted from the experiments, the rather long life time, which must be longer than the typical flight time of up to 100 microseconds, indicates a substantial well depth in the potential energy curve of the observed species. However, a deep potential well does not automatically ensure a long lifetime for helium cations.

Table 6. Ionization energies I_n^a (in eV)

Element	n	I_n	Element	n	I_n
Al	2	18.828	La	3	19.175
	3	28.447	Ce	3	20.20
Sc	3	24.76	Pr	3	21.62
Ti	2	13.58	Tm	3	23.71
	3	27.491	Yb	3	25.2
V	2	14.65	Hf	3	23.3
	3	29.310		4	33.3
Y	3	20.52	Bi	2	16.69
Zr	3	22.99		3	25.56
	4	34.34	Th	3	20.0
Nb	2	14.32		4	28.8
	3	25.04			

[a] Ref. 85

By an ingenious analysis of the observed travel time of $HeRh^{2+}$ cations and the dissociation rate into $He+Rh^{2+}$, Tsong and Liou [92i] conclude that the dissociation is mainly due to tunneling of the He atom through the potential barrier. Tunneling phenomena are critically dependent on the mass of the tunneling atom and the width of the potential barrier. The small size of the helium atom makes the dissociation via tunneling an important mechanism.

Concerning the binding interactions in "metal halides" HeX^{n+}, CASSCF calculations by Hotokka et al. [93] predict D_e = 4.4 kcal/mol for dissociation of $HeTi^{2+}$ into $He+Ti^{2+}$. For the triply charged HeV^{3+}, which dissociates into $He^+ + V^{2+}$, a barrier for the dissociation is calculated at 17.2 kcal/mol [93]. Calculations were also performed for the $HeAl^{3+}$ cation. The barrier for dissociation into $He^+ + Al^{2+}$ is predicted as 27.4 kcal/mol [93]. The very high ionization energy of helium, which prohibits any "normal" chemistry for the lightest noble gas, is a favorable condition for the remarkable stability of these highly charged cations.

The possibility of binding helium in highly charged cations has also been recognized by Radom and coworkers [94, 95]. They calculated $HeSi^{n+}$ with n = 1 – 4 and found computationally [94] that the $HeSi^{4+}$ tetracation has the shortest bond (1.550 Å) of the four charged species, although the exothermicity of the dissociation into $He^+(^2S) + Si^{3+}(^2S)$ is enormous: 385.7 kcal/mol. I_4 of Si is 45.141 eV [85]. The attractive interactions are explained using molecular orbital arguments [94]. There are only two valence electrons in $HeSi^{4+}$ which occupy the 4σ bonding orbital. In $HeSi^{3+}$ and $HeSi^{2+}$, the 5σ-antibonding orbital is singly and doubly occupied, respectively. This yields longer interatomic distances especially for $HeSi^{2+}$ (2.568 Å), although $HeSi^{2+}$ is thermodynamically stable towards dissociation into $He+Si^{2+}(^1S)$, albeit only by 2 kcal/mol [94]. $HeSi^{4+}$ is an example for the situation shown in Fig. 4a, with the lower dissociation limit being He^+ and Si^{3+} and the higher limit as $He+Si^{4+}$.

4.5 *The Nature of Bonding in Diatomic Noble Gas Ions*

Figure 6 shows a contour line diagram of the electron density distribution of the van der Waals complex He_2 (He,He distance 2.74 Å). The electron density at the midpoint between the two He atoms is just 0.008 e/Å^3, quite different from the values found for a typical covalent bond between first-row elements (1–5 e/Å^3). Despite the smallness of ρ(r) in the internuclear region, the He nuclei are linked by a MED path and the midpoint is the position of a (3, – 1) critical point (Fig. 6). As pointed out above this does not imply the existence of a chemical bond. The energy density H(r) is positive at the (3, – 1) critical point, which means that the kinetic energy rather than the potential energy dominates in the internuclear region. There is no chemical bond between the He atoms.

If one electron is removed to yield He_2^+, the equilibrium distance between the two He nuclei decreases to 1.08 Å. This is caused by the contraction of the

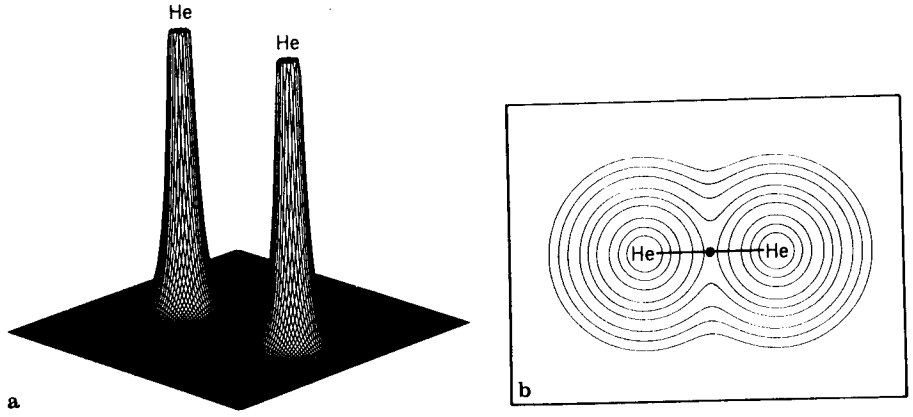

Fig. 6a and b. Perspective drawing (**a**) and contour line diagram (**b**) of the electron density distribution $\rho(\mathbf{r})$ of He_2 at its van der Waals distance (2.74 Å) shown with regard to a plane that contains the nuclei. MED path and (3, − 1) critical point are indicated in the contour line diagram. (HF/6-31G(*p*) calculations)

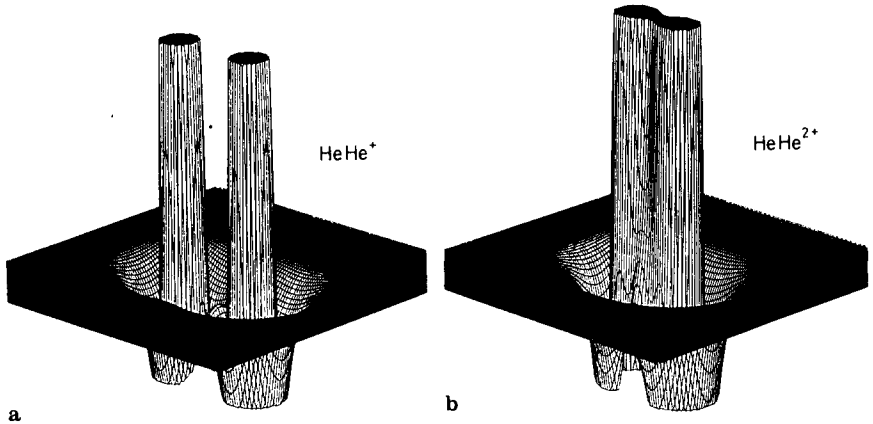

Fig. 7a and b. Perspective drawings of the Laplace concentration, $-\nabla^2\rho(\mathbf{r})$, of (**a**) He_2^+ and (**b**) He_2^{2+} ions at their equilibrium distance shown with regard to a plane containing the nuclei

orbitals due to the positive charge. Electronic charge is drawn closer to the nuclei which is reflected by the calculated Laplace concentration. The nuclei are more shielded, while at the same time repulsion between the He electrons is decreased. This leads to a reduction of the internuclear distance relative to that of the van der Waals complex He_2.

There is a MED path connecting the two nuclei of He_2^+. The electron density ρ_B at the (3, − 1) critical point, the midpoint between the two He atoms, is 1.2 e/Å^3, which is typical of a covalent bond. More convincing is the result that

the energy density H_B is negative (− 0.73 hartree/Å^3), indicating that the kinetic energy has become smaller than the potential energy in the internuclear region. A covalent bond has been formed. This description is in line with the common understanding that bonding is accompanied by a decrease in kinetic energy [18].

If a second electron is removed as in He_2^{2+}, the internuclear distance decreased to 0.70 Å for the same reasons described for He_2^+. The electron density at the (3, − 1) critical point is 4.4 e/Å^3, while the energy density H_B is − 4.4 hartree/Å^3, both indicating covalent bonding.

The Laplace concentrations of the two molecules He_2^+ and He_2^{2+} reflect these trends nicely as can be seen from Fig. 7. For the monocation, the Laplace concentration is increased in the bond region relative to that of the separated atoms, which possess in the outer valence region a sphere with depletion of negative charge. However, depletion is not totally compensated in the cation: the Laplace concentration is still negative, i.e. $-\nabla^2\rho(\mathbf{r}) < 0$. For the dication, the Laplace concentration becomes positive, i.e. $-\nabla^2\rho(\mathbf{r}) > 0$. Obviously, covalent bonding implies an increase of the Laplace concentration in the bonding region relative to the Laplace concentration of the noninteracting atoms.

Mono- and dications Ng_2^{n+} possess covalent bonds comparable to those of other homonuclear diatomics such as H_2, N_2, or F_2. This, however, is not necessarily true for cations and dications NgX^{n+} with X being different from Ng. Since the electronegativity of Ng is higher than that of X, positive charge is preferentially located at X and Ng will be polarized by the positive charge at X. Hence, Ng and X are attracted by charge-induced dipole interactions proportional to the amount of positive charge q at X and the value of the static electric dipole polarizability α of Ng. Predictions on the stability of NgX^{n+} can be made by using Eq. (4), which estimates the electrostatic interaction energy ΔE_{elec} from the known values of q, α, and the Ng, X distance r [4].

$$\Delta E_{elec} = -0.5\alpha q^2/r^4 \tag{4}$$

Whether or not the stability of NgX^{n+} is enhanced by additional covalent interactions depends on the electronic structure of X^{n+}. As mentioned above, a covalent Ng,X bond can only be achieved by donation of Ng electrons to X which implies that X must be a sufficiently strong electron acceptor. Inspection of Table 7 reveals that for the electronic ground states of HeX^+ none of the first-row elements X is capable of withdrawing electrons from He thereby establishing a covalent bond. The electron density ρ_B at the (3, − 1) critical point is extremely small, ranging from 0.01 (X = Be) to 0.09 e/Å^3 (X = F). Only $HeNe^+(X^3\Sigma^-)$ has a somewhat larger value of ρ_B (0.26 e/Å^3, Table 7). All H_B values are larger than zero, indicating electrostatic interactions rather than covalent bonds.

Nevertheless, covalent bonding between He and X^+ is possible for the monocations HeX^+. It requires a rearrangement of electrons in the valence shell of X^+ thus yielding an excited electronic state of X^+ and, subsequently, HeX^+. The electron rearrangement must be such that the electron acceptor ability of

X^+ increases. This is best achieved by creating a *s*- or *pσ*-hole in the valence shell that is prone to accept *s*-electrons from He. An *s*- or σ-hole in connection with a sufficiently large nuclear charge is the prerequisite for covalent He,X bonding (Table 7).

All excited states of HeX^+ listed in Table 7 possess a He,X bond with covalent character according to the properties of the calculated electron and energy distribution [4]. The ρ_B and H_B data in Table 7 suggest that the He,B bond is the weakest Ng, X bond, actually more electrostatic than covalent. The strongest covalent bond is found for $HeN^+(^3\Pi)$, which is in line with the frontier orbital model (Sect. 4.3) and the Laplace description of He, X interactions.

Investigation of the Laplace concentration $-\nabla^2\rho(\mathbf{r})$ of HeX^+ provides additional information. In Fig. 8, perspective drawings and contour line diagrams of $-\nabla^2\rho(\mathbf{r})$ are given for both the $X^3\Sigma^-$ ground state and the $^3\Pi$ excited state of HeN^+. The valence shell concentration of $N^+(^3P)$ is highly anisotropic. There are concentration lumps in the direction of the singly occupied $2p(\pi)$ orbitals and deep concentration holes in the direction of the unoccupied $2p(\sigma)$

Table 7. Nature of bonding in HeX^{n+} ions according to ab initio calculations[a]

HeX^{n+} (state)	Electronic structure of X^{n+}	Hole	ρ_b [eÅ^{-3}]	H_b [hartree Å^{-3}]	D_e [kcal/mol]	Nature of bonding
		Ground States of HeX^+ and HeX^{2+}				
$HeLi^+(X^1\Sigma^+)$	$1s^2$	2*s*	0.04	0.02	1.5	electrostatic
$HeBe^+(X^2\Sigma^+)$	K $2s$	2*s*	0.01	0.00_2	0.3	electrostatic
$HeB^+(X^1\Sigma^+)$	K $2s^2$	2*p*	0.02	0.01	0.5	electrostatic
$HeB^{2+}(X^2\Sigma^+)$	K $2s$	2*s*	0.57	− 0.19	26.8	covalent
$HeC^+(X^2\Pi)$	K $2s^22p$	2*p*	0.05	0.02	1.1	electrostatic
$HeC^{2+}(X^1\Sigma^+)$	K $2s^2$	2*p*	0.55	− 0.11	17.7	covalent
$HeN^+(X^3\Sigma^-)$	K $2s^22p^2$	2*p*	0.26	0.07	4.1	electrostatic
$HeN^{2+}(X^2\Pi)$	K $2s^22p$	2*p*	1.19	− 0.80	48.2	covalent
$HeO^+(X^4\Sigma^-)$	K $2s^22p^3$	2*p*	0.04	0.01	0.8	electrostatic
$HeO^{2+}(X^3\Sigma^-)$	K $2s^22p^2$	2*p*	1.96	− 1.86	98.4	covalent
$HeF^+(^3\Pi)$	K $2s^22p^4$	2*p*	0.09	0.03	1.4	electrostatic
$HeF^{2+}(^2\Pi)$	K $2s^22p^3$	2*p*	2.82	− 2.93	143.0	covalent
$HeNe^+(X^2\Pi)$	K $2s^22p^5$	2*p*	0.80	0.01	10.4	(electrostatic)
$HeNe^{2+}(X^1\Sigma^+)$	K $2s^22p^4$	2*p*	2.92	− 2.58	240.1	covalent
		Excited States of HeX^+ and HeX^{2+}				
$HeB^+(^3\Pi)$[b]	K $2s2p$	2*s*	0.34	− 0.08	5.6	(covalent)
$HeB^{2+}(^2\Pi)$	K $2p$	2*s*	0.82	− 0.16	64.5	covalent
$HeC^+(^4\Sigma^-)$[b]	K $2s2p^2$	2*s*	0.98	− 0.76	29.3	covalent
$HeC^{2+}(^3\Pi)$[b]	K $2s2p$	2*s*	1.24	− 1.39	67.0	covalent
$HeN^+(^3\Pi)$	K $2s2p^3$	2*s*	2.06	− 3.51	68.9	covalent
$HeN^{2+}(^4\Sigma^-)$	K $2s2p^2$	2*s*	2.16	− 4.06	127.9	covalent
$HeO^+(^2\Pi)$	K $2s2p^4$	2*s*	1.51	− 1.21	4.4	covalent
$HeO^{2+}(^3\Pi)$	K $2s2p^3$	2*s*	2.88	− 3.59	223.3	covalent
$HeF^+(X^1\Sigma^+)$	K $2s2p^5$	2*s*	2.63	− 2.72	47.5	covalent

[a] Values of ρ_b and H_b from HF/6-31G(*d*, *p*) calculations [4]. For HeX^{2+}, IA values are given. [b] A minimum rather than a maximum was found in a direction perpendicular to the internuclear axis indicating a poor description of $\rho(\mathbf{r})$.

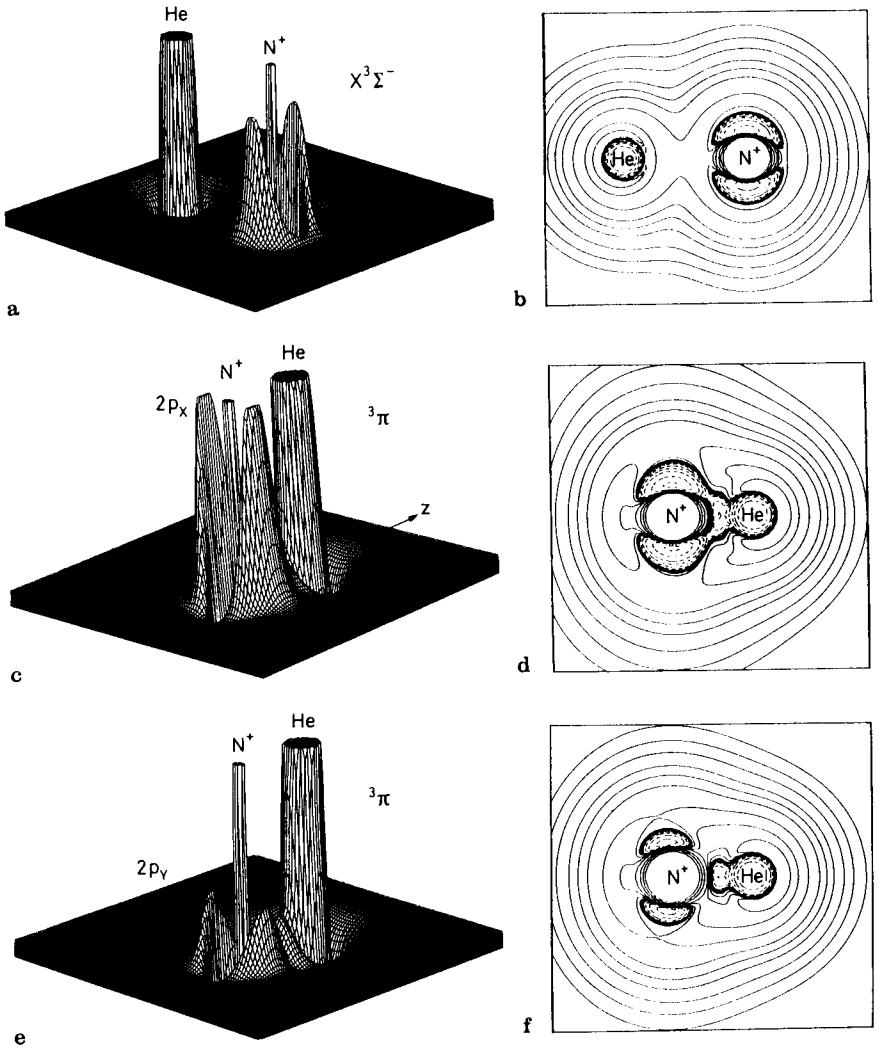

Fig. 8a–f. Perspective drawings and contour line diagrams of the Laplace concentration $-\nabla^2\rho(\mathbf{r})$ of HeN^+. Dashed contour lines are in regions of concentration of negative charge, solid contour lines in regions of charge depletion. Inner-shell concentration of N^+ is not shown in the contour line diagrams. (**a**) and (**b**) $HeN^+(X^3\Sigma^-)$ in xz-plane. (**c**) and (**d**) $HeN^+(^3\Pi)$ in xz-plane. (**e**) and (**f**) $HeN^+(^3\Pi)$ in yz-plane. (HF/6-31G(*d*, *p*) calculations). Ref. [4]

orbital. If a van der Waals complex is formed with He (Fig. 8a, b), the noble gas atom approaches $N^+(^3P)$ in the direction of the *pσ*-holes. The nucleus of N is less shielded in this direction and, accordingly, the electrons of He "feel" the attracting positive charge of the nucleus most strongly in this direction.

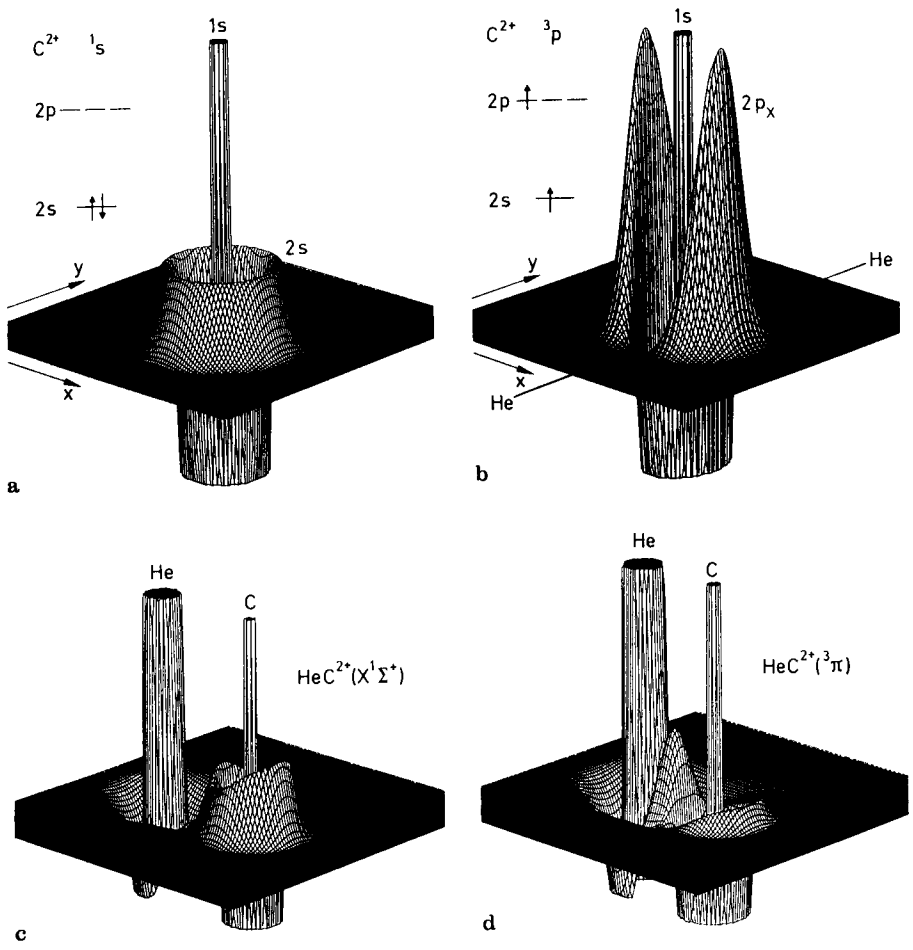

Fig. 9a–d. Perspective drawings of the Laplace concentration, $-\nabla^2\rho(\mathbf{r})$, of (**a**) $C^{2+}(^1S)$, (**b**) $C^{2+}(^3P)$, (**c**) $HeC^{2+}(X^1\Sigma^+)$, and (**d**) $HeC^{2+}(^3\Pi)$. Inner shell and valence shell concentrations are indicated

The contour line diagram in Fig. 8b reveals that the electronic structure of both He and $N^+(^3P)$ are hardly distorted in the $X^3\Sigma^-$ ground state of HeN^+. The $p\sigma$-hole slightly widens on the side of the He atom (the elliptic concentration areas are shifted slightly to the back) such as to increase stabilizing electrostatic interactions. This is in line with the description given above.

When the ground state ^3P of N^+ is excited to $N^+(^3D)$ the concentration holes in the valence shell of N^+ deepen significantly due to the transfer of a *2s* electron to a *2p* orbital. Inspection of Fig. 8c shows that the acceptor ability of N^+ is significantly enhanced. The electronic charge is concentrated in the

internuclear region of $HeN^+(^3\Pi)$ because negative charge is shifted from He to the σ-hole at $N^+(^3D)$. A semipolar bond between He and $N^+(^3D)$ is formed. In the contour line diagram of the Laplace concentration of $HeN^+(^3\Pi)$ the semipolar bond appears as a droplet like appendix of the spherical He concentration (Fig. 8d). This pattern of $-\nabla^2\rho(\mathbf{r})$ has been found to be typical of all semipolar covalent He,X bonds investigated so far [4, 7, 13].

Increase of the positive charge at atom X enhances the acceptor ability for X^{2+}. All HeX^{2+} dications are covalently bonded according to the calculated ρ_B and H_B values listed in Table 7. This holds also for X^{2+} ions with isotropical charge distribution, i.e. species without holes in the valence sphere. The Laplace concentration of $C^{2+}(^1S)$ is shown in Fig. 9a. Although isotropical, the charge concentration in the valence shell is so small that the C nucleus is insufficiently shielded and an oncoming He atom is attracted by $C^{2+}(^1S)$. A weakly covalent bond is formed (D_e = 17.9 kcal/mol) which shows up in the Laplace concentration only by distortion in the valence shell concentration of $C^{2+}(^1S)$ (Fig. 9c). The charge concentration is more pronounced along the bond axis rather than perpendicular to it.

Again, covalent bonding is much stronger when an *s*-hole is available, for example in the ^3P excited state of C^{2+} (Fig. 9b). Due to the excitation of a *2s* electron to a *2p* orbital, the carbon nucleus is deshielded in the direction of the unoccupied *2p* orbitals. There are deep concentration holes in these directions, while in the direction of the occupied *2p* orbital there are large concentration lumps. Electronic charge of He is shifted toward the concentration holes upon collision of He and $C^{2+}(^3P)$. A strong covalent semipolar bond can be formed between He and $C^{2+}(^3P)$. This is clearly reflected by the Laplace concentration of $HeC^{2+}(^3\Pi)$, the calculated ρ_B and H_B values, and the dissociation energy (Table 7). Similar descriptions can be given for the ground and excited states of other HeC^{2+} ions. Donor-acceptor interactions increase with

a) the nuclear charge,
b) the total charge of X and
c) the enlargement of the σ-holes.

Covalent semipolar bonds result if an *s*-hole is available in the valence shell of X. This is in line with the donor-acceptor description given above.

What are the differences between the helium ions HeX^{n+} and the neon and argon analogues NeX^{n+} and ArX^{n+}? This question has been answered by basically applying the same analysis as used for the HeX^{n+} ions [5]. However, a simplified energy analysis may already provide important informations. The stabilization arising from charge-induced dipole interactions can be estimated from Eq. (4) using calculated equilibrium distances and dipole polarizabilities α taken from the literature. The resulting electrostatic interaction energies ΔE_{elec} are larger than the actual electrostatic attraction, because Eq. (4) is not strictly valid at small internuclear distances [96]. Nevertheless, covalent bonding can be assumed if the calculated D_e values are significantly larger than the electrostatic attraction energy ΔE_{elec}.

In Table 8 the results of this analysis are summarized for NgX^+ ions in their electronic ground states. There are no covalent bounded HeX^+ ions, since $D_e - \Delta E_{elec}$ is in all cases negative. NeN^+ ($D_e - \Delta E_{elec} = 2.5$ kcal/mol) and ArC^+ ($D_e - \Delta E_{elec} = 5.5$ kcal/mol) are predicted as slightly covalent, ArN^+ ($D_e - \Delta E_{elec} = 25$ kcal/mol) and ArF^+ ($D_e - \Delta E_{elec} = 37$ kcal/mol) seem to be clearly covalent. All other NgX^+ ions are electrostatically bound without significant covalent contribution according to the energy criterion. These predictions are confirmed by the analysis of $\rho(\mathbf{r})$ and $H(\mathbf{r})$ (Table 9). Electrostatic interactions increase with the polarizability of Ng. Since the value of α differs not very much for He and Ne, the D_e values are comparable. But for Ar with α being five times as large as the values for Ne and He, electrostatic interactions gradually change to covalent bonding.

If the positive charge of X is increased to X^{2+}, or if X is excited to a state with pronounced *s*-holes, then the corresponding NeX^+ and Ar^+ species are covalently bound for the same reasons discussed for HeX^+. The semipolar bond between Ng and X^{n+} is formed by sharing of the two $2p\sigma$ electrons of Ne or Ar. Alternatively, two $2p\pi$ electrons of Ne or Ar could be donated to X^+. However, the acceptor ability of X with regard to π electrons is much lower. There is no π-donation by Ne or Ar towards X^+.

It is interesting to note that the $p\pi$ electrons of Ne and Ar may lead to some destabilization of NgX^{2+}. In Fig. 10, contour line diagrams and perspective drawings of $-\nabla^2\rho(\mathbf{r})$ are shown for the $^1\Sigma^+$ ground state and the $^3\Pi$ excited state of ArC^{2+} [5]. The ground state corresponds to $C^{2+}(^1S)$ which does not possess any *p* electrons; the excited state corresponds to $C^{2+}(^3P)$, which possesses a σ-hole but also a *2p* electron (compare with Fig. 9). In the ArC^{2+} states, the valence shell concentration of the Ar atom is distorted in a characteristic way. There are holes in the direction of the bond while there are concentration lumps in the nonbonding region of Ar. Distortions in the valence shell concentration of the C atom are complementary to those at the Ar atom, i.e. the concentration lumps are in the direction of the molecular axis while the holes are in the nonbonding region. The distortions are the result of a transfer of $3p\sigma$ electrons from Ar to C^{2+}, either into a *2p* (C^{2+}, ^1S) or *2s* (C^{2+}, ^3P) orbital. In the latter case, the charge transfer is more pronounced and the concentration holes at Ar are much deeper (Fig. 10c) than in the former case (Fig. 10a). Figure 10 also shows that $ArC^{2+}(^3\Pi)$ suffers from $2p\pi$, $3p\pi$ repulsion (see concentration lumps in the nonbonding regions of C and Ar in Fig. 10c) which is absent in $ArC^{2+}(^1\Sigma^+)$ (Fig. 10a). Because of the difference in $p\pi$-$p\pi$ electron repulsion, the Ng,C bond strength in the triplet states is almost four times as large than in the singlet state if Ng = He, but only twice as large for Ng = Ne, and less than twice as large for Ng = Ar. In the latter case it is also important that donation from a $3p\sigma$ orbital to a *2s* ($2p\sigma$) orbital is less efficient than from a $2p\sigma$ to a *2s* ($2p\sigma$) orbital.

Table 8. Nature of bonding in NgX^+ monocations according to Eq. (4)[a]

X	He	Ne	Ar
Li	electrostatic	electrostatic	electrostatic
Be	electrostatic	electrostatic	electrostatic
B	electrostatic	electrostatic	electrostatic
C	electrostatic	electrostatic	covalent
N	electrostatic	covalent	covalent
O	electrostatic	electrostatic	electrostatic
F	electrostatic	electrostatic	covalent
Ne	electrostatic	covalent	electrostatic

[a] Electrostatic bonding is assumed for $\Delta E^{elec} > D_e$, covalent bonding for $\Delta E^{elec} < D_e$.

Table 9. Nature of bonding in NeX^+ and ArX^+ ions according to ab initio calculations[a]

NgX^+ (state)	Electronic structure of X^+	Hole	ρ_b [eÅ^{-3}]	H_b [hartree Å^{-3}]	D_e [kcal/mol]	Nature of bonding
A. NeX^+ ions						
$NeLi^+(X^1\Sigma^+)$	$1s^2$	*2s*	0.10	0.06	2.8	electrostatic
$NeBe^+(X^2\Sigma^+)$	K $2s$	*2s*	0.16	0.04	− 0.1	electrostatic
$NeB^+(X^1\Sigma^+)$	K $2s^2$	*2p*	0.10	0.01	1.1	electrostatic
$(^3\Pi)$[b]	K $2s2p$	*2s*	0.30	− 0.10	7.3	covalent
$NeC^+(X^2\Pi)$	K $2s^22p$	*2p*	0.23	− 0.01	3.0	electrostatic
$(^4\Sigma^-)$[b]	K $2s2p^2$	*2s*	0.59	− 0.51	21.7	covalent
$NeN^+(X^3\Sigma^-)$	K $2s^22p^2$	*2p*	0.50	− 0.07	9.2	covalent
$NeO^+(X^4\Sigma^-)$	K $2s^22p^3$	*2p*	0.14	0.04	1.2	electrostatic
$(^2\Pi)$	K $2s2p^4$	*2s*	0.92	− 0.20	6.3	covalent
$NeF^+(^3\Pi)$	K $2s^22p^4$	*2p*	0.30	0.07	3.6	electrostatic
$(X^1\Sigma^+)$	K $2s^22p^5$	*2s*	1.29	− 0.34	39.8	covalent
$NeNe^+(X^2\Pi)$	K $2s^22p^5$	*2p*	0.65	0.14	29.8	(electrostatic)
B. ArX^+ ions						
$ArLi^+(X^1\Sigma^+)$	$1s^2$	*2s*	0.07	0.03	5.8	electrostatic
$ArBe^+(X^2\Sigma^+)$	K $2s$	*2s*	0.27	− 0.01	10.7	electrostatic
$ArB^+(X^1\Sigma^+)$	K $2s^2$	*2p*	0.12	0.01	5.0	electrostatic
$(^3\Pi)$	K $2s2p$	*2s*	0.61	− 0.41	35.2	covalent
$ArC^+(X^2\Pi)$	K $2s^22p$	*2p*	0.53	− 0.14	20.6	covalent
$(^4\Sigma^-)$	K $2s2p^2$	*2s*	1.15	− 1.26	56.5	covalent
$ArN^+(X^3\Sigma^-)$	K $2s^22p^2$	*2p*	0.98	− 0.49	48.7	covalent
$ArO^+(X^4\Sigma^-)$	K $2s^22p^3$	*2p*	0.30	0.05	10.0	electrostatic
$(^2\Pi)$	K $2s2p^4$	*2s*	1.53	− 1.08	50.5	covalent
$ArF^+(X^1\Sigma^+)$	K $2s^22p^5$	*2s*	1.59	− 1.02	43.2	covalent
$(^3\Pi)$	K $2s^22p^4$	*2p*	0.43	0.01	16.6	electrostatic
$ArNe^+(X^2\Pi)$	K $2s^22p^5$	*2p*	0.15	0.02	1.8	electrostatic

[a] Values of ρ_b and H_b from HF/6-31G(*d*, *p*) calculations [5]; [b] A maximum rather than a saddle point was found. [5]

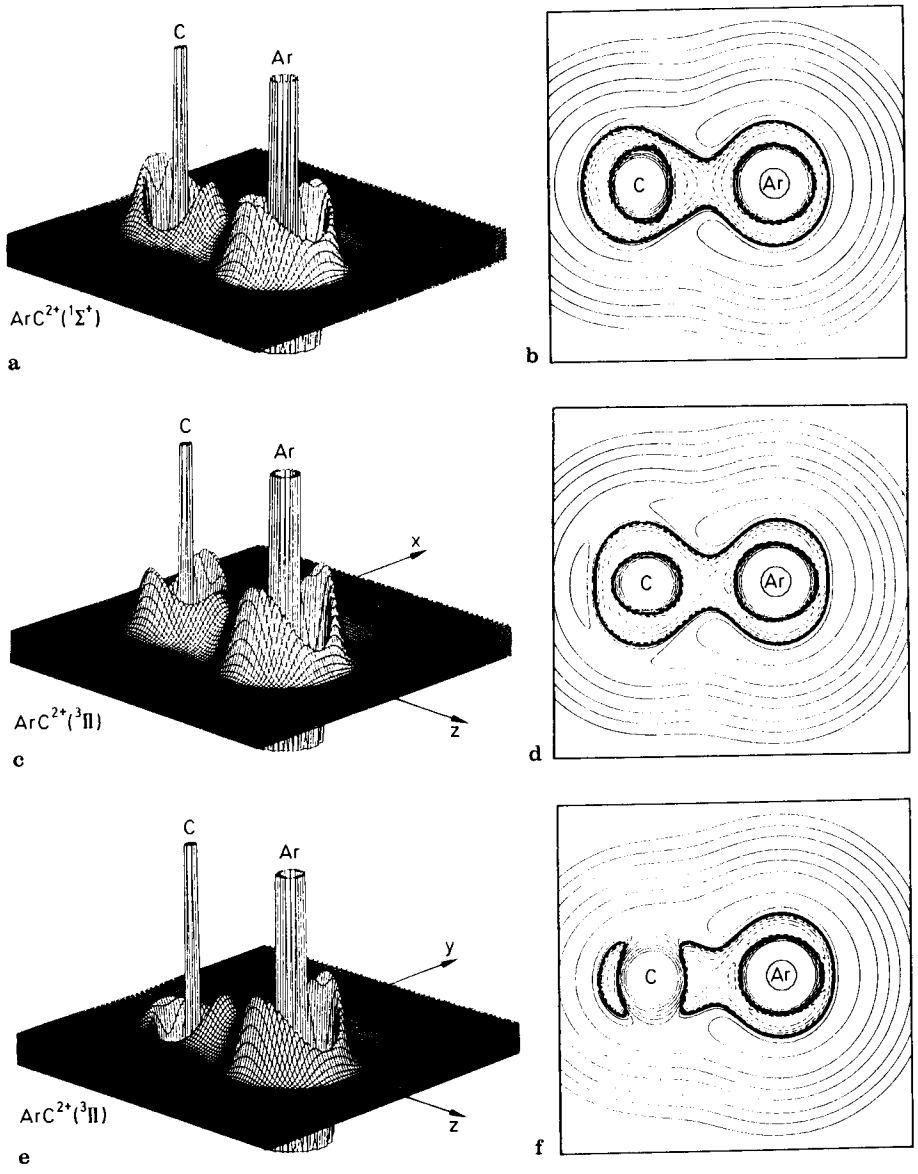

Fig. 10a–f. Contour line diagrams and perspective drawings of the Laplace concentration, $-\nabla^2\rho(\mathbf{r})$, of ArC^{2+}: (**a**, **b**) $^1\Sigma^+$ state, (**c**, **d**) $^3\Pi$ state, direction of filled π-orbital and (**e**, **f**) $^3\Pi$ state, direction of unfilled π-orbital. In the contour line diagrams inner shell concentrations are no longer shown. Ref. [13]

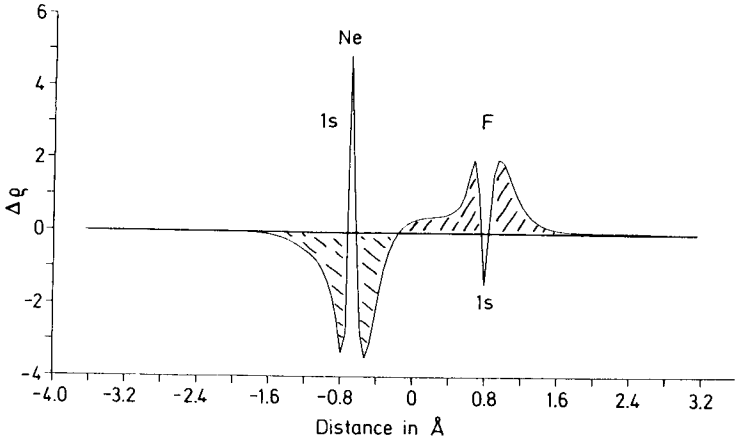

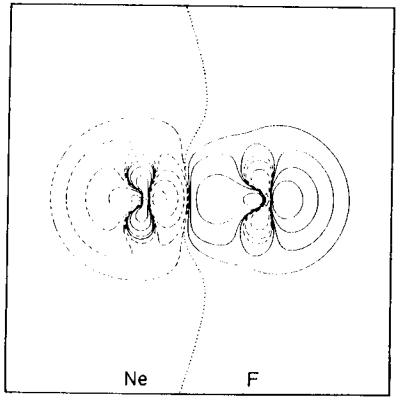

Fig. 11. Profile plot along the internuclear axis (*above*) and contour line diagram (*below*) of the difference electron density $\Delta\rho(\mathbf{r}) = \rho(\mathbf{r})^{molecule} - \rho(\mathbf{r})^{promolecule}$ calculated for $NeF^+(X^1\Sigma^+)$. (HF/6-31G(*d*) calculations). Ref. [5]

The bonding mechanism in NgX^{n+} and ArX^{n+} becomes even more clear when calculating the difference electron density distribution $\Delta\rho(\mathbf{r})$. In Fig. 11, a profile plot and a contour line diagram of $\Delta\rho(\mathbf{r})$ of $NeF^+(X^1\Sigma^+)$ are given [5]. Both diagrams indicate that electron density is transferred from Ne to F^+. It accumulates in the bonding and nonbonding region of F^+. Ne becomes partially positive while F^+ looses some of its positive charge. As a consequence, negative charge residing in the *2pπ* or the *1s* orbitals, which are not involved in the charge transfer from Ne to F^+, is contracted toward the Ne nucleus but becomes more diffuse at the F nucleus. Also, some of the *2pπ* charge may be transferred from F to Ne atom via back donation. As a consequence, $\Delta\rho(\mathbf{r})$ is positive (negative) in the region of the *2pπ* and *1s* orbitals of Ne (*2pπ* and *1s* orbitals of F). This confirms that the formation of a covalent Ng,X bond is different for Ng = Ne or Ar than for Ng = He.

5 Polyatomic Ions of Helium, Neon and Argon

Most research of light noble gas chemistry has focussed on diatomic ions, because only very few polyatomic cations have been observed experimentally. Under the conditions of a mass spectrometer, where most gas-phase experiments are performed, it is difficult to detect more complex molecules containing He, Ne and Ar. The experimental technique of flowing-afterglow mass spectrometry [193] helped to investigate the formation of more complex noble gas ions. For example, it was found by Bohme et al. [98] that Ar_2^+ reacts with CO and forms, among other products, the triatomic cation $ArCO^+$. Under the same condition, the formation of $HeCO^+$ and $NeCO^+$ from CO and He_2^+ of Ne_2^+, respectively, was not observed [99]. In a similar way, Munson et al. [99] report the formation of $ArCO^+$ and ArN_2^+ in a mass spectrometer, while the helium and neon analogs could not be detected in analog reactions. In recent years, theoretical studies of small noble gas ions have been reported [7, 13, 83, 90d, 95, 97] and these may help experimentalists to tailor their experiments to more promising candidates. The results of these studies let us expect that more promising candidates. The results of these studies let us expect that more focussed experiments guided by theory will find new cations of He, Ne and Ar.

The presentation of the reported research on polyatomic cations will be made analogous to the diatomic species. As shown above, atomic ions X^{n+} may bind a light noble gas element with a binding energy up to 96.1 kcal/mol (ArH^+). We will first ask the question how many noble gas atoms may the atomic ions X^{n+} bind in polyatomic cations Ng_mX^{n+}. Then, we will proceed to cations which are formally formed from diatomic ions XY^{n+} and He, Ne or Ar. The reader will see that the available information on polyatomic cations is well understood using this scheme and that it is possible to make an "educated guess" about the stability of unknown species without even performing quantum mechanical calculations.

5.1 Ng_mH^+ Cations

Of all the atomic cations X^+ in the ground state, hydrogen(+) forms the strongest bonds with Ng. Therefore, it can be expected that the proton should be capable of attracting more than one noble gas atom in hydrogen-bonded cluster ions Ng_mH^+. In fact, the formation of Ng_2H^+ (H = He, Ne, Ar) using the flowing afterglow technique has been reported by Adams et al. [100]. The triatomic molecules were formed in reaction (1):

$$Ng_2^+ + H_2 \longrightarrow Ng_2H^+ + H \qquad (1)$$

The reaction rates of reaction (1) have been measured for the three light noble gases but only for Ar_2H^+ was the bond energy deduced as $> 3.82 - D(Ar_2)$ eV [100]. Theoretical studies at the Hartree-Fock level have been reported by Matcha, Milleur and coworkers for He_nH^+ [101], Ne_nH^+ [102] and Ar_nH^+ [103]. The results for Ng_2H^+ are shown in Chart 1. All three ions have a linear geometry and a $^2\Sigma_g^+$ ground state. This dissociation energy of the triatomic species into $NgH^+ + Ng$ is nearly the same (10–12 kcal/mol) for the three species. A more recent calculation of He_2H^+ by Dykstra [104] using self consistent electron pair (SCEP) and double-substitution coupled-cluster (CCD) methods gave slightly higher values of $D_e = 13.2$ kcal/mol (SCEP) and 13.3 kcal/mol (CCD). The lower D_e value for Ar_2H^+ may be caused by the relatively low theoretical level. Thus, the interactions between NgH^+ and Ng are much weaker than between Ng and H^+. This is because NgH^+ is a weaker Lewis acid than a proton. The bonds in Ng_2H^+ are significantly longer and weaker than in NgH^+. Milleur et al. also calculated [101] that He_3H^+ and He_4H^+ are energetically unstable toward dissociation into He_2H^+ and helium. The same has been assumed for Ar_nH^+ without explicit calculations being carried out [102]. For the argon analogs it was speculated [103] that stable Ar_nH^+ clusters with $n > 2$ may be possible because of the greater bond strength in ArH^+ than for NeH^+ and HeH^+. However, the nearly identical dissociation energies for the reaction $Ng_2H^+ \rightarrow NgH^+ + Ng$ for Ng = He, Ne and Ar argues against this. While the donor ability increases for He < Ne < Ar, there is a parallel decrease in Lewis acidity for $HeH^+ > NeH^+ > ArH^+$ which seems to cancel each other, thereby explaining the similar D_e values. It seems unlikely that thermodynamically stable Ng_nH^+ cluster ions exist for the light noble gases with $n > 2$.

Matcha and coworkers [105] also reported theoretical results based on Hartree-Fock SCF calculations for the mixed triatomic cation $HeNeH^+$. They

Chart 1. Optimized interatomic distances at MP2/6-31G(*d, p*) for NgH^+ and $NgHNg^+$ ions (in Å) and calculated dissociation energies D_e at MP4(SDTQ)/6-31G(*2df, 2pd*)//MP2/6-31G(*d, p*) for the loss of Ng atom.

He ···(0.770)··· H^+	D_e = 44.5 kcal/mol[a]
	Δ = 11.0 kcal/mol
He——(0.926)——H·····He^+	D_e = 55.5 kcal/mol[a]
Ne ···(0.973)··· H^+	D_e = 49.6 kcal/mol[b]
	Δ = 11.0 kcal/mol
Ne——(1.143)——H·····Ne^+	D_e = 61.1 kcal/mol[b]
Ar ···(1.292)··· H^+	D_e = 82.6 kcal/mol[c]
	Δ = 9.3 kcal/mol
Ar——(1.586)——H·····Ar^+	D_e = 91.9 kcal/mol[c]

[a] Ref. 101; [b] Ref. 102; [c] Ref. 103

predicted dissociation energies of 9.4 kcal/mol for the loss of He and 14.5 kcal/mol for the loss of Ne. These numbers, which are smaller (for He loss) and larger (for Ne loss) compared with the D_e values for He_2H^+ and Ne_2H^+ agree nicely with the donor-acceptor model. Ne is a better donor than He and HeH^+ is a better acceptor than NeH^+ which explains the calculated reaction energies. No experimental reports are known to us about mixed cations $NgNg'H^+$.

5.2 Ng_mX^{n+} Cations with First-Row Elements X

In 1970, Clampiti and Jefferies [106] reported their molecular beam experiments for various ion clusters. For Ne_mLi^+, they found the largest peak for m = 1 followed by nearly identical signals for m = 2, 3, 4, 5, 6. The yield of ion clusters decreases abruptly beyond He_6Li^+. The same result was found for hydrogen clusters $(H_2)_mLi^+$. A remarkable feature of the mass spectrum was the relative insignificance of clusters with m > 6. It was concluded [106] that "six molecules around an ion probably constitute a complete shell". This result is important in comparison with theoretical studies of Ng_mBe^{2+} ions.

As noted above, I_2 of beryllium is lower than I_1 of helium and neon, which causes $HeBe^{2+}$ and $NeBe^{2+}$ to the thermodynamically stable by ca. 18 kcal/mol [4, 90] and 37 kcal/mol [90d], respectively. Harrison et al. [90b] found computationally that the binding energy for the stepwise attachment of the first (18.6 kcal/mol) helium atom is only slightly higher than the second (17.7 kcal/mol) He forming He_2Be^{2+}. Also the bond lengths in $HeBe^{2+}$ (1.434 Å) and linear He_2Be^{2+} (1.439 Å) are nearly the same [90b]. This is strikingly different to what is reported for the hydrogen analogs He_nH^+ discussed above [101]. Schleyer [90d] has extended these studies to helium, neon and argon clusters Ng_mBe^{2+} with m = 8 for He, m = 6 for Ne and m = 3 for Ar. The calculated association energies are shown in Table 10. As can be seen from the predicted binding energies, cluster ions He_mBe^{2+} and Ne_mBe^{2+} are stable toward the loss of a noble gas atom with $m \leq 6$. These clusters all have the highest symmetry possible, i.e. linear for m = 2, trigonal for m = 3, tetrahedral for m = 4, trigonal bipyramidal for m = 5 and octahedral for m = 6. Schleyer [90d] speculated that the break in calculated binding energies for He_mBe^{2+} from m = 4 to m = 5 may be a hint toward octet rule consideration. However, such a break is found for Ne_mBe^{2+} with only the addition of a third and, to a lesser degree, for a fourth atom. In the case of Ar_mBe^{2+}, there is a significant decrease in binding energy even for the second and third argon. This result rather points toward the size of the noble gas atoms as the most important factor. Also, the change from negative to positive association energies for He_mBe^{2+} clusters for m > 6 shows some similarity to the experimental results for He_mLi^+ species which hints that the optimum shell size may be 6. For the Ar_mBe^{2+} clusters it should be kept in mind that the calculated association energies do not refer to the most favorable dissociation products. Since I_1 of Ar

Table 10. Calculated association energies for He_nBe^{2+}, Ne_nBe^{2+}, and Ar_nBe^{2+} clusters (in kcal/mol)[a]

Reactions	Ng		
	He	Ne	Ar
$Be^{2+} + Ng \longrightarrow NgBe^{2+}$	− 18.2	− 37.1	− 69.7
$NgBe^{2+} + Ng \longrightarrow Ng_2Be^{2+}$	− 17.2	− 35.3	− 49.4
$Ng_2Be^{2+} + Ng \longrightarrow Ng_3Be^{2+}$	− 15.2	− 25.1	− 24.1
$Ng_3Be^{2+} + Ng \longrightarrow Ng_4Be^{2+}$	− 13.0	− 20.7	
$Ng_4Be^{2+} + Ng \longrightarrow Ng_5Be^{2+}$	− 6.1	− 17.0	
$Ng_5Be^{2+} + Ng \longrightarrow Ng_6Be^{2+}$	− 6.5	− 18.9	
$Ng_6Be^{2+} + Ng \longrightarrow Ng_7Be^{2+}$	+ 2.6		
$Ng_7Be^{2+} + Ng \longrightarrow Ng_8Be^{2+}$	+ 5.6		

[a] Taken from Ref. 90d

is lower than I_2 of Be, $ArBe^{2+}$ will dissociate into $Ar^+ + Be^+$ for which no dissociation energy is given.

The principle of donor-acceptor interactions in noble gas cations is further exemplified by the theoretical study of Radom and coworkers [95a,c] on the series He_nC^{n+}. Figure 12 shows the optimized geometries for the four cations. The intriguing result of the theoretical studies is the rather short He,C bond length for the triply and quadruply charged species He_3C^{3+} and He_4C^{4+}. The latter molecule, which is isoelectronic with methane CH_4, has also been calculated by Schleyer [90d]. He_3C^{3+} and He_4C^{4+} are "explosive" molecules with highly exothermic dissociation reactions of 246 and 383 kcal/mol, respectively [95c]. However, the barriers for these processes are calculated as 36.3 kcal/mol for He_3C^{3+} and 17.2 kcal/mol for He_4C^{4+}, which are sufficiently large to make experimental observation feasible [95c], although the experimental obstacles to proving the theoretical predictions are enormous.

The calculated interatomic distances shown in Fig. 12 for He_nC^{n+} can be rationalized when the interactions between n helium atoms and the atomic ion C^{n+} are considered. The acceptor strength (Lewis acidity) of C^{n+} increases with n, C^{4+} has no valence electrons and is a very strong Lewis acid. However, the higher charge means increasing Coulomb repulsion. While the increase in attractive orbital interactions dominates for He_3C^{3+} compared with He_2C^{2+}, the two opposing effects seem to nearly cancel each other when going from He_3C^{3+} to He_4C^{4+} as indicated by the nearly constant bond length.

The dihelium carbene dication He_2C^{2+} has also been studied theoretically by the groups of Frenking and Cremer [7, 11] together with the nitrogen and oxygen analogs He_2N^{2+} and He_2O^{2+}. The interatomic distances for the ground states of He_2X^{2+} decrease with C > N > O just like the diatomic HeX^{2+} (see above). The calculated geometries are shown in Fig. 13.

He_2C^{2+} is isoelectronic with methylene CH_2 which is known to have a $^3B_1$ ground state 9.0 kcal/mol lower than the $^1A_1$ excited state [107]. In the case of He_2C^{2+}, the $^1A_1$ state is predicted to be 63.8 kcal/mol lower than the $^3B_1$ state

which is also shown in Fig. 13 [7]. The latter state has a much shorter He, C distance than the $^1A_1$ ground state. The same result has been found for the $^1\Sigma^+$ ground state and $^3\Pi$ excited state of diatomic HeC^{2+} (see Sect. 4.3) and can be explained in the same fashion. HOMO–LUMO interactions of $He(^1S)$ with the *2p* LUMO of $C^{2+}(^1S)$ are much weaker than with the half empty AO of $C^{2+}(^3P)$ (Fig. 2). But the stronger binding interactions do not compensate for the excitation energy which is the reason that the weakly bound $^1A_1$ state of He_2C^{2+} is the ground state and the stronger bound $^3B_1$ state is the excited state.

He_2C^{2+} has not been observed experimentally (nor have He_2N^{2+} and He_2O^{2+}) but since it is predicted to be stable towards dissociation into the atomic products, it might be found in molecular beam experiments. The stabilization energy of the $^1A_1$ ground state relative to $C^{2+}(^1S)$ + 2He is 30.6 kcal/mol (Table 11) [7, 11, 13]. Thus, the association energies for helium atoms with C^{2+} in the ground state are 17.0 kcal/mol for the first He and 13.6 kcal/mol for the second He (Table 11), which indicates similar sequence as found for He_mBe^{2+} (Table 10) [90b,d]. No studies have been reported for He_mC^{2+} with $m > 2$.

The neon and argon analogs of Ng_2X^{2+} have also been studied theoretically by Frenking et al. [13]. The calculated geometries and dissociations energies are

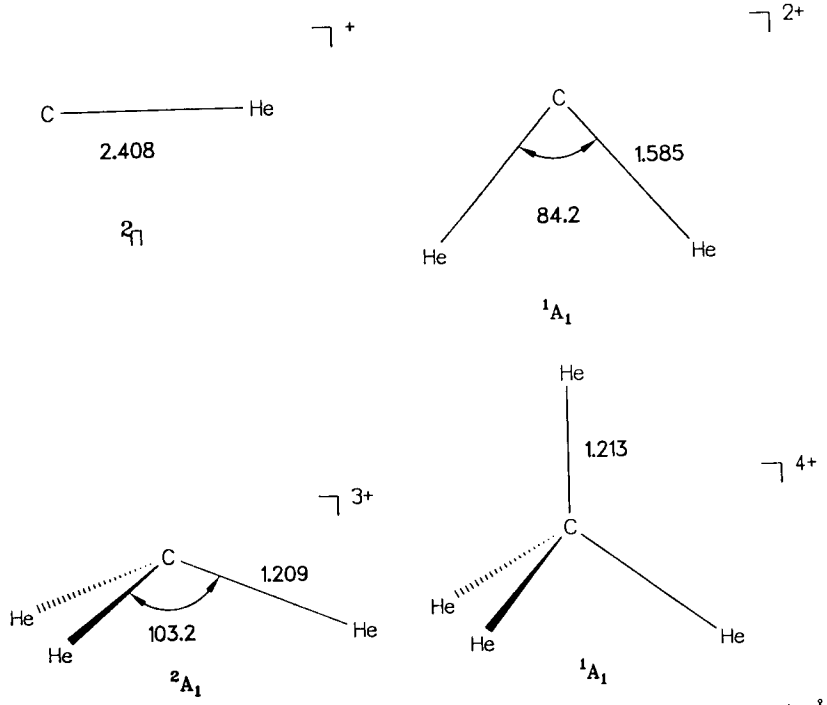

Fig. 12. Optimized geometries (MP4/6-311G(*d*, *p*)) for CHe_n^{n+} cations [95a]. Distances in Å, angles in °

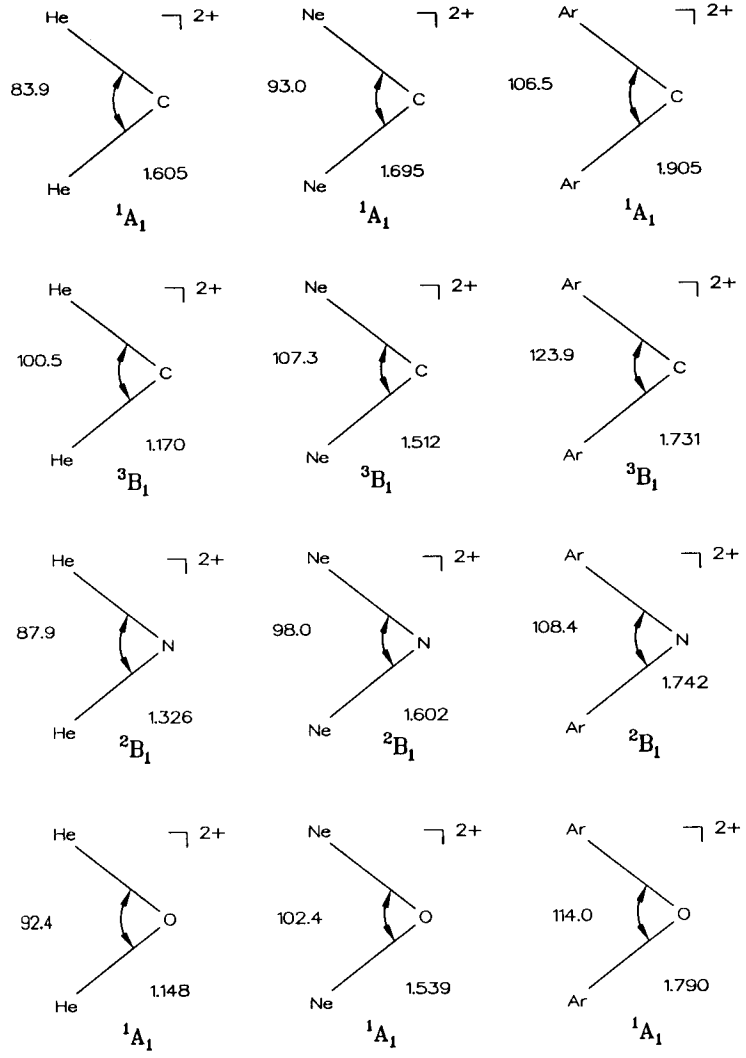

Fig. 13. Optimized geometries (MP2/6-31G(*d*, *p*)) for Ng_2X^{2+} cations [13]. Distances in Å, angles in °

shown in Fig. 13 and Table 11, respectively. The results are in total agreement to what could have been predicted from the donor-acceptor model. For Ng_2C^{2+}, the Ng,C interatomic distance is always longer in the $^1A_1$ ground state than the $^3B_1$ excited state. Accordingly, the dissociation energies for the fragmentation into Ng + C^{2+} in the corresponding electronic states are significantly higher for

Table 11. Calculated dissociation energies (kcal/mol) for Ng_2X^{2+} structures[a]

Reaction	D_e	D_o
$He_2C^{2+}(^1A_1) \longrightarrow HeC^{2+}(^1\Sigma^+) + He(^1S)$	+ 14.7	+ 13.6
$\longrightarrow C^{2+}(^1S) + 2He(^1S)$	+ 32.6	+ 30.6
$\longrightarrow C^+(^2P) + He^+(^2S) + He(^1S)$	+ 37.4	+ 35.4
$He_2C^{2+}(^3B_1) \longrightarrow HeC^{2+}(^3\Pi) + He(^1S)$	+ 50.1	+ 47.2
$\longrightarrow C^{2+}(^3P) + 2He(^1S)$	+ 117.4	+ 112.5
$\longrightarrow C^+(^2P) + He^+(^2S) + He(^1S)$	− 23.4	− 28.3
$Ne_2C^{2+}(^1A_1) \longrightarrow NeC^{2+}(^1\Sigma^+) + Ne(^1S)$	+ 27.4	+ 27.0
$\longrightarrow C^{2+}(^1S) + 2Ne(^1S)$	+ 71.9	+ 70.6
$\longrightarrow C^+(^2P) + Ne^+(^2P) + Ne(^1S)$	+ 3.9	+ 2.6
$Ne_2C^{2+}(^3B_1) \longrightarrow NeC^{2+}(^3\Pi) + Ne(^1S)$	+ 53.6	+ 52.6
$\longrightarrow C^{2+}(^3P) + 2Ne(^1S)$	+ 143.0	+ 140.8
$\longrightarrow C^+(^2P) + Ne^+(^2P) + Ne(^1S)$	− 70.7	− 72.9
$Ar_2C^{2+}(^1A_1) \longrightarrow ArC^{2+}(^1\Sigma^+) + Ar(^1S)$	+ 49.2	+ 48.8
$\longrightarrow C^{2+}(^1S) + 2Ar(^1S)$	+ 178.6	+ 177.2
$\longrightarrow C^+(^2P) + Ar^+(^2P) + Ar(^1S)$	− 26.7	− 28.1
$Ar_2C^{2+}(^3B_1) \longrightarrow ArC^{2+}(^3\Pi) + Ar(^1S)$	+ 89.2	+ 88.1
$\longrightarrow C^{2+}(^3P) + 2Ar(^1S)$	+ 294.5	+ 292.3
$\longrightarrow C^+(^2P) + Ar^+(^2P) + Ar(^1S)$	− 56.9	− 59.1
$He_2N^{2+}(^2B_1) \longrightarrow HeN^{2+}(^2\Pi) + He(^1S)$	+ 37.6	+ 35.2
$\longrightarrow N^{2+}(^2P) + 2He(^1S)$	+ 86.2	+ 82.4
$\longrightarrow N^+(^3P) + He^+(^2S) + He(^1S)$	− 30.4	− 34.0
$Ne_2N^{2+}(^2B_1) \longrightarrow NeN^{2+}(^2\Pi) + Ne(^1S)$	+ 48.6	+ 47.7
$\longrightarrow N^{2+}(^2P) + 2Ne(^1S)$	+ 133.4	+ 131.1
$\longrightarrow N^+(^3P) + Ne^+(^2P) + Ne(^1S)$	− 55.9	− 58.2
$Ar_2N^{2+}(^2B_1) \longrightarrow ArN^{2+}(^2\Pi) + Ar(^1S)$	+ 70.4	+ 67.9
$\longrightarrow N^{2+}(^2P) + 2Ar(^1S)$	+ 276.4	+ 272.8
$\longrightarrow N^+(^3P) + Ar^+(^2P) + Ar(^1S)$	− 49.5	− 53.1
$He_2O^{2+}(^1A_1) \longrightarrow O^{2+}(^1D) + 2He(^1S)$	+ 160.0	+ 154.9
$\longrightarrow O^+(^2D) + He^+(^2S) + He(^1S)$	− 66.3	− 71.4
$Ne_2O^{2+}(^1A_1) \longrightarrow O^{2+}(^1D) + 2Ne(^1S)$	+ 211.5	+ 208.9
$\longrightarrow O^+(^2D) + Ne^+(^2P) + Ne(^1S)$	− 87.6	− 90.2
$Ar_2O^{2+}(^1A_1) \longrightarrow O^{2+}(^1D) + 2Ar(^1S)$	+ 408.8	+ 407.0
$\longrightarrow O^+(^3P) + 2Ar^+(^2P)$	− 25.8	− 27.6

[a] Taken from Ref. 13

the $^3B_1$ state than for the $^1A_1$ state (Table 11). Interaction energies between Ng and C^{2+} in the corresponding electronic states are significantly higher for the $^3B_1$ state than for the $^1A_1$ state (Table 11). Interaction energies between Ng and C^{2+} in Ng_2C^{2+} become higher with He < Ne < Ar for both electronic states. The numbers for the $^1A_1$ ground state are: 32.6 kcal/mol (He), 71.9 kcal/mol (Ne), 178.6 kcal/mol (Ar); for the $^3B_1$ state the results are: 117.4 kcal/mol (He), 143.0 kcal/mol (Ne), 294.5 kcal/mol (Ar). The stability differences between the $^1A_1$ ground state and $^3B_1$ excited state of Ng_2C^{2+} are 63.8 kcal/mol (He), 56.7 kcal/mol (Ne) and 31.1 kcal/mol (Ar). As before, the difference between He and Ne is less than between Ne and Ar. However, the $^1A_1$ ground state of He_2C^{2+} is distinguished from the Ne and Ar analogs by the energetically lowest lying atomization reaction. Unlike He_2C^{2+}, which dissociates endothermic into C^{2+} + 2He, the ground states of Ne_2C^{2+} and Ar_2C^{2+} dissociate exothermic

(Ar) or nearly thermoneutral (Ne) into $Ng^+(^2P) + C^+(^2P)$ (Table 11). Somewhat paradoxic, the weaker bound He_2C^{2+} is stable toward dissociation into the atoms, whereas the stronger bound Ne_2C^{2+} and Ar_2C^{2+} are much less stable (Ne) or unstable (Ar). This is because I_1 of He is higher than I_2 of C, but I_1 of Ne and Ar are lower than I_2 of C.

The results for Ng_2N^{2+} and Ng_2O^{2+} are straightforward. The dissociation reactions into the respective $Ng^+ + N^+$ and $Ng^+ + O^+$ ions are exothermic in all cases. The interaction energies between Ng and X^{2+} increase in Ng_2X^{2+} for X with the sequence C < N < O and for Ng in the order He < Ne < Ar (Table 11). This is also reflected in the calculated geometries (Fig. 13). Again, larger differences in the interaction energies are found between Ne and Ar than between He and Ne (Table 11).

5.3 Ng_mXY^{n+} Ions

Our knowledge about binding interactions in light noble gas compounds has been extended significantly in the last couple of years by the application of modern ab initio methods to small cations which are formed from diatomic species XY^{n+} (X, Y = first-row atoms) and one or two Ng atoms. A summary of the optimized geometries is shown in Fig. 14. Table 12 shows some relevant dissociation energies.

A qualitative understanding for the structures and stabilities of Ng_mXY^{n+} ions is achieved in terms of donor-acceptor interactions between Ng and XY^{n+} in the respective electronic state. Figure 15 shows schematically the molecular orbitals of several XY^{n+} species. We will begin with molecules XY^{n+} with 8 valence electrons.

Wilson and Green [97] calculated the structures and stabilities of $HeCN^+$ at the Hartree-Fock SCF level using various basis sets. They also performed preliminary calculations for $NeCN^+$. For $HeCN^+$, they predict the bond lengths for He,C as approx. 1.10–1.17 Å and for C–N as 1.13–1.16 Å. The dissociation energy D_e for He loss was calculated between 35 and 46 kcal/mol. In case of $HeCN^+$, the Ne,C interatomic distance is predicted as being 1.593 Å. The dissociation energy D_e for $NeCN^+$ is significantly smaller (13.8 kcal/mol) compared with $HeCN^+$, but it was assumed that with a better basis set, the D_e value for the Ne,CN^+ bond would be similar to the He,CN^+ bond. Thus, $HeCN^+$ and $NeCN^+$ are predicted at the Hartree-Fock level to be bound rather strongly. However, a totally different result is found when correlation energy is included in the calculations! Using Møller-Plesset perturbation theory, Frenking et al. [13] report that $HeCN^+$ in the $^1\Sigma^+$ ground state has a very long He,C-distance of 2.515 Å, and the He,C binding energy is only D_e = 0.9 kcal/mol (Fig. 14, Table 12). The isomer $HeNC^+$ is predicted with the same reaction energy for dissociation of He, i.e. D_e = 0.9 kcal/mol. Also for the neon analogs weak interaction energies and rather long distances for the neon bonds are predicted. As shown in Table 12, the dissociation energies D_e are

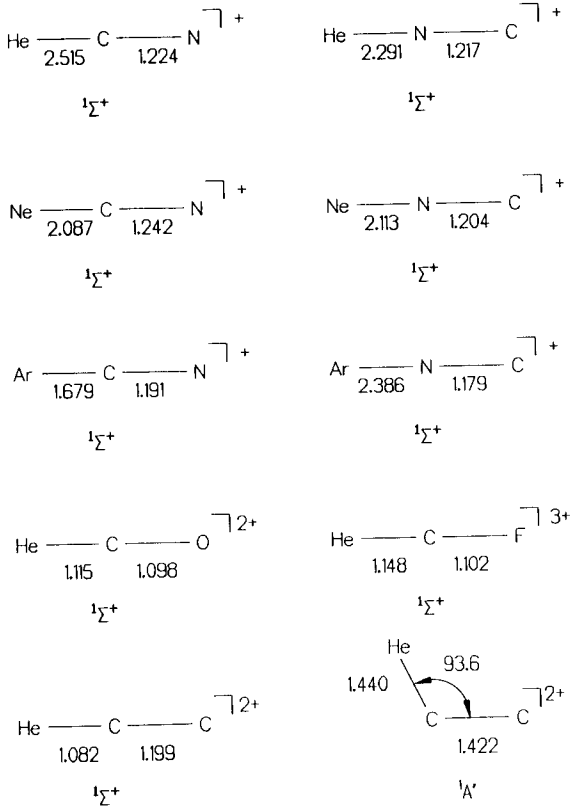

Fig. 14. Optimized geometries (MP2/6-31G(*d*, *p*)) for He, Ne, and Ar cations [7, 13]. Distances in Å, angles in °

3.6 kcal/mol for $NeCN^+$ and $NeNC^+$. Frenking et al. [13] show that the much larger stabilization energies reported by Wilson and Green [97] are an artefact of the Hartree-Fock level. Much higher stabilization energies are reported for $ArCN^+$ and $ArNC^+$ than for the helium and neon analogs. As shown in Table 12, the computed dissociation energy for $ArCN^+$ is $D_e = 35.7$ kcal/mol and for $ArNC^+$ it is $D_e = 17.5$ kcal/mol. This points towards covalent interactions in the argon compounds, but not in the helium and neon structures. As discussed in Sect. 5.5, the analysis of the electron density distribution reveals that $ArCN^+$ is indeed covalently bound, whereas the attractive interactions in $ArNC^+$ are caused by charge-induced dipole interactions.

The valence molecular orbitals of CN^+ in the $X^1\Sigma^+$ ground state are schematically shown in Fig. 15 (XY(8e)). The 3σ, 4σ and the degenerate 1π MO are occupied, and the lowest unoccupied MO is the 5σ orbital. Thus, HOMO–LUMO interactions with Ng involve the 5σ LUMO of CN^+. Because

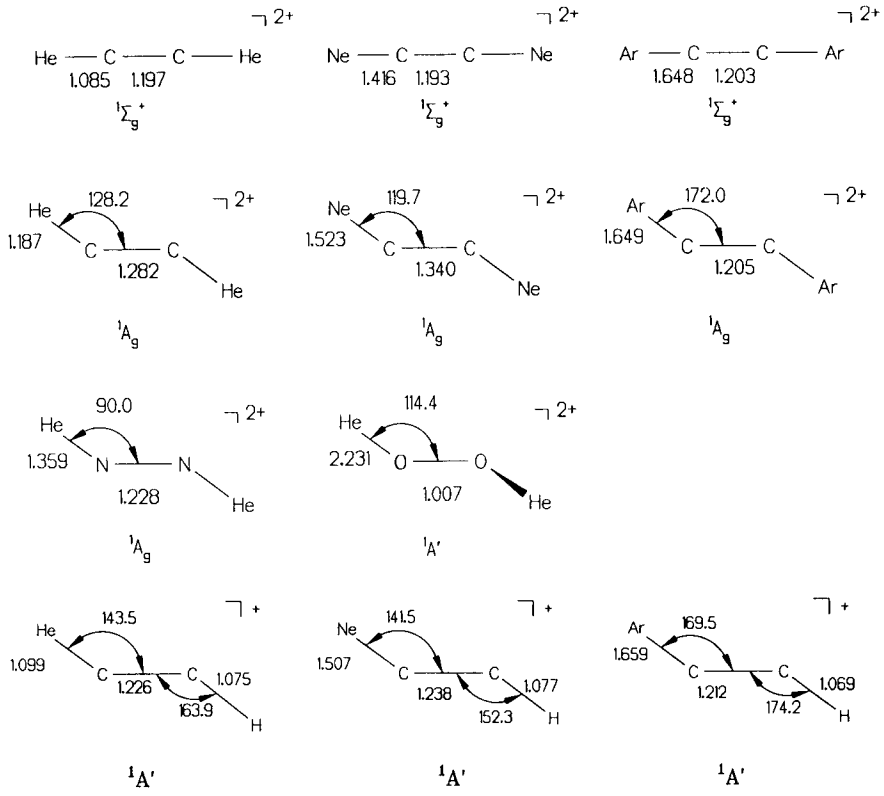

this orbital is dominantly located at the carbon atom, the $ArCN^+$ isomer is clearly more stable than $ArNC^+$. The identical dissociation energies for the He and Ne isomers indicate that the weak binding is mainly caused by charge-induced dipole interactions and that orbital interactions are negligibly small.

The same orbital scheme as for CN^+ is found for isoelectronic CO^{2+}, CF^{3+} and CNe^{4+}. The interactions between He and the multiply charged cations have been reported by Radom and coworkers [95b,c]. $HeCNe^{4+}$ is predicted not to be a minimum on the potential energy hypersurface. For $HeCO^{2+}$ and $HeCF^{3+}$ rather short helium bond lengths are calculated (see Fig.14). This is reasonable, because the higher nuclear charge in the multiply charged XY^{n+} cations yields lower-lying orbitals, which in turn caused stronger orbital interactions with He. The interaction energies between He and $(^1\Sigma^+)CO^{2+}$ are calculated including correlation energy as $D_o = 43.2$ kcal/mol [95b]. $HeCO^{2+}$ has also been calculated by Cooper and Wilson [83] who reported a well depth of approx.

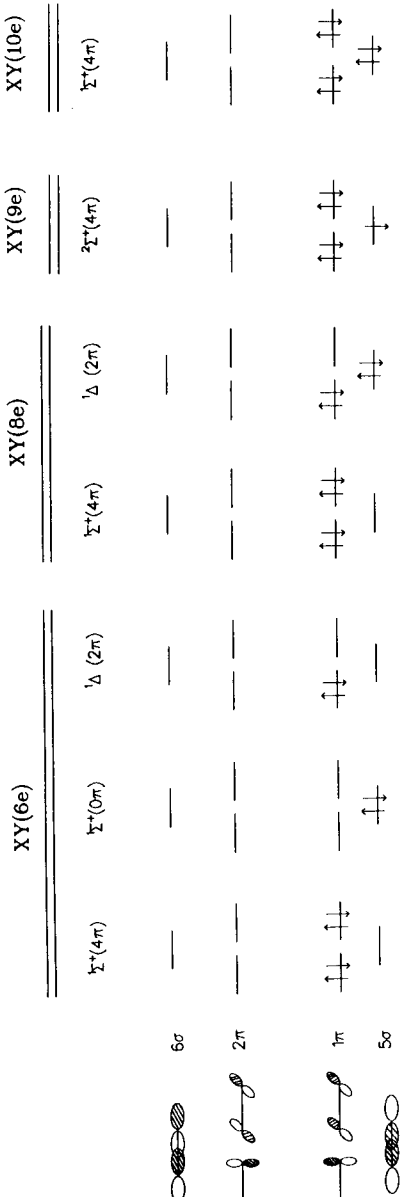

Fig. 15. Schematic representation of some electronic states of XY diatomics with 6, 8, 9, and 10 electrons. In the case of the Δ-states only one possible electron configuration is shown

Table 12. Theoretically predicted dissociation energies D_e and D_o (in kcal/mol)[a]

Reaction	D_e	D_o
$HeCN^+(^1\Sigma^+) \longrightarrow CN^+(^1\Sigma^+) + He(^1S)$	+ 0.9	+ 0.6
$HeNC^+(^1\Sigma^+) \longrightarrow CN^+(^1\Sigma^+) + He(^1S)$	+ 0.9	+ 0.4
$NeCN^+(^1\Sigma^+) \longrightarrow CN^+(^1\Sigma^+) + Ne(^1S)$	+ 3.6	+ 2.0
$NeNC^+(^1\Sigma^+) \longrightarrow CN^+(^1\Sigma^+) + Ne(^1S)$	+ 3.6	+ 2.2
$ArCN^+(^1\Sigma^+) \longrightarrow CN^+(^1\Sigma^+) + Ar(^1S)$	+ 35.7	+ 34.6
$ArNC^+(^1\Sigma^+) \longrightarrow CN^+(^1\Sigma^+) + Ar(^1S)$	+ 17.5	
$HeCO^{2+}(^1\Sigma^+) \longrightarrow CO^{2+}(^1\Sigma^+) + He(^1S)$	+ 45.9[b]	+ 43.2[b]
$\longrightarrow CO^+(^2\Sigma^+) + He^+(^2S)$	+ 19.8[b]	+ 17.7[b]
$HeCF^{3+}(^1\Sigma^+) \longrightarrow CF^{2+}(^1\Sigma^+) + He^+(^2S)$	− 228.6[b]	− 232.4[b]
$HeCC^+(^2\Sigma^+) \longrightarrow CC^+(^2\Sigma_u^+) + He(^1S)$	+ 34.0[d]	− 28.8[d]
$\longrightarrow CC^+(^2\Pi_u) + He(^1S)$	− 32.9[d]	− 39.1[d]
$HeCC^{2+}(^1\Sigma^+) \longrightarrow CC^{2+}(^1\Sigma_g^+, 4\pi) + He(^1S)$	+ 34.0[d]	− 28.8[d]
$\longrightarrow CC^{2+}(^1\Sigma_g^+, 0\pi) + He(^1S)$	− 32.9[d]	− 39.1[d]
$HeCC^{2+}(^1A') \longrightarrow CC^{2+}(^2\Sigma_g^+, 0\pi) + He(^1S)$	− 34.0[d]	− 28.8[d]
$HeCCHe^{2+}(^1\Sigma_g^+) \longrightarrow 2He(^1S) + CC^{2+}(^1\Sigma_g^+, 4\pi)$	+ 174.6	
$\longrightarrow 2He(^1S) + CC^{2+}(^1\Sigma_g^+, 0\pi)$	+ 18.9	+ 10.0
$\longrightarrow He(^1S) + He^+(^2S) + CC^+(^2\Pi_u)$	+ 86.0	+ 78.6
$\longrightarrow 2HeC^+(^2\Pi)$	− 103.6	− 112.6
$HeCCHe^{2+}(^1A_g) \longrightarrow 2He(^1S) + CC^{2+}(^1\Delta_g)$	+ 58.2	
$\longrightarrow 2He(^1S) + CC^{2+}(^1\Sigma_g^+, 0\pi)$	+ 22.8	+ 14.2
$\longrightarrow He(^1S) + He^+(^2S) + CC^+(^2\Pi_u)$	+ 89.9	+ 82.8
$\longrightarrow 2HeC^+(^2\Pi)$	− 99.7	− 108.6
$NeCCNe^{2+}(^1\Sigma_g^+) \longrightarrow 2Ne(^1S) + CC^{2+}(^1\Sigma_g^+, 4\pi)$	+ 169.6	
$\longrightarrow 2Ne(^1S) + CC^{2+}(^1\Sigma_g^+, 0\pi)$	+ 13.9	+ 8.3
$\longrightarrow Ne(^1S) + Ne^+(^2P) + CC^+(^2\Pi_u)$	+ 8.2	+ 4.1
$\longrightarrow 2NeC^+(^2\Pi)$	− 116.0	− 121.5
$NeCCNe^{2+}(^1A_g) \longrightarrow 2Ne(^1S) + CC^{2+}(^1\Delta_g)$	+ 75.6	
$\longrightarrow 2Ne(^1S) + CC^{2+}(^1\Sigma_g^+, 0\pi)$	+ 34.2	+ 28.4
$\longrightarrow Ne(^1S) + Ne^+(^2P) + CC^+(^2\Pi_u)$	+ 28.5	+ 24.2
$\longrightarrow 2NeC^+(^2\Pi)$	− 95.6	− 101.6
$ArCCAr^{2+}(^1\Sigma_g^+) \longrightarrow 2Ar(^1S) + CC^{2+}(^1\Sigma_g^+, 4\pi)$	+ 336.7	
$\longrightarrow 2Ar(^1S) + CC^{2+}(^1\Sigma_g^+, 0\pi)$	+ 173.4	+ 168.2
$\longrightarrow Ar(^1S) + Ar^+(^2P) + CC^+(^2\Pi_u)$	+ 34.9	+ 31.2
$\longrightarrow 2ArC^+(^2\Pi)$	+ 14.3	+ 9.4
$ArCCAr^{2+}(^1A_g) \longrightarrow 2Ar(^1S) + CC^{2+}(^1\Delta_g)$	+ 222.8	
$\longrightarrow 2Ar(^1S) + CC^{2+}(^1\Sigma_g^+, 0\pi)$	+ 173.3	+ 168.1
$\longrightarrow Ar(^1S) + Ar^+(^2P) + CC^+(^2\Pi_u)$	+ 34.8	+ 31.1
$\longrightarrow 2ArC^+(^2\Pi)$	+ 14.2	+ 9.3

[a] Unless otherwise noted, data are taken from Ref. 13; [b] Ref. 95 b; [c] Ref. 83; [d] Ref. 7

63 kcal/mol at the Hartree-Fock level. However, the energetically lowest lying dissociation products of $HeCO^{2+}$ are $He^+ + CO^+(^2\Sigma^+)$. But even for the energetically favored charge separation reaction, the $HeCO^{2+}$ dication is predicted not only to be kinetically stable but also thermodynamically stable by 17.7 kcal/mol [95b,c]. The dissociation of $HeCO^{2+}$ into $He^+ + CO^+$ is another example of Fig. 4b. Fragmentation of $HeCF^{3+}$ $(^1\Sigma^+)$ into $He^+ + CF^{2+}(^2\Sigma^+)$ is

highly exothermic by 232.4 kcal/mol [95b,c]. Nevertheless, a sufficiently high (29.5 kcal/mol) barrier makes the observation even of the trication feasible. The fragmentation of $HeCF^{3+}$ into $He^+ + CF^{2+}$ is an example for Fig. 4a, whereas $HeCNe^{4+}$ is an example for Fig. 4d.

The 8-valence electron systems CN^+, CO^{2+}, CF^{3+} and CNe^{4+} may form stable ions with noble gas atoms not only in the $^1\Sigma^+$ state but also in other electronic states. Figure 15 shows schematically the $^1\Delta$ state (XY(8e)) of the diatomics when approached by another atom [108]. In the $^1\Delta$ state, the LUMO is the 1π(Y) orbital (the 1π(X) is occupied). Because this orbital is usually higher in energy than the 5σ MO, HOMO–LUMO interactions with Ng will be weaker. Also, the resulting $NgXY^{n+}$ species is expected to be non-linear, because the LUMO has π symmetry. This has been found for the interactions between He and another 8-valence electron system XY^{n+}, i.e. NN^{2+}. Cooper and Wilson [83] calculated a bond angle of 92.3° for the non-linear equilibrium structure of $HeNN^{2+}$ with a He,N bond length of only 1.50 Å. The N,N distance is 1.44 Å, which indicates that the corresponding state of NN^{2+} has not $^1\Sigma_g^+$ symmetry. The interaction energy between He and NN^{2+} is computed at the Hartree-Fock level as approx. 86 kcal/mol [83]. No data were presented for the dissociation of $HeNN^{2+}$ into $He^+ + NN^+$, which is the energetically lowest-lying fragmentation reaction. Also the electronic state of the calculated species was not given. Since there is a balance between the excitation energy of the acceptor cation and the donor-acceptor interaction with Ng, it is not always easy to predict the energetically lowest-lying state of $NgXY^{n+}$ molecules. A striking example is presented below.

After discussion the interactions between Ng and 8-valence electron systems XY^{n+}, we now turn to XY^{n+} species with 6-valence electrons. In particular, we will discuss interactions between Ng and CC^{2+}. Koch et al. [7] investigated theoretically the structures of $HeCC^{2+}$ in several electronic states. They found a strongly $^1\Sigma^+$ state with a He,C distance of only 1.082 Å and an interaction energy of 89.9 kcal/mol. The corresponding $^1\Sigma_g^+(4\pi)$ state of C_2^{2+} is schematically shown in Fig. 15 (XY(6e) $^1\Sigma^+(4\pi)$). The short He,C bond and linear geometry can be rationalized with strong HOMO–LUMO interactions involving the low-lying 4σ LUMO [109]. A second energy minimum with a non-linear geometry was found for $HeCC^{2+}$ ($^1A'(2\pi)$) with a longer He,C bond (1.440 Å) and a bond angle of 93.6° (Fig. 14), which is similar to what is found for $HeNN^{2+}$. This structure corresponds to the $^1\Delta_g$ state of CC^{2+} which is also shown in Fig. 15 (XY(6e), $^1\Delta(2\pi)$). Here, the LUMO is the higher-lying 5σ orbital, which explains the weaker interactions in the bent form of $HeCC^{2+}$. The energetically lowest-lying state of CC^{2+} is the $^1\Sigma_g^+(0\pi)$ state, which has an even higher-lying (1π) LUMO (Fig. 15, XY(6e) $^1\Sigma^+(0\pi)$). Not surprisingly, no bound $HeCC^{2+}$ structure was found with the $X^1\Sigma_g^+(0\pi)$ ground state of CC^{2+}. The $^1A'(2\pi)$ state of $HeCC^{2+}$ is computed to be 51.0 kcal/mol lower in energy than the stronger bound $^1\Sigma^+$ state [7]. Also triplet states were investigated and the lowest lying state of $HeCC^{2+}$ is predicted to have $^3A''(1\pi)$ symmetry [7]. The model of donor-acceptor interaction has also been used to explain the structures and stabilities of the triplet states of $HeCC^{2+}$ and $HeCCHe^{2+}$ [7, 50].

Koch et al. [7] studied also the interactions of CC^{2+} with two He atoms. When both He are attached to the same carbon, vinylidene analogs He_2CC^{2+} are formed. When He is bound to the terminal carbon atoms, acetylenic structures $HeCCHe^{2+}$ are found. The $^1\Sigma_g^+$ state of $HeCCHe^{2+}$ has a very short He,C bond length of 1.085 Å (Fig. 14) and the dissociation energy D_e into CC^{2+} ($^1\Sigma_g^+(4\pi)$) + 2 He is very high, 174.6 kcal/mol (Table 12) [7, 50]. The dissociation energy corresponds to a He,C binding energy of 87.3 kcal/mol. The strong binding interaction compensates even for the excitation energy of CC^{2+} from the $X^1\Sigma_g^+(0\pi)$ state to the $^1\Sigma_g^+(4\pi)$ state. The dissociation of $HeCCHe^{2+}$ ($^1\Sigma_g^+$) into the ground state of $CC^{2+}(^1\Sigma_g^+,0\pi)$ + 2He is still endothermic by 10.0 kcal/mol (Table 12) [7, 50]. The $^1\Sigma_g^+$ state is also lower in energy than the triplet states of $HeCCHe^{2+}$ which were calculated by Koch et al. [7]. However, the linear singlet form of $HeCCHe^{2+}$ is not the lowest lying bound state!! A later investigation of $NgCCNg^{2+}$ (Ng = He, Ne, Ar) by Frenking et al. [13] showed that the $^1\Delta_g$ state of CC^{2+} may bind two helium atoms forming the trans-planar ^1A_g state of $HeCCHe^{2+}$ shown in Fig. 14. The ^1A_g state of $HeCCHe^{2+}$ is predicted to be 4.2 kcal/mol lower in energy than the linear $^1\Sigma_g^+$ state. The He,C bonds are slightly longer and weaker in the *trans*-form, but the weaker He,C binding interactions are compensated by the deexcitation energy of CC^{2+} from the $^1\Sigma_g^+(4\pi)$ state to $^1\Delta_g$ (Fig. 15, XY(6e)).

Also for $NeCCNe^{2+}$, the trans-planar ^1A_g state is calculated to be lower in energy than the linear $^1\Sigma_g^+$ form by 20.2 kcal/mol [13]. In the case of $ArCCAr^{2+}$, a linear and slightly bent structure were optimized (Fig. 14) which are nearly degenerate in energy. The calculation of the potential energy hypersurfaces of $HeCCHe^{2+}$ and $NeCCNe^{2+}$ at MP2/6-31G(*d*, *p*) as a function of the NgCC angle gave a maximum energy structure that was only slightly higher than the corresponding linear structures. At MP4(SDTQ)/6-311G(*2df*, *2pd*), the energy of the "transition states" were even lower than for the linear forms [13]. This result indicates that the linear structures of $HeCCHe^{2+}$ and $NeCCNe^{2+}$ may not even be true minima on the potential energy surface.

Considering the linear and *trans*-bent forms of $NgCCNg^{2+}$ as products of Ng and CC^{2+} in the $^1\Sigma_g^+(4\pi)$ and $^1\Delta_g$ state, respectively, the following binding energies per Ng,C bond are computed: for the linear forms 87.3 kcal/mol (He,C), 84.8 kcal/mol (Ne,C), and 168.4 kcal/mol (Ar,C); for the *trans*-bent forms 29.1 kcal/mol (He,C), 37.8 kcal/mol (Ne,C) and 111.4 kcal/mol (Ar,C) (Table 12). The slightly lower bond strength in the linear form of $NeCCNe^{2+}$ than calculated for linear $HeCCHe^{2+}$ can be explained by the p-π repulsion in the former structure. In the linear and *trans*-bent forms of $NgCCNg^{2+}$, Ar is much stronger bound than He an Ne. $ArCCAr^{2+}$ is theoretically predicted to be stable not only kinetically, but also thermodynamically. Unlike $HeCCHe^{2+}$ and $NeCCNe^{2+}$, the charge separation reaction into $2NgC^+$ is endothermic for Ng = Ar by 9.3 kcal/mol. The corresponding dissociation reactions of $HeCCHe^{2+}$ and $NeCCNe^{2+}$ are exothermic by 108.6 kcal/mol and 101.6 kcal/mol, respectively (Table 12).

Koch et al. [7] also investigated the changes in the noble gas structures for the series $HeCCHe^{2+}$, $HeNNHe^{2+}$, and $HeOOHe^{2+}$. Figure 14 shows that the

helium bonds are much longer for $HeNNHe^{2+}$ and especially $HeOOHe^{2+}$. This can be explained by donor-acceptor interactions between He and the respective diatomic dication. Figure 15 shows the molecular orbitals of the diatomics with 4 π-electrons (XY with 6, 8, 10 electrons, $^1\Sigma^+(4\pi)$). The lowest-lying orbital of $CC^{2+}(^1\Sigma_g^+(4\pi))$ is the 4σ MO [109]. NN_2^{2+} and O_2^{2+} have two and four more electrons, respectively. HOMO–LUMO interactions involve the 5σ MO of N_2^{2+} and the 2π MO of O_2^{2+} [109], which are higher in energy (Fig. 15). The predicted geometry for $HeNNHe^{2+}$ by Koch et al. [7] is in agreement with the calculated structure of $HeNN^{2+}$ by Cooper and Wilson [83].

There are very few experimental reports about light noble gas ions Ng_mXY^{n+}. For the 9-valence electron systems CO^+ and NN^+, interactions with noble gases have been studied in a mass spectrometer by Munson et al. [99]. Besides the corresponding krypton and xenon compounds, $ArNN^+$ and $ArCO^+$ were observed, but not the helium and neon analogs. $ArNN^+$ had already earlier been detected in a mass spectrometer by Kaul and Fuchs [110]. Assuming that NN^+ and CO^+ were in the $^2\Sigma^+$ ground state ($^2\Sigma_g^+$ for NN^+), interactions with Ng should be weaker than between Ng and the 8-valence electron system CN^+ in the $^1\Sigma^+$ ground state. This is, because the 5σ orbital is empty in CN^+, but singly occupied in NN^+ and CO^+ (Fig. 15, XY(9e) $^2\Sigma^+(4\pi)$). Teng and Conway [111] determined the dissociation energy for the Ar,NN^+ bond experimentally using a mass spectrometer as $D_0 = 24.5$ kcal/mol, significantly less than what is calculated for $ArCN^+$ ($D_0 = 34.6$ kcal/mol [13]). Theoretical studies for $NgNN^+$ are needed to determine the electronic state of the experimentally observed $ArNN^+$ ion and the binding energies for $HeNN^+$ and $NeNN^+$.

5.4 *Other Light Noble Gas Ions*

There are not many studies reported for molecular ions of the light noble gases that do not fall into one of the prior categories. Related to the acetylenic dications $NgCCNg^{2+}$ are the singly charged acetylene analogs $NgCCH^+$, which have also been studied theoretically. Cooper and Wilson [83] calculated $HeCCH^+$ at the Hartree-Fock level with a linear geometry and a He,C interatomic distance of 1.24 Å. Koch et al. [7] performed higher-level calculations and found that the linear structure is not a minimum on the potential energy surface when correlation energy is included. Rather, a *trans*-bent ($^1A'$) structure was found as minimum with a much shorter (1.099 Å) He,C bond. Also for $NeCCH^+$ and $ArCCH^+$, the energy minimum structure is predicted [13] to have a *trans*-bent geometry with bond lengths of 1.507 Å (Ne, C) and 1.659 Å (Ar, C) (Fig. 14). The linear $^1\Sigma^+$ form of $NgCCH^+$ may be thought as the product of Ng and CCH^+ in the $^1\Sigma^+(4\pi)$ state. However, this is not the ground state of CCH^+. There are three singlet states [112, 113] lower in energy than the $^1\Sigma^+(4\pi)$ state, $^1\Pi$, $^1\Delta$ and $^1\Sigma^-(2\pi)$. The $^1\Pi$ state appears to be the energetically lowest-lying linear singlet state of CCH^+ [113]. The interaction energies between Ng and ($^1\Pi$) CCH^+ are predicted as 15.4 kcal/mol for He [114], 7.1 kcal/mol for Ne and 55.7 kcal/mol for Ar (Table 13) [13]. Again, much stronger interactions are found for argon than for helium and neon. The decrease in binding energy from $HeCCH^+$ to $NeCCH^+$ may be caused by the π-repulsion between Ne and CCH^+, which does not exist between He and CCH^+ in $HeCCH^+$.

Table 13. Calculated reaction energies D_e and D_0 (in kcal/mol) for $NgCCH^+$ structures[a]

Reaction	D_e	D_0
$HeCCH^+(^1A') \longrightarrow He(^1S) + CCH^+(^1\Pi)$	15.4	12.5
$NeCCH^+(^1A') \longrightarrow Ne(^1S) + CCH^+(^1\Pi)$	7.1	5.9
$ArCCH^+(^1A') \longrightarrow Ar(^1S) + CCH^+(^1\Pi)$	55.7	54.3

[a] Taken from Ref. 13

A very interesting ab initio study of β-decay in OHT, NH_2T, and CH_3T has been reported by Ikuta et al. [115]. β-decay of tritium yields (besides a neutrino particle υ) the helium isotope $^3He^+$. Because of the relatively short half-life of tritium (12.26 years), tritiated compounds may be thought of as a convenient source of helium-containing molecular ions:

$$RT \longrightarrow RHe^+ + \beta^- + \upsilon \qquad (2)$$

Ikuta et al. [115] calculated the transition probabilities in reaction (2) for the three tritiated compounds listed above, and they calculated the potential curves for the product ions containing He at the Hartree-Fock level. The transition probabilities to the ground state daughter ions were predicted as ca. 0.61 for all the parent molecules studied. $OHHe^+$ and NH_2He^+ were calculated with small barriers for helium dissociation, but the energy release upon relaxation of the daughter ion from the parent geometry to the equilibrium structure was higher than the dissociation energy in both cases. For CH_3He^+, a repulsive potential curve for the helium dissociation was computed. The results of Ikuta et al. [115] are in essential agreement with earlier Hartree-Fock calculations by Cooper and Wilson [83] who predict approximate well depths for $OHHe^+$, NH_2He^+, and CH_3He^+ as ca. 4.3 kcal/mol, 0.7 kcal/mol and 0.1 kcal/mol, respectively. The theoretical calculations show that it is very unlikely that helium cations might be observed via β-decay of OHT, NH_2T and CH_3T.

The relative abundances of the ionic fragment from the decay of CH_3T in a mass spectrometer have been measured by Snell and Pleasonton [116]. They detected small amounts of CH_3He^+ with $0.06 \pm 0.01\%$ abundancy, the main product being CH_3^+. A recent higher-level calculation including correlation energy predicts a small barrier for He dissociation of < 0.25 kcal/mol for CH_3He^+ and a r_{CHe} equilibrium distance of 2.053 Å [95a]. It is surprising that the very weakly bound CH_3He^+ has been detected, albeit with very low abundancy, as the product of β-decay of CH_3T [116]. There are other helium-hydrocarbon cations which have been experimentally observed in low

abundancies in a mass spectrometer via β-decay of the tritium parent compounds [117]. Perhaps the highest yield was achieved from tritiated toluenes, giving up to $0.4 \pm 0.2\%$ $C_7H_7He^+$ [117, 118]. The experiments have mostly been performed to yield gaseous hydrocarbon cations, and the investigated molecules are not expected to bind helium strongly. Higher yields of helium molecular cations may be expected for structures such as $HeCCH^+$, which are predicted by theory to have much stronger helium bonds. Such experiments have been suggested in several theoretical studies [7, 95].

β-decay of molecules containing radioactive isotopes has successfully been employed to produce molecular ions containing another noble gas element, i.e. xenon. Using ^{131}I-labeled compounds RI, xenon-organic cations have been studied in a mass spectrometer by Carson and White [119]. For example, ^{131}I-labeled CH_3I undergoes β-decay of CH_3Xe^+ with the molecular ions remaining intact in 69% of the decays [119a]. The much higher abundancy of the xenon molecular ion compared with the helium analog can be explained by the significantly higher Xe,C bond strength, which has been determined experimentally as 43 ± 8 kcal/mol [120]. Also, the kinetic energy release resulting from the β-decay is deposited to a higher degree in the He,C bond than the Xe,C bond in CH_3Ng^+. Also CH_3Kr^+ has been produced in a mass spectrometer via β-decay of ^{82}Br-labeled CH_3Br. Here, the abundancy of CH_3Kr^+ was only 0.4% [119b]. The Kr–C bond strength in CH_3Kr^+ has experimentally been estimated as 21 ± 15 kcal/mol [120].

5.5 *The Nature of Bonding in Polyatomic Noble Gas Ions*

A description of the electronic structure and the nature of bonding in polyatomic noble gas ions follows exactly the same lines pursued in the case of diatomic noble gas molecules (Sect. 4.5). Once the electronic wave function has been determined by ab initio calculations, the electron density distribution can be calculated, the MED path and (3, −1) critical points can be found, and the properties of $\rho(\mathbf{r})$ and $H(\mathbf{r})$ can be evaluated at the critical points of $\rho(\mathbf{r})$. This has been done for Ng_2X^{2+} (X = C, N, O), $NgCCNg^{2+}$, $NgCCH^+$, and $NgCN^+$ ions. We will review in this section the results of these investigations [7, 13].

Ng_2X^{2+} ions: All NgX bonds, with one exception, are semipolar covalent bonds. According to the ρ_B and H_B data summarized in Table 14, they fulfil necessary and sufficient condition for covalent bonding. The only exception is $He_2C^{2+}(^1A_1)$, which possesses electrostatic bonds. The exceptional electronic structure of $He_2C^{2+}(^1A_1)$ is due to the electronic configuration of $C^{2+}(^1S)$, which does not possess any σ-holes in its valence shell concentration. However, its positive charge is high enough to establish a covalent bond with one He atom (see Sect. 4.5). This is possible by a distortion of the valence shell of $C^{2+}(^1S)$ as can be seen from the perspective drawing of the Laplace concentration of $HeC^{2+}(X^1\Sigma^+)$ given in Fig. 9c.

Table 14. Nature of bonding in Ng_2X^{2+} and $NgCCNg^{2+}$ ions according to ab initio calculations[a]

Dication	State	Bond	ρ_b [eÅ^{-3}]	H_b [hartree Å^{-3}]	B_e[b] [kcal/mol]	Nature of bonding
He_2C^{2+}	$^1A_1$	He, C	0.49	−0.1	16.3	electrostatic
He_2C^{2+}	$^3B_1$	He, C	1.16	−1.2	58.7	covalent
Ne_2C^{2+}	$^1A_1$	Ne, C	0.71	−0.3	35.7	covalent
Ne_2C^{2+}	$^3B_1$	Ne, C	0.89	−1.0	71.5	covalent
Ar_2C^{2+}	$^1A_1$	Ar, C	0.90	−0.4	89.3	covalent
Ar_2C^{2+}	$^3B_1$	Ar, C	1.28	−1.1	147.3	covalent
He_2N^{2+}	$^2B_1$	He, N	1.13	−0.7	43.1	covalent
Ne_2N^{2+}	$^2B_1$	Ne, N	0.96	−0.4	66.7	covalent
Ar_2N^{2+}	$^2B_1$	Ar, N	1.36	−0.9	138.2	covalent
He_2O^{2+}	$^1A_1$	He, O	1.97	−1.9	80.0	covalent
Ne_2O^{2+}	$^1A_1$	Ne, O	1.17	−0.4	105.7	covalent
Ar_2O^{2+}	$^1A_1$	Ar, O	1.17	−0.5	204.4	covalent
$HeCCHe^{2+}$	$^1\Sigma_g^+$	He, C	1.38	−1.3	87.3	covalent
$HeCCHe^{2+}$	^1A_g	He, C	1.25	−1.2	89.2	covalent
$NeCCNe^{2+}$	$^1\Sigma_g^+$	Ne, C	0.97	−1.0	84.8	covalent
$NeCCNe^{2+}$	^1A_g	Ne, C	0.80	−0.9	94.9	covalent
$ArCCAr^{2+}$	$^1\Sigma_g^+$	Ar, C	1.53	−2.0	168.3	covalent
$ArCCAr^{2+}$	^1A_g	Ar, C	1.53	−2.0	168.4	covalent

[a] From Ref. 13; [b] B_e = Bond energy, using one half of the D_e values for Ng dissociation listed in Tables 11 and 12

A second He atom can not be bound in the same way. If two He atoms approach $C^{2+}(^1S)$ from different sides, then the net distortion of this valence shell will be much smaller than in the case of $HeC^{2+}(X^1\Sigma^+)$ as can be seen from Fig. 16. As a consequence, the stability of $He_2C^{2+}(^1A_1)$ is due to electrostatic interactions such as charge-induced dipole attraction rather than covalent bonding [7].

Since the donor ability of Ng increases from He to Ar, both $Ne_2C^{2+}(^1A_1)$ and $Ar_2C^{2+}(^1A_1)$ possess covalent bonds with increasing bond energies. This increase can also be observed for the other Ng_2C^{2+} ions (Table 14).

Another feature of bonding, which is nicely reflected in the electron density distribution $\rho(\mathbf{r})$ at the (3, −1) critical point of the Ng,C bond, is the dependence of the strength of the bond in the electronic structure of X^{2+} (see also Sect. 4.5). For example, the value of ρ_b(Ng, C) is higher of the $^3B_1$ states than for the $^1A_1$ states of Ng_2C^{2+}. This increase reflects the fact that $C^{2+}(^3P)$ contrary to C^{2+} (^3P) possesses distinct σ-holes in its valence shell configuration, which are prone to accept electronic charge from Ng thereby establishing semipolar bonds with Ng. This interpretation is in line with calculated dissociation energies and geometries.

Bonding in Ng_2N^{2+} and Ng_2O^{2+} can be explained in the same way. In Fig. 17a and b, perspective drawings of the Laplace concentration of $N^{2+}(^2P)$ and $O^{2+}(^1D)$ are shown. Both dications possess concentration holes in their valence shell, which can be filled with electrons of a suitable donor. The holes correspond to low lying unoccupied *2p* orbitals, which split into *2pσ* and *2pπ*

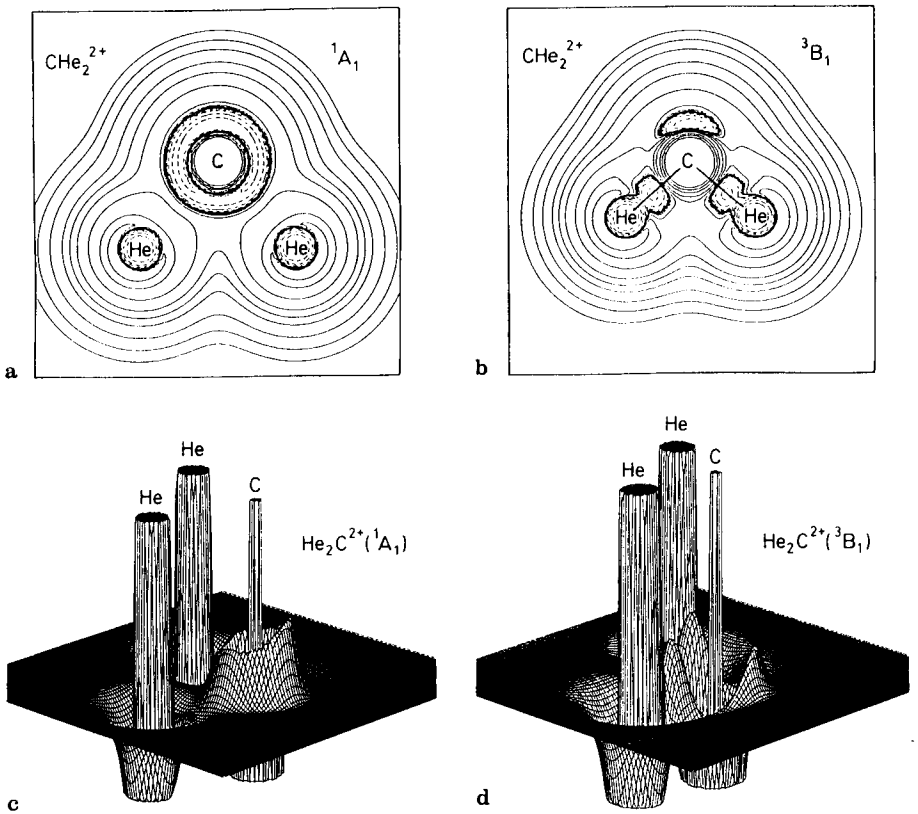

Fig. 16a–d. Contour line diagrams and perspective drawings of the Laplace concentration, $-\nabla^2\rho(\mathbf{r})$, of He_2C^{2+}: (**a**, **b**) $^1A_1$ state, (**c**, **d**) $^3B_1$ state, given with regard to the molecular plane. In the contour line diagrams, inner shell concentrations are no longer shown

components upon approach of an Ng atom. The seize of the $2p\sigma$ holes can be estimated by the difference $\nabla^2\rho(\mathbf{r})_{max} - \nabla^2\rho(\mathbf{r})_{min}$ where the subscripts max and min denote maximum and minimal concentration values in the valence shell. According to this difference the seize increases with the atomic number, i.e. going from $C^{2+}(^1S)$ to $O^{2+}(^1D)$ leads to a stronger electron acceptor, which binds Ng atoms better. In MO language, one can say that the $2p\sigma$ MO becomes lower in energy and, hence, frontier orbital interactions between donor and acceptor increase.

This is exactly what is reflected by the calculated bond properties of ions Ng_2X^{2+}. All ions with X = N and X = O possess covalent bonds according to the data collected in Table 14 [13].

$NgCCNg^{2+}$ ions: The analysis of bonding in NgX^{n+} and Ng_2X^{2+} ions reveals that the electronic structure of the acceptor determines whether or not

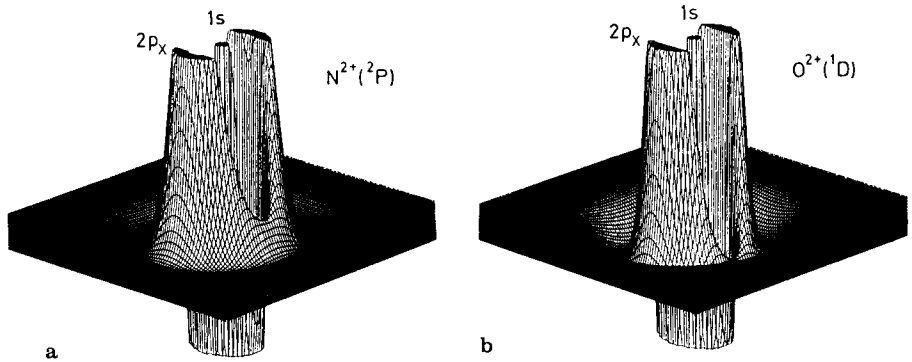

Fig. 17a and b. Perspective drawings of the Laplace concentration, $-\nabla^2\rho(\mathbf{r})$, of (**a**) $N^{2+}(^2P)$, and (**b**) $O^{2+}(^1D)$ influenced by an approaching Ng atom. Note that ion states change in this situation to $^2\Pi$ and $^1\Delta$, respectively. Inner shell and valence shell concentrations are indicated. (HF/6-31G(*d*) calculations)

a covalent bond is formed with Ng. σ-Holes in the valence shell, i.e. low-lying unoccupied σ-MOs, are essential for the nature of the Ng,X interactions. The same observations have also been made in the case of the Ng acceptor CC^{2+}. As explained already above (see also Fig. 18) the CC^{2+} ion is an excellent electron acceptor in its $^1\Sigma_g^+(4\pi)$ excited state, but it does not interact at all with Ng atoms in its $^1\Sigma_g^+(0\pi)$ ground state [7, 13].

The reason for the different reactivities of the two states can nicely be illustrated by the Laplace concentrations given in Fig. 18. In the case of the ground state, there are four concentration lumps along the molecular axis, two in the internuclear region and two in the lone pair regions. They correspond to σ-electrons that shield the nuclei with regard to each other and with regard to an attacking nucleophile. In this way, nuclear repulsion is reduced and the dication is stabilized. In addition, its ability of reacting with a σ-electron donor is diminished. CC^{2+} in its ground state is only a (weak) π-acceptor as is reflected by the π-holes at the nuclei. However, this π-acceptor ability is irrelevant for the bonding of Ng atoms.

In the excited $^1\Sigma_g^+(4\pi)$ state of CC^{2+}, the concentration lumps are in regions where one should expect the four π-electrons, while concentration holes appear in the lone pair regions along the internuclear axis. That means that the concentration holes qualify as σ-holes that impart to the CC^{2+} ion distinct σ-electron acceptor ability. CC^{2+} in its $^1\Sigma_g^+(4\pi)$ state possesses the right electron configuration to undergo reaction with Ng atoms. Noble gas compounds with one or two Ng atoms can be formed as already discussed above.

There are no longer concentration lumps in the internuclear region of $CC^{2+}(^1\Sigma_g^+(4\pi))$. Accordingly, nuclear repulsion is high and the stability of the dication is low. On the other side, the energy gain by bonding Ng atoms can be so large that it compensates the excitation energy of CC^{2+} ions as was discussed in Sect. 5.3.

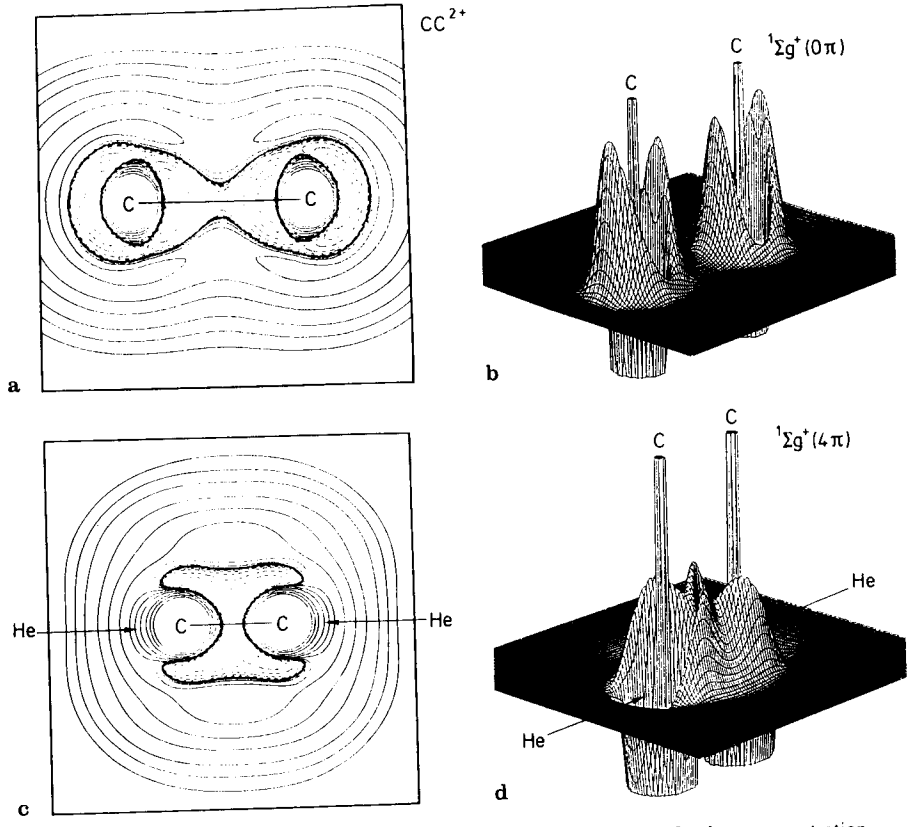

Fig. 18a–d. Contour line diagrams and perspective drawings of the Laplace concentration, $-\nabla^2\rho(\mathbf{r})$, of CC^{2+}: (**a**, **b**) $^1\Sigma^+(0\pi)$ ground state, (**c**, **d**) $^1\Sigma^+(4\pi)$ excited state with regard to the plane containing the nuclei. In the contour line diagrams inner shell concentrations are no longer shown. (HF/6-31G(*d*) calculations). Ref. [7]

All Ng,C bonds of cations $NgCCNg^{2+}(^1\Sigma_g^+)$ investigated so far are covalent. This is suggested by the properties of the electron and the energy density evaluated at the bond critical points (Table 14). The density data also reflect the fact that the Ne,C bond is actually weaker than the He,C bond due to $2p\pi$-π_u electron repulsion absent in the He compound.

Analysis of the electron density distribution confirms that Ng,C bonding in $NeCCNe^{2+}$ and $HeCCHe^{2+}$ is due to *s*-electron donation from He while in $ArCCAr^{2+}$ it is due to $p\sigma$-electron donation from Ng. Again, this is nicely reflected by the calculated Laplace concentrations (Fig. 19).

Figure 19a depicts a perspective drawing of the calculated Laplace concentration of $ArCCAr^{2+}$. There are concentration holes in the valence shell of the Ar atoms where one would expect the $3p\sigma$-electrons, however concentration

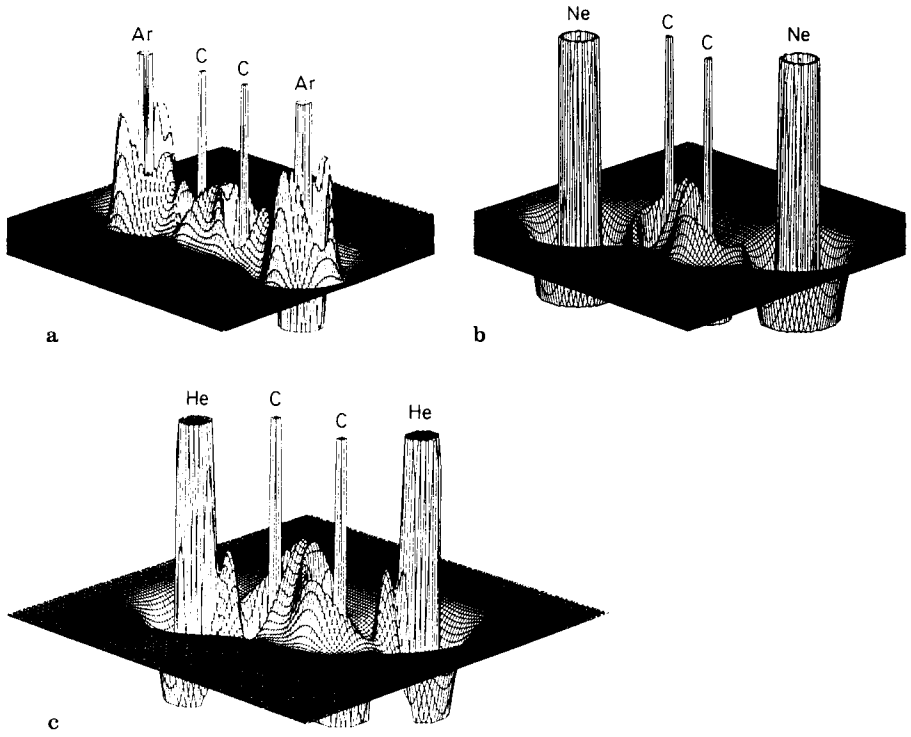

Fig. 19a–c. Perspective drawings of the Laplace concentration, $-\nabla^2\rho(\mathbf{r})$, of (**a**) $ArCCAr^{2+}(^1Ag)$, (**b**) $NeCCNe^{2+}(^1Ag)$, and (**c**) $HeCCHe^{2+}(^1A_g)$. Inner shell and valence shell concentrations are indicated. (HF/6-31G(*d*, *p*) calculations). Ref. [13]

lumps in the regions of the $3p\pi$-electrons. Furthermore, there is a distinct increase of electron concentration in the Ar,C bond region indicative of a semipolar covalent bond between noble gas atom and carbon. Similar features can be observed in the Laplace concentration of $NeCCNe^{2+}$ although the Ne atoms are still surrounded in the molecule by the outer depletion sphere, which is now less pronounced than in the free atom (Fig. 19b).

For $HeCCHe^{2+}$ the semipolar He,C bond is reflected by an appendix like deformation of the *s*-electron distribution of He in the bonding region which is exactly opposite of the σ-hole at CC^{2+}. As noted above this is typical of all semipolar He,X bonds and becomes easy detectable in the contour line diagrams of the Laplace concentration.

While the electronic structure of the acceptor allows reasonable predictions on its possibilities to bind Ng atoms, it does not provide a basis to predict the geometry of the most stable $NgCCNg^{2+}$ form calculated by ab initio theory. For example, it is difficult to predict the *trans*-bent form of $HeCCHe^{2+}$ and

$NeCCNe^{2+}$ on the basis of the electronic structure of the acceptor $CC^{2+}(^1\Sigma_g^+(4\pi))$. However, this can be rationalized by simple MO arguments as has been shown in Ref. [13].

Normally, a 10-valence electron system such as acetylene, HCCH, possesses a linear structure, which can be rationalized by the shape of its bonding σ-MOs, namely the C,C bonding ($2\sigma_g$) MO and the two C,H bonding MOs ($2\sigma_u$ and $3\sigma_g$) [121]. The later MO is formed by bonding overlap of $2p\sigma$(C) orbitals, which means that bending of acetylene leads to a decrease of C,H bonding and, hence, to an increase of the molecular energy.

In the case of $HeCCHe^{2+}$, the nature of the three σ-MOs changes due to the larger electronegativity of Ng relative to C. The $2\sigma_g$- and the $2\sigma_u$-MO possess He,C bonding character, while the $3\sigma_g$-MO is responsible for C,C bonding (Fig. 20). Accordingly, bending of the molecule leads only to an insignificant increase of the energy of the $3\sigma_g$-MO. On the other hand, the in-plane π_u-MO can overlap in a bonding fashion with σ-type He orbitals upon bending of the molecule, thus stabilizing the nonlinear form. Since antibonding overlap between non-nearest neighbors is minimized in the *trans*-bent form, this structure represents the energy minimum of the $HeCCHe^{2+}$ ions. For the same reason $HeCC^{2+}$ in its ground state possesses a bent rather than a linear geometry [7].

In the case of the $NeCCNe^{2+}$ ion bending leads also to a reduction of $2p\pi$-π_u repulsion in the linear form. This is clearly reflected in the relative energies of

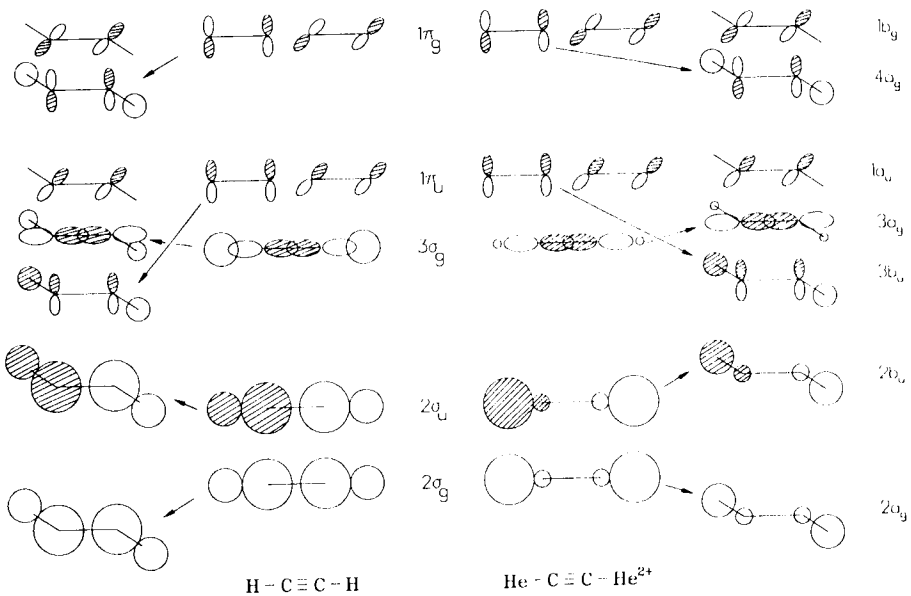

Fig. 20. Orbital correlation diagrams for bending of (**a**) acetylene and (**b**) $HeCCHe^{2+}$. Ref. [13]

linear and bent forms. In the case of $ArCCAr^{2+}$, this energy difference is negligible thus indicating that $2p\pi$(C)-$3p\pi$(Ar) electron repulsion is less important than $2p\pi$(C)-$2p\pi$(Ne) electron repulsion [13].

$NgCCH^+$ ions: The investigation of the NgX^{n+}, Ng_2C^{2+}, and $NgCCNg^{2+}$ ions clearly shows that σ-holes in the valence shell of the acceptor are more important than positive charges. This led Frenking and coworkers to investigate the acceptor ability of suitable monocations such as the HCC^+ ion [7]. In Fig. 21, the Laplace concentration of the ground state and two excited states of the HCC^+ ion are depicted. They show that only the excited $^1\Sigma^+(4\pi)$ state with its deep σ-concentration hole at the terminal C atom should be suited to bind a Ng atom. This has been confirmed by ab initio calculations [7]. The contour line diagram of the Laplace concentration of $HeCCH^+$ is given in Fig. 22. It shows the droplet like appendix in the charge concentration of the He atom that is typical of a semipolar covalent He,C bond. The covalent nature of the He, C bond is confirmed by the properties of electron and energy density distribution in the bonding region (see Table 15). Necessary and sufficient condition for covalent bonding are fulfilled [7, 13].

As noted in Sect. 5.3, $HeCCH^+$ possesses a *trans*-bent geometry, which can be rationalized in the same way as the nonlinear structures of $NgCCNg^{2+}$ discussed above. The MO correlation diagram in Fig. 20 suggests that due to the larger electronegativity of He compared to that of H the HeCC bending angle should be much smaller than the HCC angle. This is confirmed by the calculated bond angles shown in Fig. 4.

In the case of $NeCCH^+$ bending of the molecule leads also to a reduction of electron repulsion between the lone pair electrons of Ne and the π-electrons of the CC unit. Again, $p\pi$-$p\pi$ electron repulsion is stronger for the Ne compound than the Ar compound (see above). As a consequence, the ArCC angle is close to 180° while the NeCC angle is smaller than the HeCC angle (see calculated geometries in Fig. 14).

Two of the three $NgCCH^+$ ions, namely $HeCCH^+$ and $ArCCH^+$, possess covalent Ng,C bonds (see Table 15). For $NeCCH^+$, however, the analysis of the

Table 15. Nature of bonding in NgX^+ monocations according to ab initio calculations[a]

Dication	State	Bond	ρ_b [eÅ^{-3}]	H_b [hartree Å^{-3}]	D_e [kcal/mol]	Nature of bonding
$HeCCH^+$	$^1A'$	He, C	1.17	−0.9	15.4	covalent
$NeCCH^+$	$^1A'$	Ne, C	—[b]	—[b]	7.1	electrostatic
$ArCCH^+$	$^1A'$	Ar, C	1.36	−1.9	55.7	covalent
$HeCN^+$	$^1\Sigma^+$	He, C	0.04	0.0	0.9	electrostatic
$HeNC^+$	$^1\Sigma^+$	He, N	0.08	0.0	0.9	electrostatic
$NeCN^+$	$^1\Sigma^+$	Ne, C	0.21	−0.0	3.6	electrostatic
$NeNC^+$	$^1\Sigma^+$	Ne, N	0.24	0.0	3.6	electrostatic
$ArCN^+$	$^1\Sigma^+$	Ar, C	1.38	−1.7	35.7	covalent
$ArNC^+$	$^1\Sigma^+$	Ar, N	0.27	0.0	17.5	electrostatic

[a] From Ref. 13; [b] No (3, −1) critical point found. Characterization of the bond has been done on the basis of the Laplacian of ρ(r) and the D_e value.

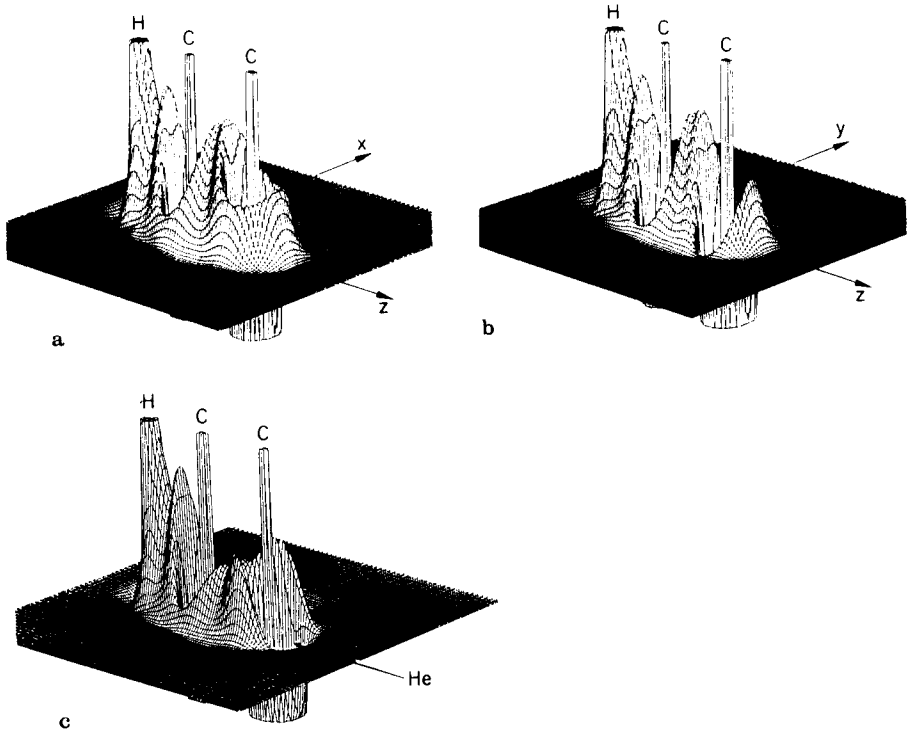

Fig. 21a–c. Perspective drawings of the Laplace concentration, $-\nabla^2\rho(\mathbf{r})$, of (**a**, **b**) $HCC^+(^1\Pi)$ shown for both the plane with one (a) and with the two paired π-electrons (b), and (c) $HCC^+(^1\Sigma^+, 4\pi)$. Inner shell and valence shell concentrations are indicated. (HF/6-31G(*d*, *p*) calculations)

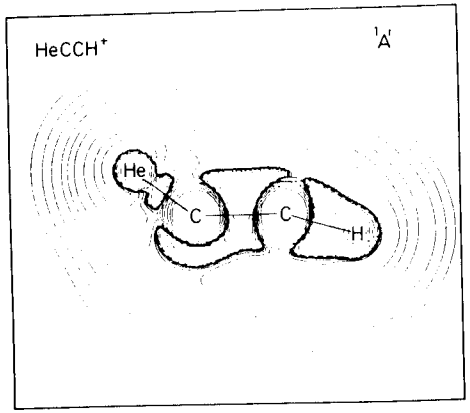

Fig. 22. Contour line diagram of the Laplace concentrations, $-\nabla^2\rho(\mathbf{r})$, of $HeCCH^+$. The inner shell concentrations are no longer shown. (HF/6-31G(*d*, *p*) calculations). Ref. [7]

energy density H_b reveals that the bond possesses only weak covalent character. Electrostatic interactions between Ne and CCH^+ should play a more important role, which is in line with the relatively low dissociation energy of 7 kcal/mol (Table 15).

It is likely that a replacement of H in $NgCCH^+$ ions by alkyl, aryl or other organic groups does not lead to a significant change in Ng,C bonding and, therefore, monohelium or monoargon alkyne cations should be stable possessing semipolar covalent Ng,C bonds. This is one of the important conclusions of the bond analysis of Ng compounds [7, 13].

$NgCN^+$ ions: The $CN^+(^1\Sigma^+)$ ion is another suitable acceptor for Ng electrons. This is clearly reflected by the Laplace concentration of $CN^+(^1\Sigma^+)$ shown in Fig. 23. There is a σ-hole at the C atom, which is not as deep as the σ-hole at the terminal C atom of $HCC^+(^1\Sigma^+)$ shown in Fig. 21. But it is much deeper than the σ-hole at the N atom of $CN^+(^1\Sigma^+)$ (Fig. 23b). This is indicative of the fact that the $3\sigma_g$ LUMO of $CN^+(^1\Sigma^+)$ has a larger amplitude at the C atom. The $CN^+(^1\Sigma^+)$ ion is an electron acceptor that can pull electrons into its valence shell holes both at the C and the N atom where binding should be stronger via the C atom than the N atom.

He and Ne form only weakly stable van der Waals complexes with CN^+ (Sec. 5.3), which is confirmed by the analysis of $\rho(\mathbf{r})$ and $H(\mathbf{r})$ (Table 15). Obviously, the acceptor ability of $CN^+(^1\Sigma^+)$ does not suffice for the formation of covalently bonded molecules. The properties of $\rho(\mathbf{r})$ and $H(\mathbf{r})$ indicate just weak dipole-induced dipole interactions.

Contrary to He and Ne, Ar forms a covalently bound $ArCN^+(^1\Sigma^+)$ ion with $CN^+(^1\Sigma^+)$ (see Ar, C in Table 15). This is in line with the enhanced donor ability of Ar and the distinct acceptor ability of $CN^+(^1\Sigma^+)$ at its carbon end. Figure 24, which contains contour line diagrams and perspective drawings of calculated Laplace-concentration of $ArCN^+$ and $ArNC^+$, reveals pronounced $3p\sigma$-donation of the Ar atom and concentration of negative charge in the ArC bonding

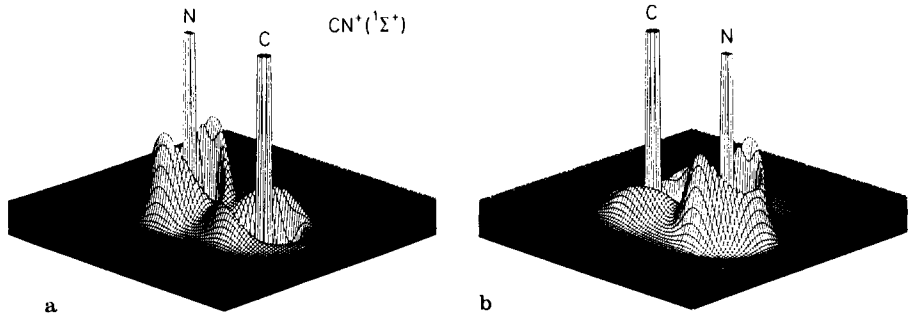

Fig. 23a and b. Perspective drawings of the Laplace concentration, $-\nabla^2\rho(\mathbf{r})$, of the $CN^+(^1\Sigma^+)$ shown (**a**) from the side of the carbon atom, (**b**) from the side of the N atom. (HF/6-31G(*d*) calculations)

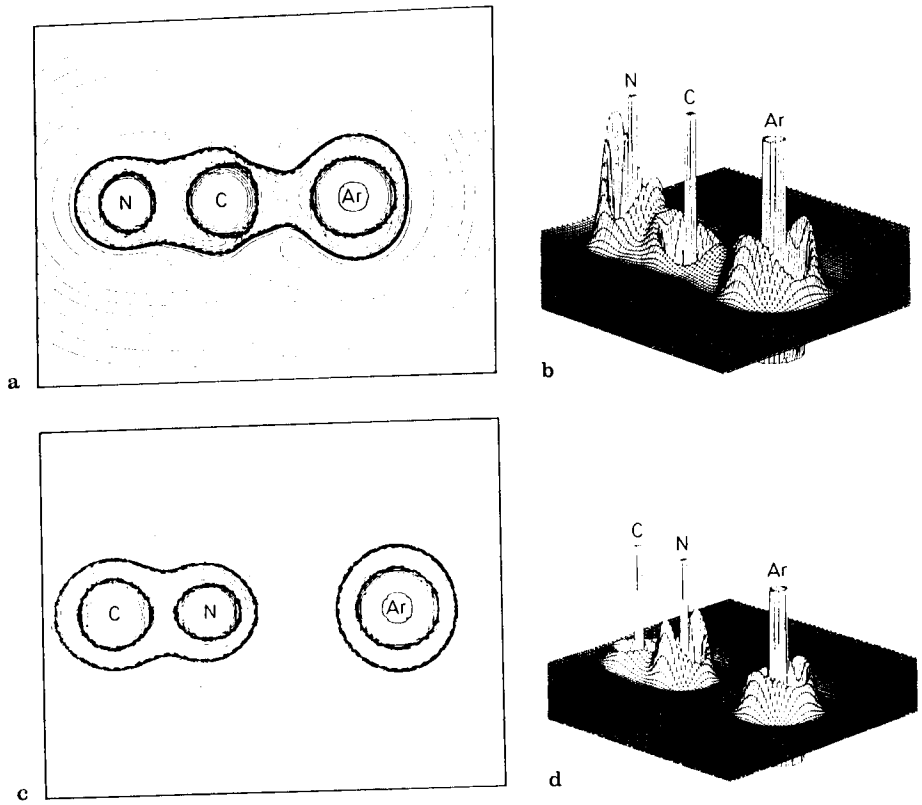

Fig. 24a–d. Contour line diagrams and perspective drawings of the Laplace concentration, $-\nabla^2\rho(\mathbf{r})$, of (**a**, **b**) $ArCN^+$ and (**c**, **d**) $ArNC^+$. In the contour line diagrams inner shell concentrations are no longer shown. (HF/6-31G(*d*) calculations). Ref. [13]

region. Electron donation from Ar to $CN^+(^1\Sigma^+)$ leads to a reorganization of electronic structure in the CN part of $ArCN^+$, which is nicely illustrated by the perspective drawings of $-\nabla^2\rho(\mathbf{r})$ in Fig. 23 ($CN^+(^1\Sigma^+)$) and Fig. 24b.

The calculated electronic structure is completely different in ion $ArNC^+$ as can be seen from Fig. 24c and d. Obviously, there are just electrostatic interactions between Ar and the noble gas atom in line with what has been found for $HeNC^+$ and $NeNC^+$. There is no concentration of negative charge in the region between Ar and N (Fig. 24d) and the electronic structure of the $CN^+(^1\Sigma^+)$ ion seems to be hardly changed by the Ar atom (compare Fig. 24d and 23). This result clearly demonstrates that the σ-hole at the N atom is too small to make $CN^+(^1\Sigma^+)$ an ambident noble gas acceptor with equal strength at the C and N end. The D_e value for $ArNC^+$ is relatively large in view of the electrostatic nature of the interactions (Table 15). However, investigation of ArX^+ ions has

shown that ion-induced dipole forces can lead to as much as 25 kcal/mol attraction between Ar and ions such as N^+ [5]. Calculations show that despite the fact that CN^+ is isoelectronic with HCC^+, only $ArCN^+$ of the six possible $NgCN^+$ and $NgNC^+$ systems represents a covalently bonded ion.

6 Neutral Compounds of Helium, Neon and Argon

Soon after the discovery of the noble gas elements, many laboratories made great efforts to induce chemical reactions with Ng. Unsuccessful attempts were made to enforce reactions with compounds known to be very reactive, such as Cl_2, $KMnO_4$, red-hot Mg, alkaline metals, and many others. A survey of unsuccessful attempts to induce chemical reactions with Ng is given in Ref. 122. By 1916 it was established that He, Ne, Ar as well as the other noble gases were chemically inert.

An early report of weakly bound noble gas species came from Druyvesteyn [123] in 1931. He observed two regions of band structure in the violet region for a mixture of helium and neon. Because the resolution of his spectrometer was low, it is difficult to know whether such spectra originate from neutral molecules such as HeNe or from molecular ions such as $HeNe^+$. Reliable information of neutral diatomics NgX was available for the mercury species NgHg as early as 1941, when Heller [124] reported the vibrational wave numbers and dissociation energies for NgHg with Ng = He, Ne, Ar, Kr, Xe. HeHg was reported by Manley as early as 1924 [125].

In the following, we will shortly summarize the knowledge about neutral compounds of the light noble gas elements bound by van der Waals interaction including the "border-line" structures NgBeO. Although no chemically bound molecule of He, Ne, and Ar is known as yet, there is reason to believe that argon compounds are feasible. This is discussed at the end of this section.

6.1 Clathrates and van der Waals Complexes

Clathrates are host-guest complexes in which a crystalline cage of the host compound holds the guest molecule by weak intermolecular forces. Often, the cavities of the guest molecule are formed by a network of hydrogen bonds between covalently bound compounds. Powell [126] names them 'clathrates' from the Latin word 'clathratus', which means enclosed. It is interesting to note that the lattice structure of the host in the clathrate is not its normal crystalline form; the former becomes thermodynamically more stable than the latter only by the formation of the host-guest complex.

The first known clathrate was a gas hydrate of chlorine, discovered by Davy in 1811 [127]. By 1900, many clathrate compounds had been prepared [128],

but the nature of these substances was not understood until the X-ray work of Powell and coworkers [126, 129] provided detailed structural information. Although the composition of the clathrate nH . mG (H = host, G = guest) can vary over a long range, the maximum composition formula, which corresponds to completely filled cavities, is stoichiometric. For example, hydroquinone forms a clathrate with many guest molecules with the ratio 3H : 1G [130]. This corresponds to 69 ml gas per gramm clathrate.

The best-known noble gas clathrates are hydrates, hydroquinone and phenol clathrates, which have found an increasing number of uses [131]. Clathrates may serve as convenient "storage" for noble gases. Because of the different affinity hydroquinone clathrate prepared from an equal mixture of krypton and xenon liberates 3 times the amount of Xe than Kr [132]. Clathrates are also of interest for nuclear technology. Radioactive isotopes of argon, xenon and krypton can more easily be handled in the compact form of a solid rather than in gas form [133–136].

Hydroquinone clathrates of the nobles gases with the maximum composition formula $(C_6H_4(OH)_2)_3Ng$ are known for Ng = Ar [137], Ng = Kr [138], and Ng = Xe [139]. Attempts to form He or Ne clathrates were unsuccessful. The molecular structures are well known [130, 140]. Each Ng atom is enclosed in a cubic cage formed by 6 benzene rings as shown in Fig. 25 [130]. The stability of the clathrates shows the order Ar < Kr < Xe. The stability order is readily explained by the increase in electric polarizability of the noble gas atoms. One reason that clathrates of He and Ne are not formed is the lower polarizability. But perhaps more important is the size of the cage; the cavity is too large, the phenyl rings are too far away to allow for stabilizing interactions. In fact, up till now there are no clathrates of He and Ne known with any host molecule. A suitable host compound for the two lightest noble gases should provide small cavities; but this yields repulsive intramolecular interactions within the host compound which apparently can not be compensated for by the weak stabilization energy of a He or Ne clathrate.

Hydrates of Ar, Kr, and Xe were first synthesized by Villard in 1896 [141]. They were further studied, as well as hydrates of krypton and xenon, by de Forcrand [142]. Several structures for noble gas hydrates are known [143–146]. All the hydrate structures are different from that of ordinary hexagonal ice. In the two fundamental structures, the water molecules form pentagonal dodecahedra which are stacked with different degrees of distortion from their ideally regular forms [146]. The two types of structures are shown in Fig. 26a and 26b [140]. One structure contains 46 water molecules in the unit cell with 2 small and 6 larger cavities. The other structure has 136 water molecules in the unit cell with 16 small and 8 larger cavities. The formation of the two fundamental types of hydrates depends mainly on the size of the guest species. More detailed data for the two principal clathrate hydrate structures are available from the literature [147].

The phenol clathrates of argon, krypton, and xenon have been prepared by Lahr and Williams [148] by direct combination of the gas with crystalline

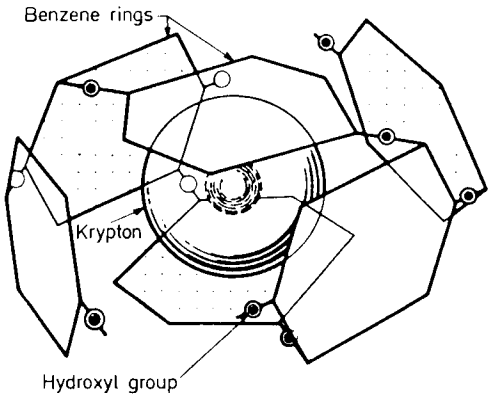

Fig. 25. Schematic display of krypton hydroquinone clathrate [130]

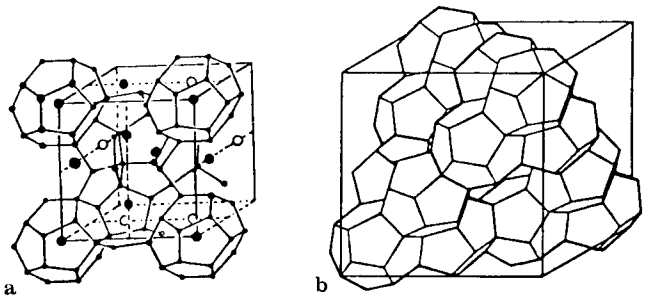

Fig. 26a and b. Schematic representation of the dodecahedra of noble gas hydrates of (**a**) type I and (**b**) type II. [140]

phenol. In the cases of krypton and xenon, clathrates were also formed with molten phenol. The gas/phenol mole ratio was 1 : 4 for argon and krypton, and 1 : 3 for xenon [148]. Also substituted phenol form clathrates with the three noble gas elements [149]. Details on other substances which form clathrates with argon, neon, and xenon may be found in the literature [139]. As mentioned above, no stable clathrates of helium and neon have been prepared. A semi-empirical quantum mechanical calculation [150] of the stability of cubane clusters with He and Ne came to the conclusion that there is a lesser chance of retaining a Ne atom in comparison with a He atom in a cubane cage.

A different class of noble gas compounds bound by van der Waals interactions are small molecules NgX, where X is either an atom or a diatomic or triatomic species such as HF, HCl, HBr, ClF, NO, HCN, Cl_2, Br_2. The experimental and theoretical techniques for studying such weakly bound complexes and the concepts and theoretical models to understand them have recently been reviewd in several articles and monographs [151–154] and will not be discussed here. It should be mentioned, however, that detailed structural and dynamical

information of small van der Waals complexes in the gas phase is available from molecular beam experiments using methods such as electric resonance spectroscopy [155] and Fourier transform microwave spectroscopy [156]. The spectroscopic study of these species has accelerated enormously since the advent of the supersonic nozzle [157], which allows the investigation of van der Waals complexes at an extremely low translational temperature. Table 16 shows the dissociation energies of some well studied examples of NgX compounds with X = HF, HCl, HBr, Cl_2, Br_2, J_2, NO. Attractive interactions in these compounds is mainly due to dipole-induced dipole interactions (X = HF, HCl, HBr, NO) or dispersion forces between two induced dipoles (X = Cl_2, J_2). Unlike the clathrates, van der Waals complexes are known for neon and helium.

The data in Table 16 indicate typical dissociation energies D_o for HeX in the range 10–20 cm^{-1}, for NeX they are 20–80 cm^{-1}, and for ArX 80–240 cm^{-1}. As expected, the dissociation energy in NgX increases for a given X with the size of Ng (see the discussion in Sect. 4.5). With 350 cm^{-1} being equal to 1 kcal/mol,

Table 16. Dissociation enrgies D_o (in cm^{-1}) and equilibrium distances r_{NgX}[a] (in Å)

X		He	Ne	Ar	Kr	Xe
HF	D_o			102[f]	133[f]	181[f]
	r_{NgX}			2.63[g]	2.75[h]	2.92[h]
	Structure			lin.[f]	lin.[f]	lin.[f]
HCl	D_o		68[l]	115[f]	154[f]	206[f]
	r_{NgX}		2.41[m]	2.60[i]	2.71[k]	
	Structure		lin.[m]	lin.[f]	lin.[f]	lin.[f]
HBr	D_o			206[j]	247[j]	
	r_{NgX}			2.72[j]	2.83[j]	
	Structure			lin.[j]	lin.[j]	
Cl_2	D_o	9[b]	55[b]	175[b]		
	r_{NgX}	3.8[b]	3.57[b]	4.0[b]		
	Structure	T[b]	T[b]	T[b]		
Br_2	D_o		70[b]			
	r_{NgX}	3.7[b]	3.67[b]			
	Structure	T[b]	T[b]			
J_2	D_o	18[b]	75[b]	235[b]		
	r_{NgX}	4.5[b]				
	Structure	T[b]	T[b]			
NO	D_o	8.5[d]	20[d]	87[d]	130[d]	210[d]
	r_{NgX}	3.63[c]		3.77[e]	3.88[e]	
	Structure	T[e]		T[e]	T[e]	

[a] For linear structures, r_{NgX} is the distance between Ng and the nearest atom; for T-shaped complexes, r_{NgX} is the distance between Ng and center of mass of X; [b] Ref. 182; [c] Ref. 183; [d] Ref. 184; [e] Ref. 185; [f] Ref. 186; [g] Ref. 154b. [h] Ref. 187; [i] Ref. 188; [j] Ref. 189. [k] Ref. 190; [l] D_e value taken from Ref. 191; [m] Ref. 191

binding in van der Waals complexes NgX is very weak with typical dissociation energies $D_o < 1$ kcal/mol. Especially the He and Ne complexes exhibit very weak binding. In agreement with the weak attractive interactions, interatomic distances Ng, X in van der Waals complexes are very large as shown in Table 16. The equilibrium distance between Ng and the nearest atom is always larger than 2.5 Å. van der Waals complexes show distinctively smaller dissociation energies and larger interatomic distances for the 'van der Waals-bond' than typical covalent compounds.

In the course of their systematic theoretical investigation of positively charged helium compounds, Frenking, Cremer, and coworkers found [4, 7, 11, 12] that the electronic structure rather than the charge of the binding fragment X is crucially important for the strength of the interactions in HeX. By extending this concept to neutral molecules, they detected computationally the stable molecule HeBeO [7, 14, 15]. The calculated dissociation energy into He + BeO at the MP4(SDTQ)/6-311G(*2df*, *2pd*)//MP2/6-31G(*d*, *p*) level of theory is D_o = 3.0 kcal/mol. The equilibrium distance for the linear molecule in the $^1\Sigma^+$ ground state is predicted as r_{HeBe} = 1.538 Å [7]. They also performed full-valence CASSCF calculations which give similar results, i.e. D_e = 3.5 kcal/mol at r_{HeBe} = 1.577 Å [7]. Later, they studied the analogs NeBeO and ArBeO and found [15] for the neon structure D_o = 2.2 kcal/mol at r_{NeBe} = 1.758 Å, and for ArBeO D_o = 7.0 kcal/mol at r_{ArBe} = 2.036 Å. A critical evaluation of the theoretical results obtained at several computational levels suggests [15] that the dissociation energies are rather lower bounds to the correct values, and that HeBeO is probably bound by 3–4 kcal/mol. The theoretically predicted results for NgBeO shown in Table 17 differ significantly from the typical data found for van der Waals complexes as shown in Table 16. In particular, the D_o value for HeBeO of 3–4 kcal/mol, which is much higher than the 10–20 cm^{-1} (0.03–0.06 kcal/mol) found for weakly bound helium structures (Table 16), points towards chemical bonding, albeit very weak. In fact, a subsequent natural bond orbital analysis of the electronic structure of HeBeO, NeBeO, and ArBeO by Hobza and Schleyer [158] came to the conclusion that the essential nature of the interactions is charge transfer. For HeBeO they found that the overlap between the donor *1s* orbital of He with the acceptor σ* orbital of BeO is quite large (0.42).

In contrast to the natural bond orbital [159] picture, a detailed analysis of the electron density distribution and its associated Laplace field suggests that bonding in HeBeO, NeBeO and ArBeO is caused by strong charge induced

Table 17. Calculated dissociation energies D_o (kcal/mol) and interatomic distances r_{NgBe} (in Å) [15]

	HeBeO	NeBeO	ArBeO
D_o	3.1	2.2	7.0
r_{NgBe}	1.538	1.758	2.036

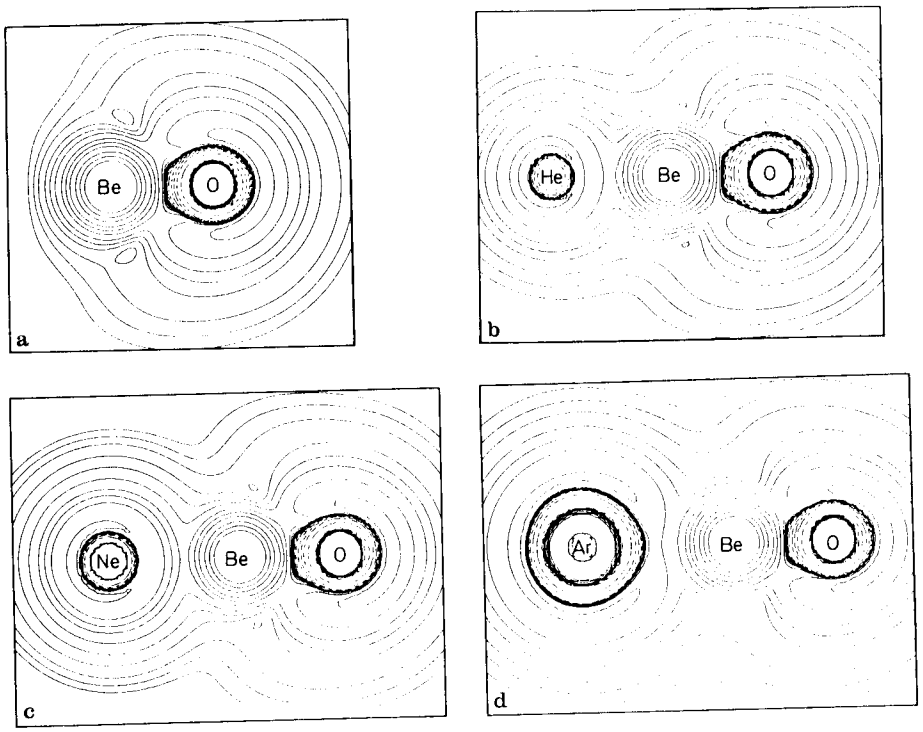

Fig. 27a–d. Contour line diagrams of the Laplace concentration, $-\nabla^2\rho(\mathbf{r})$, of (**a**) BeO, (**b**) HeBeO, (**c**) NeBeO, (**d**) ArBeO. Inner shell concentrations are not shown. (HF/6-31G(*d*, *p*) calculations). Ref. [15]

dipole interactions without covalent contributions [15]. Figure 27 shows the contour line diagrams of the Laplace concentrations of BeO, HeBeO, NeBeO, and ArBeO. The Laplace fields indicate (i) a strong charge transfer from Be to O in BeO as well as in NgBeO, (ii) nearly identical contour line diagrams for BeO as isolated species and for NgBeO, and (iii) hardly any distortion for Ng atoms in NgBeO compared with isolated Ng (Fig. 3). Only for ArBeO there is a small distortion of the Laplace field of the Ar atom. The energy density H_b at the bond critical point for Ng, Be is + 0.120 (HeBeO), + 0.102 (NeBeO), − 0.005 (ArBeO) [15]. Thus, for ArBeO there is a tendency toward beginning covalency.

The natural bond orbital analysis has been claimed [159] to correct many of the deficiencies [160] of the Mulliken population analysis [161]. But it seems to favor orbital interactions compared with electrostatic interactions as is evident by the results for hydrogen bonding which are also interpreted [159] as resulting from charge-transfer rather than electrostatic interactions. Using a multipole expansion scheme, Dykstra and coworkers [162] concluded that electrostatic forces are the dominant factor in hydrogen bonding. In any case, the light noble

gas species HeBeO, NeBeO and ArBeO seem to be examples of molecules in the 'border-line' between typical van der Waals complexes such as shown in Table 16 and covalent compounds.

BeO seems to be a very peculiar acceptor species mainly because of the beryllium atom. Calculations show that, while the oxygen atom may be replaced by isoelectronic NH or CH_2, substitution of Be by any other atom such as Mg, Al, B, does not yield a NgX species which is comparable to NgBeO [163]. The very unique acceptor ability of BeO is demonstrated by the strong complexes formed with CO and N_2, which are calculated with a dissociation energy of D_0 = 30.0 kcal/mol (NNBeO) and 40.8 kcal/mol (OCBeO) [164]. Also, neutral BeO is a stronger acceptor for He and Ne than cationic CN^+, as is evident by a comparison of the calculated binding energies for $NgCN^+$ (Table 12) and NgBeO (Table 17).

The idea of using a strong Lewis acid rather than a strong oxidizing agent for binding Ng atoms is not new. In the 1930s, much effort was devoted especially to the investigation of the Ng + BF_3 systems, and for some time it was believed that a helium compound was formed. For a survey of the literature see Ref. 165. For example, a thermal analysis of the system Ar + BF_3 was reported by Booth and Wilson [166] in 1935. A detailed study of the van der Waals molecule $ArBF_3$ was first made by Janda et al. [167] in 1978. Kaufman and Sachs [168] in 1969 investigated theoretically the systems HeLiH and $HeBeH_2$. They found that $HeBeH_2$ was marginally unstable with respect to He + BeH_2 [168b], but HeLiH was bound by 1.8 kcal/mol [168a]. Although more recent highly accurate calculations [15] predict that HeLiH is bound by only ca. 0.1 kcal/mol, the basic idea of Kaufmann and Sachs pointed toward the right direction. The systematic study of binding in light noble gas compounds [7, 13–15] show that Lewis acids exhibit the strongest attracting force toward Ng.

6.2 *Chemical Compounds of Helium, Neon and Argon*

Soon after the preparation of the first stable noble gas compound by N. Bartlett [1], the isolation of many other noble gas molecules followed [169], it was quickly recognized that many noble gas salts can be classified as derivatives of binary fluorides or oxide fluorides such as $(NgF)^+(A)^-$, $(NgF_3)^+(A)^-$, $(NgOF_3)^+(A)^-$, and many others where Ng = Xe, Kr, and sometimes Rn [170]. Although all attempts to synthesize argon analogs were unsuccessful, stability considerations pointed toward ArF^+ salts as the most promising candidate. Suggestions for possible argon salts are (ArF) (PtF_6) [87] and (ArF) (BF_4) [86]. As discussed in Sect. 4.3, the binding energy of ArF^+ in its $^1\Sigma^+$ ground state has recently been calculated very accurately as $D_0 = 49 \pm 3$ kcal/mol [6]. This value and an estimate of the lattice energies of the possible salt compounds was used by Frenking et al. [6] to predict that (ArF) (SbF_6) and (ArF) (AuF_6) could be stable. However, experimental obstacles to synthesizing these compounds are enormous, because neither AuF_6 nor SbF_6 would probably oxidize the Ar atom,

and the need to generate ArF^+ or F^+ ions as precursors for the salts is experimentally a formidable task. Nevertheless, the theoretical study encourages further experimental attempts to synthesize argon salt compounds, which apparently represent the limit of possible neutral, chemical compounds of the noble gas atoms. Unless one includes the (experimentally not yet found) NgBeO structures in the chemical realm!

7 Summary

The research on light noble gas chemistry may be summarized in the following way. For many years chemists tried to induce chemical reactions with noble gas elements using the most reactive agents known. Until 1962, the only success was the observation of various gas phase cations and weakly bound van der Waals complexes and clathrates. Because of the little information on binding interactions in these compounds, the knowledge on the principles of chemical interactions involving noble gas atoms was scarce and not very systematic. It was only known that attractive interactions between Ng and other atoms or molecules increase with the size of Ng. The Lewis paradigm served as a theoretical explanation for the apparent inability of Ng to form any neutral chemical compound. It was so effective that experimental efforts to disprove the strict validity of the octet rule were for some time not very strong.

With Bartlett's landmark experiment in 1962 [1], noble gas chemistry became synonymous with the chemistry of Xe and Kr and very soon became a standard field of inorganic research. Since the obstacles to synthesizing Xe and Kr compounds were shown to be only technical, a renewed search for compounds of the lighter homologues He, Ne, and Ar was started. It was soon realized that experiments, that were successful for Xe and Kr, did not materialize for helium, neon and argon. The explanation for this was the increase in ionization energy with decreasing size of Ng. The ionization energy of Ng replaced the Lewis paradigm as a rationalization for the unreactivity of Ng = He, Ne, Ar. Experimentally obtained information about bonding of the light noble gas elements is still very scarce.

The situation has changed in the last few years by theoretical studies which culminated in a model for chemical bonding in light noble gas compounds, i.e. donor-acceptor interactions [4, 5, 7, 13, 15]. Earlier attempts at a systematic theoretical study of bonding in light noble gas compounds was performed by Liebman and Allen [82, 87]. Because of the crude methods and limited computer facilities available at that time, the results were quantitatively not very reliable. Modern methods of molecular quantum mechanics together with high-speed computers allow theoretical predictions for small molecules with an accuracy that is competitive with high-quality experiments. Using the tools of modern theoretical chemistry, Frenking, Cremer and coworkers [4–15] reported the results of very accurate calculations and extracted a binding model that explains the binding features for light noble gas compounds. The scattered experimental results for NgX molecules could be shown to be examples of molecular species whose bond strength Ng,X should be discussed in terms of donor-acceptor interactions between Ng and X. It is the Lewis acidity (acceptor strength) of X, rather than the electronegativity or electronic charge, that determines the strength of the binding interactions in neutral and ionic NgX molecules. Based on this model, the search for new and strongly bound molecules was focussed on binding partners that were strong σ-acceptors. The surprising results were the predictions of strong covalent Ng,C bonds in molecular cations and the unusually strong interaction in NgBeO. Table 18 shows a list of theoretically predicted stable or metastable Ng compounds [6, 7, 13, 14].

Table 18. Potentially stable or metastable He, Ne, Ar containing compounds for the thermodynamically stable molecules, the calculated reaction energy ΔE_o (in kcal/mol) for the least endothermic reaction is given. Unless otherwise specified, the results are taken from Ref. 13

Thermodynamically stable molecule	ΔE_o	Metastable
A. Dications		
$He_2C^{2+}(^1A_1)$	13.6	$He_2C^{2+}(^3B_1)$; $He_2N^{2+}(^2B_1)$; $He_2O^{2+}(^1A_1)$; $Ne_2C^{2+}(^1A_1)$; $Ne_2C^{2+}(^3B_1)$; $Ne_2N^{2+}(^2B_1)$; $Ne_2O^{2+}(^1A_1)$; $Ar_2C^{2+}(^1A_1)$; $Ar_2C^{2+}(^3B_1)$; $Ar_2N^{2+}(^2B_1)$; $Ar_2O^{2+}(^1A_1)$;
$ArCCAr^{2+}$	9.4	$HeCCHe^{2+}$; $NeCCNe^{2+}$;
$HeCO^{2+}$	17.7[b]	$HeCF^{3+}$[b]
B. Monocations		
$HeCCH^+$	12.5	
$NeCCH^+$	5.9	
$ArCCH^+$	54.3	
$ArCN^+$	34.6	
$ArNC^+$	17.5 (ΔE_e)	
C. Neutral Compounds		
HeBeO	3.1[a]	
NeBeO	2.2[a]	
ArBeO	7.0[a]	
$ArFSbF_6$	49[c]	

[a] Ref. 15; [b] Ref. 95; [c] $D_o(Ar, F^+)$, Ref. 6

It should be pointed out that the theoretical predictions listed in Table 18 are results *a priori* and not *a posteriori*. The experimental obstacles to verify the theoretical predictions are substantial, however. Light noble gas chemistry has become an area of chemical research where theory and experiment combine and challenge each other.

Acknowledgement. The authors would like to thank the following colleagues and coworkers for stimulating discussions and dedicated cooperation: Prof. C. K. Jørgensen, Prof. N. Bartlett, Prof. J.

F. Liebman, Dr. W. Koch, Dr. J. Gauss, Dr. J. R. Collins, Dr. C. Deakyne, Dr. B. T. Luke, Dipl. Chem. F. Reichel. Part of this research has been supported by the Fonds der Chemischen Industrie.

8 References

1. Bartlett N: Proc. Chem. Soc. 1962: 218
2. For a recent review on the history of the discovery of noble gas compounds see: Laszlo P, Schrobilgen G (1988) Angew. Chem. 100: 495; (1988) Angew. Chem. Int. Ed. Engl. 27: 479
3. Hogness TR, Lunn EG (1925) Phy. Rev. 26: 50
4. Frenking G, Koch W, Gauss J, Cremer D, Liebmann JF (1989) J. Phys. Chem. 93: 3397
5. Frenking G, Koch W, Gauss J, Cremer D, Liebman JF (1989) J. Phys. Chem. 93: 3410
6. Frenking G, Koch W, Deakyne C, Liebmann JF, Bartlett N (1989) J. Am. Chem. Soc. 111: 31
7. Koch W, Frenking G, Gauss J, Cremer, D, Collins JR (1987) J. Am. Chem. Soc. 109: 5917
8. Koch W, Frenking G, Luke BT (1987) Chem. Phys. Lett. 139: 149
9. Koch W, Frenking G (1987) J. Chem. Phys. 86: 5617
10. Koch W, Liu B, Frenking G (in print) J. Chem. Phys.
11. Koch W, Frenking G: J. Chem. Soc. Chem. Commun. 1986: 1095
12. Koch W, Frenking G (1986) Int. J. Mass Spectrom. Ion Proc. 74: 133
13. Frenking G, Koch W, Reichel F, Cremer D (in print) J. Am. Chem. Soc.
14. Koch W, Collins JR, Frenking G (1986) Chem. Phys. Lett. 132: 330
15. Frenking G, Koch W, Gauss J, Cremer D (1988) J. Am. Chem. Soc. 110: 8007
16. See e.g., Hehre WJ, Radom L, Schleyer PVR, Pople JA (1985) Ab initio molecular orbital theory, Wiley, New York
17. (a) Cremer D (1988) In: Maksić ZB (ed) Modelling of structure and properties of molecules. Ellis Horwood, Chichester, England, p 125; (b) Kraka E, Cremer D (in press) In: Maksić ZB (ed) Theoretical models of chemical bonding, vol 2, Springer Verlag, Berlin Heidelberg New York
18. (a) Bader RFW, Preston HJT (1969) Int. J. Quant. Chem. 3: 327; (b) Feinberg MJ, Ruedenberg K (1971) J. Chem. Phys. 54: 1495; (c) Kutzelnigg W (1973) Angew. Chem. 13: 551
19. Cremer D, Kraka E (1984) Croat. Chem. Acta 57: 1259
20. Bader RFW, Essen H (1984) J. Chem. Phys. 80: 1943
21. Frenking G, Koch W (1988) Int. J. Mass Spectrom. Ion Proc. 82: 335
22. (a) Coppens P, Hall MB (eds) (1982) Electron distributions and the chemical bond, Plenum, New York (b) Becker P (ed) (1978) Electron and magnetization densities in molecules and crystals, Plenum, New York
23. Hohenberg H, Kohn W (1964) Phys. Rev. 136B: 864
24. (a) Bader RFW, Nguyen-Dank TT, Tal Y (1981) Rep. Prog. Phys. 44: 893; (b) Bader RFW, Nguyen-Dang TT (1981) Adv. Quantum Chem. 14: 63
25. For a more detailed review, see Ref. 17b
26. Bader RFW, Slee TS, Cremer D, Kraka E (1983) J. Amer. Chem. Soc. 105: 5061
27. Cremer D, Kraka E (1984) Angew. Chem. 96: 612; (1984) Int. Ed. Engl. 23: 627
28. Cremer D, Kraka E (1985) J. Amer. Chem. Soc. 107: 3800, 3811
29. Cremer D, Kraka E, Slee TS, Bader RFW, Lau CDH, Nguyen-Dang TT (1983) J. Amer. Chem. Soc. 105: 5069
30. (a) Cremer D, Gauss J (1986) J. Amer. Chem. Soc. 108: 7467; (b) Cremer D, Kraka E (1988) In: Liebman JF, Greenberg A (eds) Structure and reactivity, VCH Publishers, Deerfield Beach, USA, p 65
31. Cremer D, Gauss J, Kraka E (1988) J. Mol. Struct. (THEOCHEM) 169: 531
32. Note that Bader [24] uses these terms differently by calling all MED paths, also those between closed shell systems, bond paths. This, however, is contrary to general chemical understanding.
33. Morse PM, Feshbach H (1953) Methods of theoretical physics vol 1, McGraw-Hill, New York, p 6
34. Bader RFW, MacDougall PJ, Lau CDH (1984) J. Am. Chem. Soc. 106: 1594 See also Ref. 19

35. Bader RFW (1980) J. Chem. Phys. 73: 2781. G(r) is always positive while V(r) is always negative. When integrated over total molecular space, they yield the kinetic and potential energy of a molecule: $E = \int H(r)\,dr = \int G(r)\,dr + \int V(r)\,dr$
36. Tüxen O (1936) Z. Physik 103: 463
37. Hornbeck JA, Molnar JP (1951) Phys. Rev. 84: 621
38. Inghram MG (1953) Natl. Bur. Standards (U.S.) Circ. No. 522: 204
39. (a) Fukui K (1971) Accts. Chem. Res. 4: 57; (b) Fleming I (1976) Frontier orbitals and organic chemical reactions, Wiley, Chichester
40. Munson MSB, Franklin JL, Field FH (1963) J. Phys. Chem. 67: 1542
41. Weise H-P, Mittmann H-U (1973) Z. Naturforsch. 28a: 714
42. Wadt WR (1978) J. Chem. Phys. 68: 402
43. Black JH: cited in Ref. 44
44. Yu N, Wing WH (1987) Phys. Rev. Lett. 59: 2055
45. Huber KP, Herzberg G (1979) Molecular spectra and molecular structure, vol IV, Constants of diatomic molecules. Van Nostrand Reinhold, New York
46. Christodoulides AA, McCorkle DL, Christophoru LG (1984) In: Christophorou LG (ed) Electron-molecule interactions and their applications, vol 2, Academic, London
47. Bondyby V, Pearson PK, Schaefer HF (1972) J. Chem. Phys. 57: 1123
48. Pauling L (1933) J. Chem. Phys. 1: 56
49. Guilhaus M, Brenton AG, Beynon JH, Rabenovic M, Schleyer PVR (1984) J. Phys. B17: L605
50. Frenking G, Koch W, Liebmann JF (1989) In: Liebmann JF, Greenberg A (eds) Molecular structure and energetics: From atoms to polymers. Isoelectronic analogies, VCH Publishers, p 169
51. Gill PMW, Radom L (1987) Chem. Phys. Lett. 136: 294
52. (a) Yagisawa H, Sato H, Watanabe, T (1977) Phys. Rev. A16: 1352; (b) Cohen JS, Bardsley JN (1978) Phys. Rev. A18: 104
53. Mercier E, Chambaud G, Lewy B (1985) J. Phys. B18: 3591
54. Montanbonel M-CB; Cimiraglia R, Persico M (1984) J. Phys. B17: 1931
55. The ground states on Ne^{2+} and Ar^{2+} have ^3P symmetry. The lowest lying electronic state of $Ng^{2+} + He(^1S)$ (Ng = Ne, Ar) which can mix with the (1) $^1\Sigma^+$ state is the ^1D state of Ng^{2+}. This state is 3.204 eV (Ne^{2+}) and 1.737 eV (Ar^{2+}) higher in energy than the ^3P ground state [62]
56. The situation is actually more complicated because more than two states are sometimes involved in the mixing of the ground state curves: Stärk D, Peyerimhoff SD (1986) Mol. Phys. 59: 1241
57. Stärk D (Personal communication)
58. Helm H, Stephan K, Märk TD, Huestis DL (1981) J. Chem. Phys. 74: 3844
59. Stephan K, Märk TD, Helm H (1982) Phys. Rev. A26: 2981
60. Carrington A, Softley TP (1983) In: Miller TA, Bondybey VE (eds) Molecular ions: Spectroscopy, structure and chemistry, North-Holland, Amsterdam
61. Beach JY (1936) J. Chem. Phys. 4: 353
62. Moore CE (1971) Atom energy levels as derived from the analyses of optical spectra, Nat. Stand Ref. Data Ser. Nat. Bur. Stand. (U.S.) NSRDS-NBS
63. (a) Kolos W, Peek JM (1976) Chem. Phys. 12: 381; (b) Kolos W (1976) Int. J. Quantum Chem. 10: 217
64. (a) Rosmus P (1979) Theoret. Chim. Acta 51: 359; (b) Rosmus P, Reinsch EA (1980) Z. Naturforsch. 35a: 1066; (c) Klein R, Rosmus P, (1984) Z. Naturforsch. 39a: 349; (d) Rosmus P, Reinsch EA, Werner HJ (1983) In: Berkowitz J, Groeneveld KO (eds) Molecular ions: geometric and electronic structures, Plenum, New York
65. Bernath P, Amano T (1982) Phys. Rev. Lett. 48: 20
66. Wong M, Bernath P, Amano T (1982) J. Chem. Phys. 77: 693
67. Lorenzen J, Hotop H, Ruf MW, Morgner H (1980) Z. Physik A, 297: 19
68. Ram RS, Bernath PF, Brault JW (1985) J. Mol. Spectrosc. 113: 451
69. Brault JW (1978) Proceeding of the Workshop on Future Solar Observations, Needs and Constraints, Florence
70. Johns JWC (1984) J. Mol. Spectrosc. 106: 124
71. Wells BH, Wilson S (1986) J. Phys. B19: 17
72. Butler SE, Bender CF, Dalgarno A (1979) Astrophys. J. Lett. 230: 59
73. Chambaud G, Levy B (1986) Ann. Phys. 11: Suppl. 3, 107

74. (a) Dalgano A, McDowell MRC, Williams A (1958) Phil. Trans. R. Soc. A250: 411; (b) Mason EA, Schamp HW Jr, (1958) Ann. Phys. 4: 233; (c) Polark-Dingels P, Rajan MS, Gislason EA (1982) J. Chem. Phys. 77: 3983
75. Böttner E, Dimpfl WL, Ross U, Toennies JP (1975) Chem. Phys. Lett. 32: 197
76. (a) Subbaram KV, Coxon JA, Jones WE (1976) Can. J. Phys. 54: 1535; based on the experimental data, slightly different dissociation energies have been predicted by: (b) Goble JH, Winn JS (1977) J. Chem. Phys. 67: 4206; (c) Le Roy RJ, Lam W-H (1980) Chem. Phys. Lett. 71: 544; (d) Vahala L, Havey M (1984) J. Chem. Phys. 81: 4867
77. Ding A, Karlau J, Weise J, Kendrick J, Kuntz PJ, Hillier IH, Guest MF (1978) J. Chem. Phys. 68: 2206
78. Hillier IH, Guest MF, Ding A, Karlau J, Weise J (1979) J. Chem. Phys. 70: 864
79. Estimated value in Ref. 82c.
80. Ding A, Karlau J, Weise J (1977) Chem. Phys. Lett. 45: 92
81. Berkowitz J, Chupka W (1970) Chem. Phys. Lett. 7: 447
82. (a) Liebmann JF, Allen LC (1972) Inorg. Chem. 11: 1143; (b) Liebmann JF, Allen LC (1970) J. Am. Chem. Soc. 92: 3539; (c) Liebmann JF, Allen LC (1971) Int. J. Mass Spectrom. Ion Phys. 7: 27
83. Cooper DL, Wilson S (1981) Mol. Phys. 44: 161
84. Bernardi F, Epiotis ND, Cherry W, Schlegel HB, Whangbo M-H, Wolfe S (1976) J. Am. Chem. Soc. 98: 469
85. Moore CE (1970) Ionization potentials and ionization limits derived from the analyses of optical spectra nar. Stand Ref. Data Ser. Nat. Bur. Stand. (U.S.) NSRDS-NBS 34
86. Jørgensen CK (1986) Z. Anorg. Allg. Chem. 540: 91
87. Liebmann JF, Allen JF: J. Chem. Soc. Chem. Commun. 1969: 1355
88. Jonkman HT, Michl J (1981) J. Am. Chem. Soc. 103: 733
89. Jonathan P, Boyd RK, Brenton AG, Beynon JH (1986) Chem. Phys. 110: 239
90. (a) Hayes EF, Gole JL (1971) J. Chem. Phys. 55: 5132; (b) Harrison SW, Massa LJ, Solomon P (1972) Chem. Phys. Lett. 16: 57; (c) Alvarez-Rizzatti M, Mason EA (1975) J. Chem. Phys. 63: 5290; (d) Schleyer PvR (1985) Adv. Mass Spectrom. 10a: 287
91. Harrison SW, Henderson GA, Masson LJ, Salomon P (1974) Astrophys. J. 189: 605
92. (a) Müller EW, McLane SB, Panitz JA (1969) Surf. Sci. 17: 430; (b) Tsong TT, Müller EW (1970) Phys. Rev. Lett. 25: 911; (c) Tsong TT, Müller EW (1971) J. Chem. Phys. 55: 2884; (d) Müller EW, Tsong TT (1973) Prog. Surf. Sci., 4: 1; (e) Müller EW, Krishnaswamy (1973) Phys. Rev. Lett. 31: 1282; (f) Tsong TT, Kinkus TJ (1983) Physica scripta, T4: 201; (g) Tsong TT, Kinkus TJ (1984) Phys. Rev. B29: 529; (h) Tsong TT (1984) Phys. Rev. B30: 4946; (i) Tsong TT, Liou Y (1985) Phys. Rev. Lett. 55: 2180
93. Hotokka M, Kindstedt T, Pyykkö P, Roos B (1984) Mol. Phys. 52: 23
94. Wong MW, Radom L (1988) J. Am. Chem. Soc. 110: 2375
95. (a) Wong MW, Nobes RH, Radom L: J. Chem. Soc., Chem. Commun. 1987: 233; (b) Wong MW, Nobes RH, Radom L (1987) Rapid Commun. Mass Spectrom. 1: 3; (c) Radom L, Gill PMW, Wong MW, Nobes RH (1988) Pure Appl. Chem. 60: 183
96. Hirschfelder JO, Curtiss CF, Bird RB (1986) Molecular theory of gases and liquids, Wiley, New York
97. Wilson S, Green S (1980) J. Chem. Phys. 73: 419
98. Bohme DK, Adams NG, Mosesman M, Dunkin DB, Ferguson EE (1970) J. Chem. Phys. 52: 5094
99. Munson MSB, Field FH, Franklin JL (1962) J. Chem. Phys. 37: 1790
100. Adams NG, Bohme DK, Ferguson EE (1970) J. Chem. Phys. 52: 5101
101. Milleur MB, Matcha RL, Hayes EF (1974) J. Chem. Phys. 60: 674
102. Matcha RL, Milleur MB, Meier PF (1978) J. Chem. Phys. 68: 4748
103. Matcha RL, Milleur MB (1978) J. Chem. Phys. 69: 3016
104. Dykstra CE (1983) J. Mol. Struct. THEOCHEM 103: 131
105. Matcha RL, Pettitt BM, Meier PF, Pendergast P (1978) J. Chem. Phys. 69: 2264
106. Clampiti R, Jefferies DK (1970) Nature 226: 142
107. (a) Leopold DG, Murray KK, Stevens Miller AE, Lineberger WC (1985) J. Chem. Phys. 83: 4849; (b) Bunker PR, Sears TJ (1985) J. Chem. Phys. 83: 4866
108. For the problem of graphically illustrating Δ states see: Salem S (1982) Electrons in chemical reactions: First principles, Wiley, New York
109. The orbital terms in Fig. 15 correspond to heteronuclear diatomics XY. For homonuclear species XX, the 3σMO becomes $2\sigma g$ orbital, 4σ becomes $2\sigma_u$, etc. For simplicity reasons, we have used the heteronuclear notations throughout the text.

110. Kaul W, Fuchs R (1960) Z. Naturforschg. 15a: 326
111. Teng HH, Conway DC (1973) J. Chem. Phys. 59: 2316
112. The ground state of CCH^+ is a triplet: (a) Krishnan R, Frisch M, Whiteside RA, Pople JA, Schleyer PVR (1981) J. Chem. Phys. 74: 4213; (b) Glaser R (1987) J. Am. Chem. Soc. 109: 4237
113. The $^1\Pi$ state is unstable, however, towards Renner distortion. The lowest lying singlet state of CCH^+ has $^1A'$ symmetry and is 4.8 kcal/mol lower than $^1\Pi$: Koch W, Frenking G: J. Chem. Phys. (in print)
114. In Ref. 7, the binding energy of the He–C bond in $HeCCH^+$ has been calculated using the $^1\Delta$ state of CCH^+. However, the $^1\Pi$ state of CCH^+ was later [113] calculated to be lower-lying than the $^1\Delta$ state. The dissociation energy of $HeCCH^+$ yielding He + ($^1\Pi$) CCH^+ is reported in Ref. 13
115. Ikuta S, Iwata S, Imamura M (1977) J. Chem. Phys. 66: 4671
116. Snell AH, Pleasonton F (1958) J. Phys. Chem. 62: 1377
117. Cacace F (1970) Adv. Phys. Org. Chem. 8: 79
118. Wexler S, Anderson GR, Singer LA (1960) J. Chem. Phys. 32: 417
119. (a) Carlson TA, White RM (1962) J. Chem. Phys. 36: 2883; (b) Carlson TA, White RM (1962) J. Chem. Phys. 39: 1748; (c) Carlson RT, White RM (1962) J. Chem. Phys. 38
120. Holtz D, Beauchamp JL (1971) Science 173: 1237
121. See e.g., Gimarc BM (1979) Molecular structure and bonding, the qualitative molecular orbital approach, Academic Press, New York
122. Holloway JH (1968) Noble gas chemistry, Methuen, London
123. Druyvesteyn MJ (1931) Nature 128: 1076
124. Heller R (1941) J. Chem. Phys. 9: 154
125. (a) Manley JJ (1924) Nature 114: 861; (b) Manley JJ (1925) Nature 115: 337
126. Powell HM: J. Chem. Soc. 1948: 61
127. Davy H (1811) Phil. Trans. 101: 1
128. Mylius F: J. Chem. Soc. Abstracts 1886: 50
129. (a) Palin DE, Powell HM: J. Chem. Soc. 1947: 208; (b) Palin DE, Powell HM: J. Chem. Soc. 1948: 571; (c) Palin DE, Powell HM: J. Chem. Soc. 1948: 815; (d) Rayner JH, Powell HM: J. Chem. Soc. 1952: 319; (e) Wallwork SC, Powell HM: J. Chem. Soc. 1956: 4855; (f) Lawton D, Powell HM: J. Chem. Soc. 1958: 471
130. Balek V (1970) Anal. Chem. 42: (9) 16A
131. (a) Hagan SMM (1962) Clathrate inclusion compounds, Reinhold, New York (b) Gawalek G (1969) Einschlußverbindungen, Additionsverbindungen, Clathrate. Deutscher Verlag der Wissenschaften, Berlin
132. Hagan SMM (1963) J. Chem. Educ. 40: 643
133. (a) Adams RE, Browning WE, Ackley RD (1959) Ind. Eng. Chem. 51: 1467; (b) Steinberg M, Manowitz B (1959) Ind. Eng. Chem. 51: 47
134. (a) Swift WE (1957) Nucleonis 15: 66; (b) Wilson EJ, Dibbs HP, Richards S, Eakins JD (1958) Nucleonics 16: 110
135. Mock JE (private communication) cited in: Mock JE, Myers JE, Trabant EA (1961) Ind. Eng. Chem. 53: 1007
136. McClain JW, Diethorn WS (1963) J. Appl. Radiation and Isotopes 14: 527
137. (a) Powell HM, Guter M (1949) Nature 164: 240; (b) Powell HM: J. Chem. Soc. 1950: 298
138. Powell HM: J. Chem. Soc. 1950: 300
139. Powell HM: J. Chem. Soc. 1950: 468
140. Mandelcorn L (ed) Non-stoichiometric compounds, Academic, New York, p 438
141. Villard P (1896) Compt. Rend 123: 377
142. (a) De Forcrand R (1923) Compt. Rend 176: 335; (b) De Forcrand R (1925) Compt. Rend 181: 15
143. van der Waals JH, Platteeuw JC (1959) Adv. Chem. Phys. 2: 1
144. Beurskens PT, Jeffrey GA (1964) J. Chem. Phys. 40: 906; and earlier papers cited therein
145. Barrer RM (1964) In: Mandelcoin L (ed) Non-stoichiometric compounds, Academic, New York
146. Von Stackelberg M, Müller HR (1954) Z. Elektrochem. 58: 25
147. Davidson DW, Garg SK, Gough SR, Handa YP, Ratcliffe CI, Tse JS, Ripmeester JA (1984) J. Inclus. Phenom. 2: 231

148. Lahr PH, Williams HL (1959) J. Phys. Chem. 63: 1432
149. Barrer RM, Shanson VH: J. Chem. Soc. Chem. Commun. 1976: 333
150. Bolotin AB, Bolotin VA, Balyavichus M-LZ, Gantmakher BF, Stumbris EP, Tatevskii VM, Shapiro EI, Yaravoi SS (1982) Teor. Eksp. Khim 18: 212
151. Weber A (ed) (1987) Structure and dynamics of weakly bound molecular complexes, Reidel, Dordrecht
152. See the review articles in: (1988) Chemical Review 88
153. Van Lenthe JH, van Duijneneveldt-van der Rijdt JGCM, van Duijneveldt FB (1987) Adv. Chem. Phys. 69: 521
154. (a) Legon AC, Millen DJ (1986) Chem. Rev. 86: 635; (b) Peterson KI, Fraser GT, Nelson DD Jr, Klemperer W (1985) In: Bartlett RJ (ed) Comparison of ab initio quantum chemistry with experiment for small molecules, Reidel, Dordrecht
155. English TC, Zorn JC, (1972) In: Williams D (ed) Methods of experimental physics, vol 3 (2nd edn), Academic, New York
156. Balle TJ, Campbell EJ, Keenam MR, Flygare WH (1979) J. Chem. Phys. 71: 2723
157. (a) Levy DH (1981) In: Jortner J, Levine RD, Rice SA (eds) Photoselective chemistry, Wiley, New York; (b) Levy DH (1980) Annu. Rev. Phys. Chem. 31: 197
158. Hobza P, Schleyer PvR: Coll. Czech. Chem. Commun. (in print)
159. Reed AE, Curtiss LA, Weinhold F (1988) Chem. Rev. 88: 899
160. Bachrach SM, Streitwieser A Jr (1984) J. Am. Chem. Soc. 106: 2283
161. Mulliken RS (1955) J. Chem. Phys. 23: 1833
162. Dykstra CE, Liu S-Y (1987) In: Weber A (ed) Structure and dynamics of weakly bound molecular complexes, Reidel, Dordrecht
163. Koch W, Frenking G (unpublished results)
164. (a) Frenking G, Koch W, Collins JR: J. Chem. Soc., Chem. Commun. 1988: 1147; (b) Frenking G, Koch W, Cremer D, Gauss J, Collins JR (manuscript in preparation)
165. Hawkins DT, Falconer WE, Bartlett N (1978) Noble gas compounds, Plenum, New York
166. Booth HS, Willson KS (1935) J. Am. Chem. Soc. 57: 2273
167. Janda KC, Bernstein LS, Steed JM, Novick SE, Klemperer W (1978) J. Am. Chem. Soc. 100: 8074
168. (a) Kaufman JJ, Sachs LM (1970) J. Chem. Phys. 52: 3534; (b) Kaufman JJ, Sachs LM (1969) J. Chem. Phys. 51: 2992
169. Hyman HH (ed) (1963) Noble gas compounds, University of Chicago press, Chicago
170. Selig H, Holloway JH (1984) Topics Current Chem. 124: 33
171. Miller TM, Bederson B (1977) Adv. At. Mol. Phys. 13: 1
172. Dabrowski L, Herzberg G (1978) J. Mol. Spectrosc. 73: 183
173. Liao MZ, Balasubramanian K, Chapman D, Lin SH (1987) Chem. Phys. 111: 423
174. Dabrowski L, Herzberg G, Yoshino K (1981) J. Mol. Spectrosc. 89: 491
175. Trevor DJ (1980) Ph. D. Thesis, University of California, Berkeley
176. Pratt ST, Dehmer PM (1982) J. Chem. Phys. 76: 3433
177. Dehmer PM, Pratt ST (1982) J. Chem. Phys. 76: 843
178. Dehmer PM, Pratt ST (1982) J. Chem. Phys. 77: 4804
179. Pratt ST, Dehmer PM (1982) Chem. Phys. Lett. 87: 533
180. Ng CY, Trevor DJ, Mahan BH, Lee YT (1976) J. Chem. Phys. 65: 4327
181. Balasubramanian K, Liao MZ, Lin SH (1987) Chem. Phys. Lett. 138: 49
182. Cline JI, Edvard DD, Reid BP, Sivakumar N, Thommen F, Janda KC (1987) In: Weber A (ed) Structure and dynamics of weakly bound molecular complexes, Reidel, Dordrecht
183. Beneventi L, Casacecchia P, Volpy GG (1987) In: Weber A (ed) Structure and dynamics of weakly bound molecular complexes, Reidel, Dordrecht
184. Estimated value by Miller JC (1987) J. Chem. Phys. 86: 3166
185. Casavecchia P, Lagana A, Volpi GG (1984) Chem. Phys. Lett. 112: 445
186. Pine AS (1987) In: Weber A (ed) Structure and dynamics of weakly bound molecular complexes, Reidel, Dordrecht
187. Fraser GT, Pine AS (1986) J. Chem. Phys. 85: 2502
188. Howard BJ, Pine AS (1985) Chem. Phys. Lett. 122: 1
189. Keenan, MR, Campbell EJ, Balle TJ, Buxton LW, Minton TK, Soper PD, Flygare WH (1980) J. Chem. Phys. 72: 3070
190. Balle TJ, Campbell EJ, Keenan MR, Flygare WH (1979) J. Chem. Phys. 71: 2723
191. Hutson JM, Howard BJ (1982) Molec. Phys. 45: 769
192. A noble gas atom may become an electron acceptor (Lewis acid) in molecules if electronic charge is withdrawn by other atoms or ions. An example is provided by the recently synthesized first compound with a krypton-nitrogen bond HCN–$KrF^+AsF_6^-$. In KrF^+, electronic charge is withdrawn from Kr and a donor-acceptor bond between Kr and HCN is formed, but here the (partially positively charged) Kr atom serves as electron acceptor and HCN (via the nitrogen lone-pair electrons) is the electron donor: Schrobilgen GJ: J. Chem. Soc. Chem. Commun. 1988: 863; MacDougall PJ, Schrobilgen GJ, Bader RFW (1989) Inorg. Chem. 28: 763
193. For a survey of the techniques and the method see: Bierbaum VM, Ellison GB, Leone SR (1984) In: Bowers MT (ed) Gas phase ion chemistry, vol 3, Academic, Orlando, p 2